ABSTRACT

RAJULAPATI, KOTESWARARAO VENKATA. Synthesis and mechanical properties of two phase nanostructured Al based composites. (Under the direction of Prof. Carl C. Koch).

Nanostructured materials (<100 nm) exhibit novel and superior mechanical properties in comparison to their coarse grained counterparts. However the associated deformation mechanisms are poorly understood. Synthesizing bulk nanocrystalline materials to measure the meaningful/reasonable mechanical properties is still a grand challenge. Although there exist several experimental/theoretical studies on mechanical behavior of single phase materials, studies on the effect of a second phase (soft/hard) on the mechanical behavior of nanocrystalline materials are very limited. Therefore, the thrust of the current work is to synthesize bulk nanostructured two phase materials and to establish the influence of a second phase (soft/hard) on the mechanical properties of two phase materials benchmarked against the corresponding single phase material and to identify the governing mechanics of plasticity at the nano scale.

Nanocrystalline aluminum was synthesized using ball milling at room temperature. The resultant powder material was consolidated to the bulk form using warm compaction and argon atmosphere and consolidation using high pressure torsion. The samples after high pressure torsion exhibited high end mechanical properties. The hardness of the nanostructured aluminum (of grain size 32 nm) was as high as 1200 MPa which is 6 times harder than its coarse grained counterpart.

Nanocrystalline Al-W composites with varying compositions were synthesized. With the increased addition of W, the hardness of these nanocomposites was increased. This hardness trend followed the behavior predicted by the rule of mixtures based on the volume fractions of Al and W. With the addition of 4 atomic % of W, the strength of the nanocrystalline aluminum was elevated by 70 %.

Nanocrystalline Al-Pb composites were synthesized by two routes. In the first route, the room temperature ball milled samples were compacted at 573 K in an argon atmosphere. In the second route, the alloys were consolidated in situ during ball milling using a combination of milling at cryogenic temperature and milling at room temperature. Irrespective of the processing sequence employed in the current study, the minute additions of Pb to the nanocrystalline aluminum decreased its strength drastically beyond the projections made by the rule of mixtures. The Pb segregated to the grain boundaries of nanocrystalline aluminum appeared to be making the difference.

In situ consolidated nanocrystalline Al-0.7%Pb composite was subjected to high pressure torsion at room temperature. Interestingly, the additional straining caused by the high pressure torsion further weakened the material by 25 %. The mean grain size of the nanocrystalline aluminum was the same before and after the HPT. The mechanism for this abnormal behavior is yet to be known.

The creep properties of nanostructured aluminum, synthesized using the sequential combination of ball milling at room temperature and high pressure torsion, were evaluated using the impression creep testing. The measured stress exponent values do not

correspond to the Coble creep mechanism. However the activation energy measured was that of grain boundary diffusion in aluminum.

Synthesis and mechanical properties of two phase nanostructured Al based composites

by

KOTESWARARAO VENKATA RAJULAPATI

A dissertation submitted to the Graduate Faculty of
North Carolina State University
in partial fulfillment of the
requirements for the Degree of
Doctor of Philosophy

MATERIALS SCIENCE AND ENGINEERING

Raleigh

2006

APPROVED BY

Prof. Carl C Koch
(Chair of the committee)

Prof. Ronald O Scattergood

Prof. Korukonda L Murty

Dr. Gerd Duscher

Prof. Robert J Nemanich
(Minor representative)

To……

Amma (Mother) and Nanna (Father)

BIOGRAPHY

Koteswararao V. Rajulapati was born on May 24th 1979 in the southern state of Andhra Pradesh, India. He received his Bachelor of Technology in Metallurgical Engineering from the Jawaharlal Nehru Technological University College of Engineering, Kukatpally, Hyderabad, India, in June 2000. Later he enrolled at the Indian Institute of Technology (IIT), Kharagpur, India for his Master of Technology in Metallurgical Engineering in July 2000. For his masters thesis, he worked on "Phase stability in nanoquasicrystalline Al based alloys" in the research group supervised by Prof. B. S. Murty (currently at IIT, Madras). He finished his masters degree in January 2002. Following this, he worked as a Junior Research Fellow in the same group until August 2002. He then joined the research group supervised by Prof. Carl. C. Koch at North Carolina State University in August 2002 for his doctoral studies.

ACKNOWLEDGEMENTS

I would like to express my heartfelt gratitude to my supervisor Prof. Carl C. Koch for giving me an opportunity to work with him for my Ph D. I would like to express my sincere gratefulness to him for his able guidance, involvement in the work, invaluable suggestions and scintillating discussions. I admire his strict scientific principles. I am sure that I learned how to do a quality research under his guidance and hope to continue it for the rest of my life. I would like to express my deep appreciation to Prof. Ronald O. Scattergood and Prof. K. Linga (KL) Murty for their encouragement, guidance and suggestions. It was really a great opportunity to work with them.

I would like to thank Dr. Gerd Duscher for agreeing to serve on my committee. The help that I received from him and several discussions that I had with him regarding TEM are gratefully acknowledge here. I would like to express my sincere thanks to Prof. Robert J. Nemanich for serving my committee as a minor representative.

I am grateful to Prof. Zenji Horita (Kyushu University, Japan) and Prof. Terence G. Langdon (University of Southern California) for collaborating with us. My special thanks to Prof. Horita for his timely response, patience and understanding nature.

I would like to acknowledge Dr. Thomas Rawdanowicz and Mr. Donovan Leonard for their help while working with the TEM. I am thankful to Ms. Edna Deas for her help in administrative matters right from my first day in the department.

I would like to thank my group members Dr. Khaled Youssef, Dr. Ramesh Guduru, Mr. Gopinath Trichy, Ms. Abby Griffith, Mr. Kristopher Darling, Mr. David Tucker, Mr. Patrick Wong and others. I would like to express my sincere thanks to Mr. Srikant Gollapudi and Dr. Indrajit Charit for working with me on impression creep testing.

My loyal thanks to my friends Dr. Amit Chugh, Dr. Yoganand Saripalli, Mr. Shivaraman Ramachandran, Mr. Vikram Bhosle, Mr. Deepayan Chakraborti, Mr. Ravi Shankar Aggarwal and Mr. Saral Kalanadhabhatla for their help and encouragement whenever I was in need.

My gratefulness to Prof .B. S. Murty (Indian Institute of Technology, Madras, India) who taught me the basics of research.

Finally, I am bowing down my head on the feet of my parents, without whose sacrifices and support, I would not have been what I am today.

This research is supported by the U. S. National Science Foundation under grant no. DMR-0201474.

TABLE OF CONTENTS

LIST OF TABLES

CHAPTER 3

CHAPTER 5

CHAPTER 8

LIST OF FIGURES

CHAPTER 2 BACKGROUND

Chapter 1

Introduction

Nanocrystalline materials with grain size < 100 nm exhibit novel often superior physical, chemical, magnetic and mechanical properties [1-6]. These unique properties are attributed to the presence of a high volume fraction of internal interfaces in these materials. The unique and improved mechanical properties in single phase nanocrystalline materials are well documented [3]. However, the governing deformation mechanisms in these materials are not completely understood. The deformation mechanisms observed in coarse grained materials can not be extrapolated to the nano-regime. Molecular dynamics simulations predicted that there occur fundamentally different dislocation generation mechanisms [7-8]. Grain rotation and grain boundary sliding were also predicted [9]. However the supporting real time experimental data is yet to be available.

The nano-grained materials are good candidates for structural applications because of their higher strength. Alloying elements, in majority of the cases, improves the strength in coarse grained materials. However the alloying effects at the nano scale are poorly understood. Fabricating nanomaterials to their bulk form without losing the improved properties (or the original nano-structure) is still a grand challenge. Motivated by this clear lack of knowledge, the aim of the current study is to synthesize bulk nanocrystalline two phase materials using a sequential combination of ball milling, warm compaction and high pressure torsion and to study their mechanical behavior. Al was chosen as the matrix material and W and Pb were chosen as the dispersoids. The remaining part of this dissertation is organized as follows:

Chapter 2 summarizes the available literature on methods of synthesis, structure and mechanical properties of nanocrystalline materials.

Chapter 3 gives the experimental techniques and their background used in this study to achieve the objectives.

Chapter 4 gives the details about synthesis of nanocrystalline pure aluminum by high energy ball milling and its subsequent consolidation into bulk form by warm compaction and high pressure torsion. Structural details obtained by XRD and TEM and the mechanical properties are also presented.

Chapter 5 presents the work on synthesis of bulk nanostructured Al-W composites, their microstructure and the mechanical properties. The effect of a nano scaled W phase on the nanocrystalline aluminum is also discussed.

Chapter 6 is based on the journal article, K. V. Rajulapati, R. O. Scattergood, K. L.Murty, G. Duscher, C. C. Koch, Scripta mater, 55 (2006) 155. The drastic softening observed in nanocrystalline aluminum with minute additions of Pb is discussed.

Chapter 7 is about the effects of combined sequence of ball milling and high pressure torsion on the mechanical properties of nanocrystalline in situ consolidated Al-0.7% Pb composite.

Chapter 8 is on creep properties of nanostructured aluminum evaluated by impression creep testing technique.

Chapter 9 summarizes the outcomes of the present work.

Chapter 10 is on suggestions for the future work.

References:

1. H. Gleiter, Acta Mater., 48 (2000) 1.
2. K. S. Kumar, H. Van Swygenhoven, S. Suresh, Acta mater 51 (2003) 5743.
3. M. A. Meyers, A. Mishra, D. J. Benson, Prog. Mat.Sci 51 (2006) 427.
4. V. Yamakov, D. Wolf, S. R. Phillpot, A. K. Mukherjee, H. Gleiter, Nature mat. 3 (2004) 43.
5. D. Wolf, V. Yamakov, S. R. Phillpot, A. K. Mukherjee, H. Gleiter, Acta mater 53 (2005)1.
6. H. Van Swygenhoven, J. R. Weertman, Materials Today, 9 (2006) 24.
7. Van Swygenhoven H, Derlet PM, Hasnaoui A, Phys rev B 2002; 66:024101
8. Asaro RJ, Suresh S, Acta mater 2005; 53: 3369
9. Van Swygenhoven H, Derlet PM, Phys rev B 2001; 64:224105.

Chapter 2

Background

2.1 History:

The nanostructured materials are defined as the ones with the microstructure with a characteristic length scale of which is on the order of a few nanometers, typically less than 100 nm. On December 29th 1959, while addressing the American Physical Society annual meeting at Caltech, Prof. Richard Feynman pointed out that "There is plenty of room at the bottom"-highlighting if one can arrange the structures atom-by-atom, a new field of physics can be visioned [1]. However, until the landmark publication by Prof. Herbert Gleiter saw the light of the day in 1989 [2], nobody in the field of materials science realized the scope and future of this exciting nanoscience and nanotechnology. It obviously created, in the following years, a vast amount of interest among the researchers in the field of materials science globally and led to several break-throughs in the many aspects of these nanostructured materials. However, there is still plenty of scope to explore the physics displayed by these new classes of materials and thereby to look for the direct applications to mankind. Today nanotechnology has expanded to almost all the branches of science and engineering.

2.2 Structure of nanostructured materials:

Unlike in coarse crystalline materials, nanocrystalline materials, as shown in the above Figs 1&2., contain significant volume fraction of grain boundaries, triple junctions and quadruple junctions. The fraction of these intercrystalline regions increases as the grain size decreases. Palumbo et al [4], assuming a grain as fourteen sided tetrakaidecahedron,

estimated the volume fractions of grain boundaries and triple junctions [Fig.2]. A nanocrystalline material may be regarded as a composite consisting of crystalline and intercrystalline (grain boundaries, triple junctions) components. The portion of the intercrystalline components in polycrystalline materials is so small that its effect on observed properties is negligible whereas in nanocrystalline materials, not only do grain boundaries play an important role, but also triple lines and quadruple nodes might be contributing significantly to deformation.

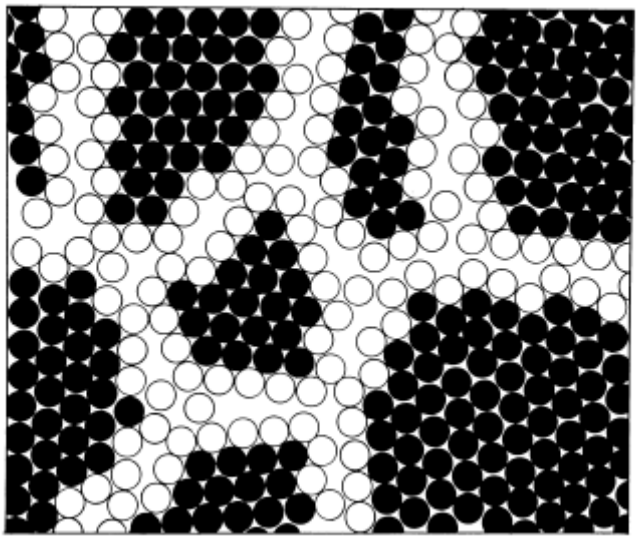

Fig 1. Two dimensional model of a nanostructured material. The atoms in the centers of the crystals are indicated in black. The ones in the boundary core regions are represented as open circles [3].

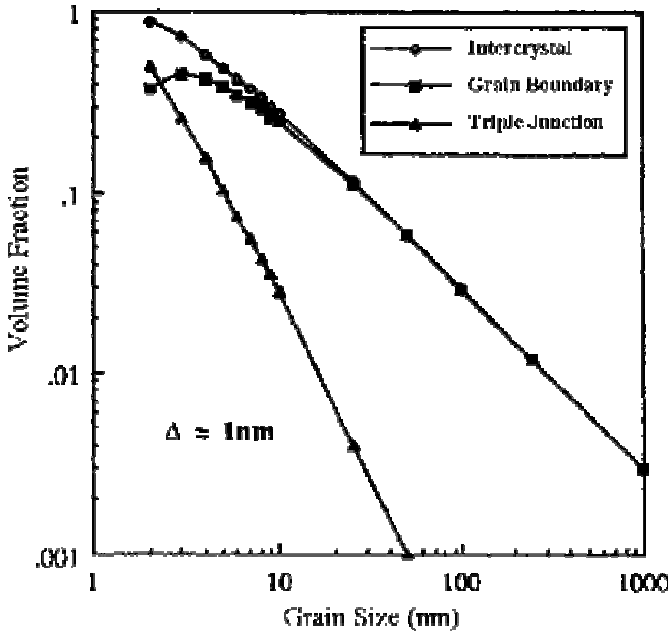

Fig 2. Effect of grain size on the calculated volume fractions for intercrystalline regions, grain boundaries and triple junctions [4]. Δ is the grain boundary width.

Hence often, the observed novel often superior properties in these advanced class of materials are attributed to the presence of these interfacial regions. However the atomistic mechanisms responsible for these novel properties are not completely understood.

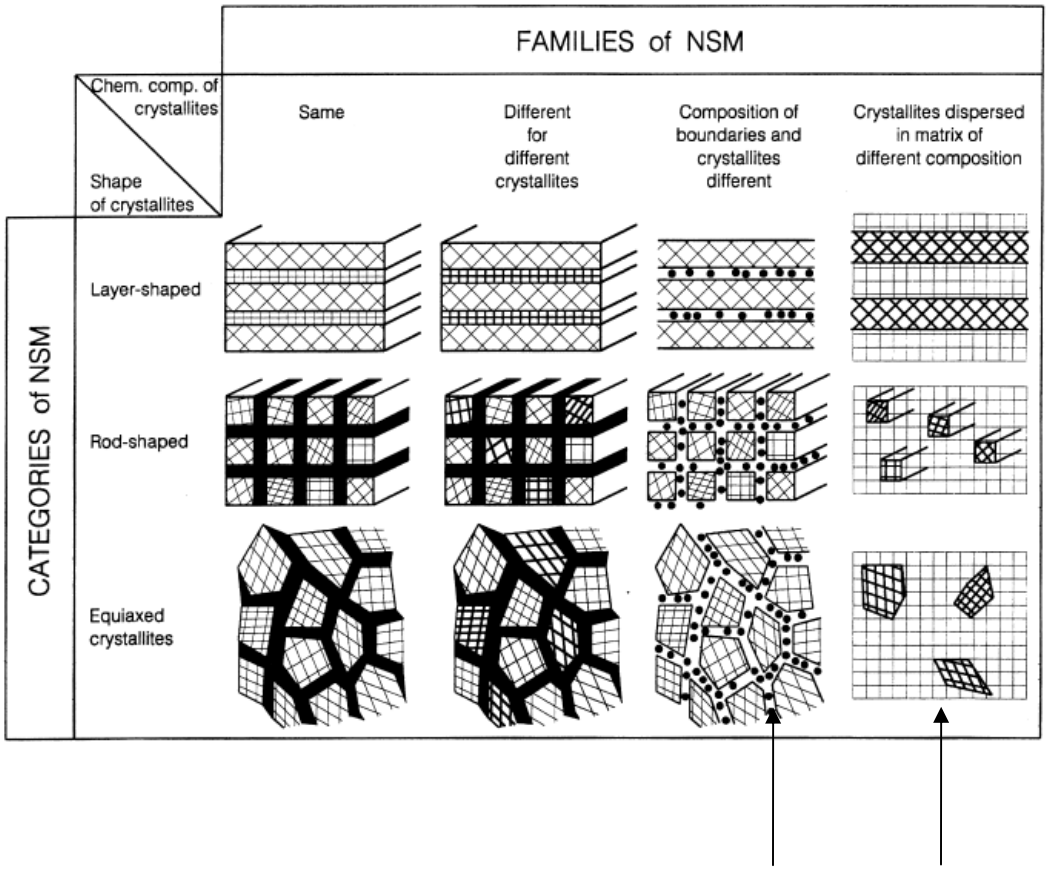

Fig 3. Classification scheme of nanostructured materials according to their chemical composition and their dimensionality (shape) of the crystallites (structural elements) forming the nanostructure [3]. The arrows indicate the materials classes of this study.

The nanostructured materials were classified into different categories [Fig 3] based on the dimensionality and composition differences between crystalline and intercrystalline regions. The boundary regions of the first and second family are indicated in black to emphasize the different atomic arrangements in the crystallites and in the boundaries [3]. The work carried out in the current study fall into those two categories (indicated with arrows in Fig 3).

2.3 Properties:

1. High strength and significant ductility
2. Improved magnetic properties
3. Increased diffusivities at room temperature
4. Reduced dimensionalities help microprocessors perform much faster, leading to the development of next generation electronic devices.

2.4 Synthesis of nanostructured materials:

The several methods to synthesize nanomaterials known to date were broadly classified into two approaches, bottom-up and top-down. The bottom-up approach involves the atom-by-atom arrangement of nanostructures whereas the top-down approach involves the disintegration of microstructure into a nanostructure. The various methods that fall in these two categories are [3]:

- Inert gas condensation [5]
- High energy ball milling [6]
- Electrodeposition [7]
- Crystallization from amorphous material [8]
- Severe plastic deformation [9]
- Plasma synthesis
- Chemical vapor deposition
- Pulsed electron deposition
- Pulsed laser deposition [10]

- Sputtering
- Physical Vapor deposition
- Spark erosion.

Should the reader be interested in knowing the full details about the above mentioned processes, he/she is advised to look at the corresponding references. Since high energy ball milling and high pressure torsion (part of severe plastic deformation) are the ones used in processing the nanostructured materials in the current study, these will be described here in detail.

2.5 High energy ball milling

High energy ball milling (HEBM) is a powder processing technique, originally employed to mix the composite powders for high temperature use, developed by Benjamin and his co-workers at INCO [11]. But over the years, it evolved as the potential technique to synthesize commercially useful and scientifically interesting materials [12, 13]. Several researchers have highlighted the potency of this process, with their landmark publications, in synthesizing several novel, scientifically interesting, metastable as well as stable materials [14, 15].

2.5.1 Attributes of HEBM **[16]**

1. Production of fine dispersion of second phase particles
2. Extension of solid solubility limits
3. Refinement of grain size down to the nanometer range
4. Synthesis of novel crystalline and quasi-crystalline materials
5. Development of amorphous phases
6. Disordering of ordered intermetallics
7. Possibility of alloying of difficult to alloy elements/metals
8. Inducement of chemical reactions at low temperatures
9. Commercially scalable process.

2.5.2 Mechanism of nanostructure formation during HEBM:

Mechanical deformation under the shear conditions and high strain rates (10^1-10^4 s^{-1}) results in the formation of nanostructures within powder particles, thin foils and at the surface of metals and alloys exposed to friction induced wear conditions [17]. The phenomenological view of the ball milling is shown in the picture below.

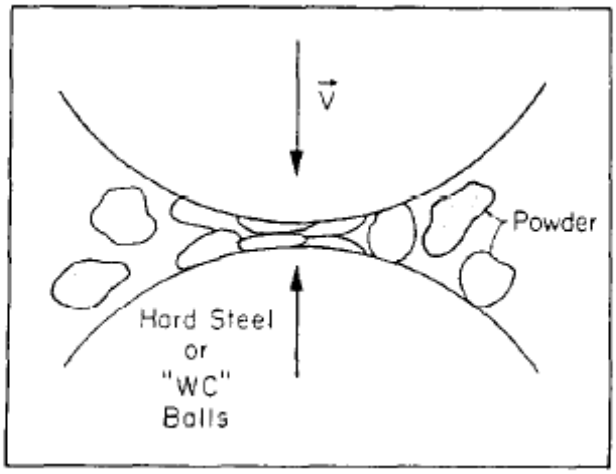

Fig 4. Phenomenology of ball milling [14].

Materials will be subjected to severe plastic deformation with ball-powder-ball collision processes [Fig 4] under high strain rate shear conditions. Consequently cold welding, fracturing and re-welding of the powder particles occurs inside the vial. Because of the deformation at high strain rates, lattice defects namely point defects, dislocations, stacking faults, twins etc. will be pumped into the material and thereby the material is brought to a high energy state. According to Fecht, during ball milling of AlRu [14], initially the deformation is localized in shear bands consisting of an array of dislocations with high density. At a certain strain level, these dislocations annihilate and recombine into low angle grain boundaries separating the individual grains. The subgrains that are formed are already in the range of 20-30 nm. During further deformation, the sample volume exhibiting small grains increases. Subsequently, the small angle grain boundaries are replaced by high angle boundaries, implying grain rotation. As a result dislocation-free nano grains are formed. Therefore the final minimum grain size achievable in a given material is

dictated by the competition between the plastic deformation via dislocation motion (in other words pumping rate) and the recovery and recrystallization characteristics of a given material. Hence if the processing temperature is decreased, one can suppress the recovery processes and can attain the minimum grain size in lesser time. This is often termed as cryomilling i.e., ball milling at cryogenic temperatures (77K).

2.5.3 Process variables:

1. Type of mill:

A wide variety of ball mills have been developed over the decades for different purposes that include shaker mills, attrition mills, vibratory mills, planetary mills and tumbler mills etc. The major difference in these mills is the variation of milling intensity as well as the impact energy from one another. Of all these, SPEX shaker mills are known to be of higher energy and one can refine the microstructures of a given material in less time compared to other mills. At the same time, the minimum (saturation) grain size that can be achieved is material dependent.

2. Milling media:

Because of the high impact of the balls on the powder material as well as on the inner walls of the container, the original powder material gets contaminated with the material of the milling media (container, balls). Generally, balls and container are made of the same material. As the material of the milling media gets into the original powder material, the chemistry of it gets altered which is undesirable. Hence one should be cautious while choosing the milling media with the ultimate goal of

minimizing the contamination if not avoiding it. Hardened steel, tool steel, hardened chromium steel, tempered steel, stainless steel, WC-Co, WC lined steel and bearing steel are the most common types of the materials that are used as milling media. Some specific materials were also used for specialized purpose, i.e., copper, titanium, sintered corundum, yittria stabilized zirconia (YTZ) etc.

3. Milling time:

Duration of milling process is an important parameter. As we increase the milling time, the grain size of the material decreases and attains a saturation value over a period of time. The general practice is that milling is carried out until a steady state in grain size is reached. Milling for about 25h at room temperature using SPEX mill (of high energy) yields a minimum grain size in most of the materials. If the milling is carried out at cryogenic temperatures, 10-12 hrs of milling should suffice to reach the minimum grain size. If other mills which are of lower energy are used more time is needed to achieve the same minimum grain size in a given material.

4. Process controlling agent (PCA):

While milling the ductile materials (for example aluminum), cold welding dominates the fracturing process and as a result the charge material gets welded to the inner walls of the container as well as to the balls. In order to avoid this, a process controlling agent (or surfactant) is added to the charge material. These surfactants can be solids, liquids or gases and are mostly organic compounds. The surfactant gets adsorbed on the surface of the fractured particle and inhibits the agglomeration. The

important PCAs include stearic acid, hexane, methanol, toluene and ethanol etc. However the presence of these PCAs in the final material is detrimental during the subsequent consolidation processes. Hence an extra processing step is often required to remove these surfactants without altering the nano-scaled microstructural features as well as the chemistry of the material.

5. Ball to powder weight ratio (BPR):

The ratio of weight of the balls to the weight of the charge material is called ball-to-powder weight ratio. As we increase the BPR, the milling intensity and the milling energy increases and microstructures can be refined in lesser durations. However the increase in the number of balls beyond a certain limit makes the deformation process ineffective. Hence the judicious selection of number of balls as well as the amount of charge material is needed for the effective processing. BPRs ranging from 1:1 to 220:1 were reported. However BPRs of 5:1 or 10:1 were employed in majority of the research studies.

6. Temperature of milling:

It is already mentioned that the final structure obtainable in the milling process is based on the competition between the strain hardening rate and the recovery rates. If the recovery rates can be suppressed to some extent (by decreasing the processing temperatures) keeping the straining rates constant, one can refine the microstructures in less time. Hence lower processing temperatures (cryogenic) are recommended.

An optimization of all the above mentioned variables is crucial for a given material or a desired objective.

2.6 Severe Plastic deformation:

For the last two decades, development of nano/ultra fine grained materials which exhibit improved properties over their coarse grained counterparts has been of primary focus. Although, the nanostructures can be obtained in powder materials via several processing techniques, there are some disadvantages in terms of powder handling, oxidation and contamination etc. In addition to that, compaction of these nano grained powders to their bulk densities without losing the nano scaled features is still a grand challenge.

To overcome a few of those shortcomings while processing the nanostructured materials, one can rely on severe plastic deformation (SPD). In SPD, the bulk material is subjected to large amounts of strains (of the order of thousands of percent) at low homologous temperatures without changing the dimensions of the material. The primary SPD techniques that were used to synthesize bulk nanostructured solids include High Pressure Torsion (HPT) and equal channel angular pressing (ECAP) [9].

2.6.1 High Pressure Torsion:

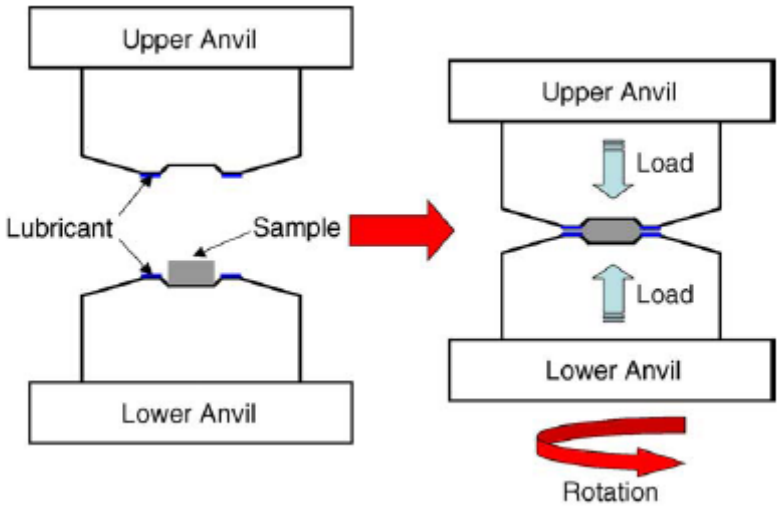

Fig 5. Schematic showing the high pressure torsion set-up [18].

The device [Fig 5] that is being used for high pressure torsional straining is the modified Bridgeman anvil type device that was first used to study the phase transformations under heavy deformation [19, 20] and the evolution of structure and recrystallization temperatures after large plastic deformations [21, 22].

A work piece is held between two anvils (upper ram and lower ram) and strained in compression under the applied pressure of several G Pa. After pressing and holding the work piece with the upper anvil, the lower anvil is rotated. The surface friction forces between the work piece and the rotating lower anvil deform the work piece by shear without changing the dimensions. The following formula is often used to calculate the strain imposed during HPT:

$$\gamma = \frac{2\pi RN}{l}. \qquad (1)$$

This formula is used in the case of usual straining for the calculation of the shear strain value at the distance R from the axis of the disk type sample where γ is the shear strain, R is the radius of the sample (disk), N is number of revolutions and l is the thickness of the sample. To compare this strain value with the strain values during the deformation by other modes, it can be converted into equivalent strain using Von-Mises criterion,

$$e_{eq} = \frac{\gamma}{\sqrt{3}} \tag{2}$$

According to equation (1), the imposed strain shall be minimum at the center and it should increase as we move towards the edge of the sample. But this was not confirmed by experiments. Secondly, the initial thickness of the sample is reduced significantly under high compressive pressures. Hence usage of l as the initial thickness may not yield the true strain imposed on the sample. Therefore the calculated strain values using equation (1) are approximate and not the true ones.

The above strain equations (1) and (2) suggest that there would not be any straining in the center of the sample. However, straining of the material using several rotations (~5) does yield homogeneous microstructures and thereby exhibits uniform mechanical properties [23].

The samples processed by severe torsional straining are usually of a disk shape, from 10 to 20 mm in diameter and 0.2-0.5 mm in thickness. In order to refine the microstructure and to have structural homogeneity several rotations are employed. Several ultra fine grained/nanostructured metals and alloys have been developed using this method starting from bulk coarse grained materials [9].

Recent investigations show that this method can be used not only to refine the microstructure but also to consolidate the nanocrystalline (ball milled) powders of Al-Mg [24], Co [25], Ni [26] and amorphous aluminum alloy [27].

2.6.2 Equal Channel Angular Pressing

This is another technique that was employed extensively to refine the microstructures of the coarse grained materials and thereby to develop the bulk high strength metals and alloys [28, 29]. As shown in the schematic [Fig 6], the ECAP processing involves pushing the material through a die. The die contains two channels, equal in cross section, intersecting at an angle close to 90^0.

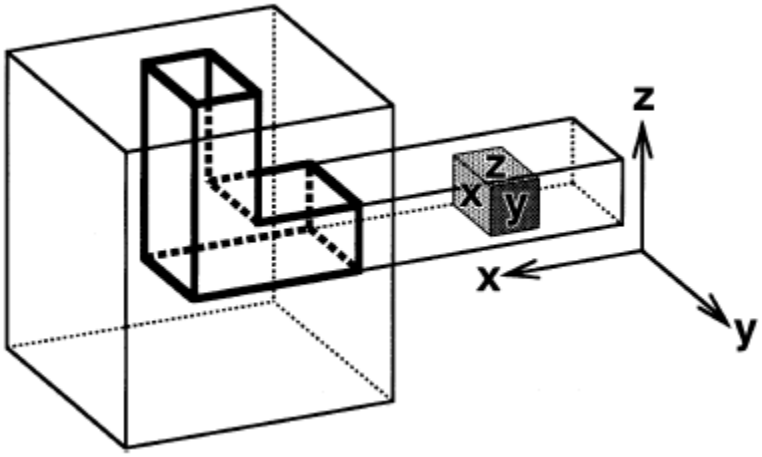

Fig 6. Schematic showing the Equal Channel Angular Pressing set up [28].

The test sample is machined to fit within these channels. The sample is directed from the top and is pushed with the help of a piston and is forced around a sharp corner. The strain imposed on the sample in ECAP is dependent upon both the channel angle between the channels, and the angle defining the outer arc of curvature where the two channels intersect. It can be shown that an equivalent strain close to ~1 is introduced when the

channel angle is 90^0 for all values of the angle defining the arc of curvature. Since the cross-sectional dimensions of the sample remain unchanged on passage through the die, repetitive pressings may be used to attain very high strains.

2.6.3 Microstructural evolution in both ECAP and HPT

Similar to the microstructural evolution in ball milling, the microstructural evolution in HPT and ECAP processes is dictated by the competition between defect accumulation and recovery processes that occurs during straining the material.

2.7 Mechanical properties of nano grained materials

It is well known and widely accepted that, plastic deformation in coarse grained materials occurs by dislocation controlled slip. However these mechanisms can't be extrapolated to the materials with the grain size in nano regime. At the smallest grain size regimes, a new deformation mechanism might dominate, such as grain boundary sliding or grain rotation accompanied by short range diffusion assisted healing events.

Hall [30] and Petch [31] developed a relation in 1950s known as Hall-Petch equation that connects the grain size and yield strength in micro crystalline materials. According to this relationship, the yield strength is inversely related to the square root of the grain size. A similar kind of relationship was also developed for hardness (based on the Tabor's relationship [32] between hardness and yield strength). Hence decreasing the grain size aids in the development of high strength materials of the same composition. Following that several researchers have investigated the validity of this relationship by refining the

grain size and thereby developed the high strength materials. The Hall Petch equation is given by:

$$\sigma_y = \sigma_0 + kd^{-1/2} \tag{3}$$

Where $\boldsymbol{\sigma_y}$ is the yield stress, $\boldsymbol{\sigma_0}$ is the friction stress and **d** is the grain size and **k** is the Hall-Petch constant.

Nanomaterials are an advanced class of materials with grain size less than 100 nm. The Hall-Petch equation predicts very high values for the hardness/strength for the grain sizes less than 20 nm. However, the experimental data available till today fall well below these Hall-Petch extrapolations to the nano regime. The slope of the Hall-Petch plot for nanocrystalline materials was found to fall well below that for coarse grained values [Figs 7 &8]. In some cases it was even found to be negative although some reports on this issue are questionable to some extent. Although there are several mechanisms proposed for the explanation of the inverse Hall-Petch effect, there was a widespread disagreement in the research community.

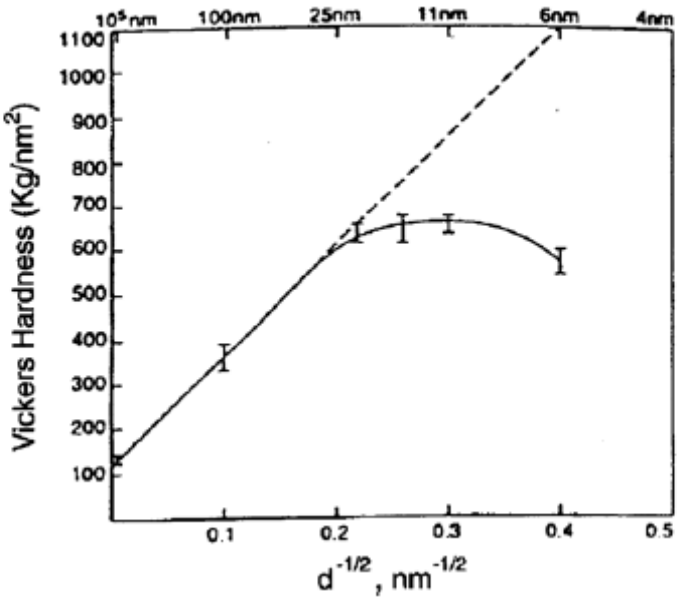

Fig 7. Hardness of Electrodeposited Ni, showing the inverse Hall-Petch effect at smaller grain sizes [33].

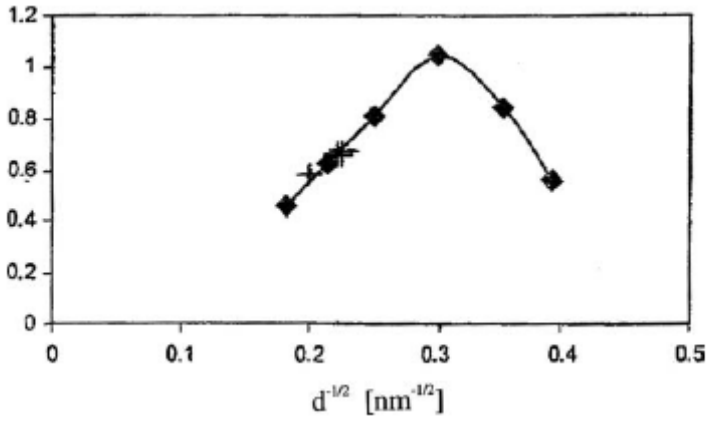

Fig 8. Hardness of nanocrystalline Zn synthesized by laser ablation or mechanical milling, exhibiting the inverse Hall-Petch effect at finer grain sizes [34].

The processing artifacts (pores, incomplete particulate bonding) will have negative effect on the strength and are the main reasons for the inverse Hall Petch effect observed in the earlier studies. However, at finer grain sizes, typically at less than 10 nm, since the existence of dislocations is of very low probability, a change in the deformation mechanism is predicted. Hence samples with a grain size less than 10 nm may exhibit the inverse Hall-Petch effect. In any case, the reasons for the Inverse Hall-Petch effect are still unknown and there is no consensus among the research community albeit the existence of several models in the literature. The data shown in Figs 7&8 are from the samples that are free from processing artifacts.

2.7.1 Elastic properties

Often the nanocrystalline materials are fabricated via the consolidation of powders. Hence the residual porosity and incomplete particulate bonding are detrimental to the mechanical properties. Sanders et al [35] investigated the effect of porosity on Young's modulus of Pd and Cu and is shown in Fig 9. This porosity dependence of Young's modulus was expressed as [36, 37]

$$E = E_0(1 - f_1 p + f_2 p^2)$$

$$= E_0 (1\text{-}f_1 p) \text{ at smaller values of p} \qquad (4)$$

Where p is the porosity and f1 and f2 are equal to 1.9 and 0.9 respectively.

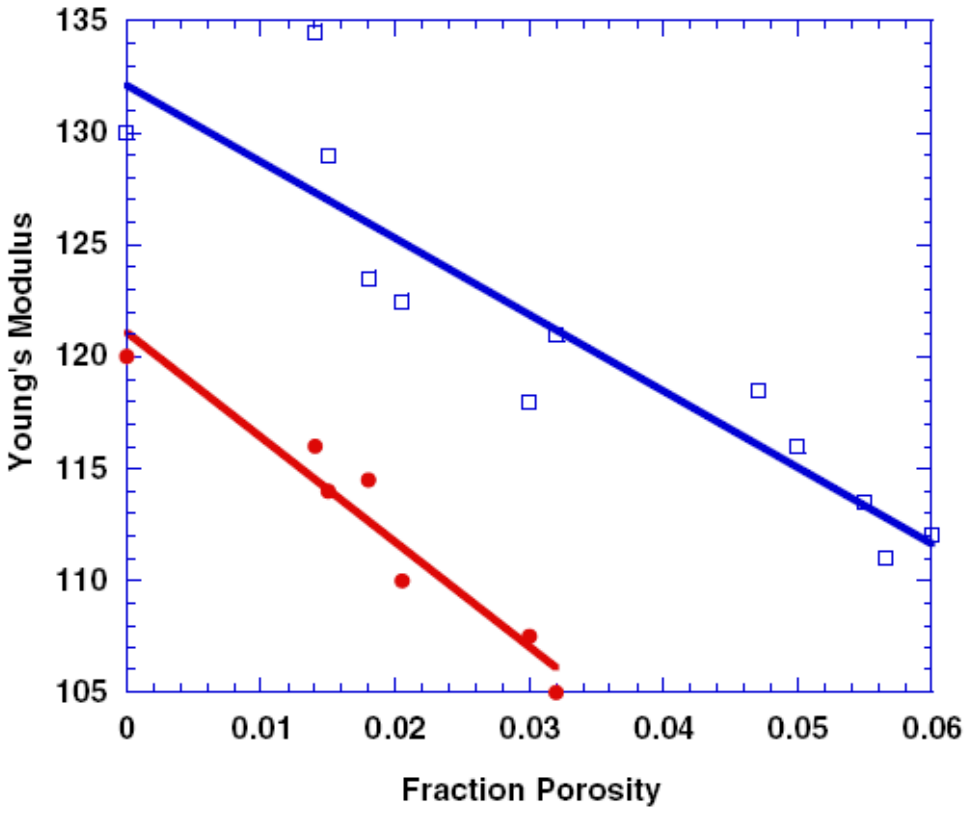

Fig 9 Young's modulus as a function of porosity for nanocrystalline Pd and Cu [35].

The yield stress and tensile ductility are expected to follow the same dependence [Fig 10]. Youngdahl et al [38] reported the density dependence of compressive yield strength and is shown in Fig 10. Therefore the processing artifacts deteriorate the mechanical properties of nanocrystalline materials with premature failure. Hence synthesizing fully dense nanomaterials with complete inter-particle bonding is still the main thrust of research in this area.

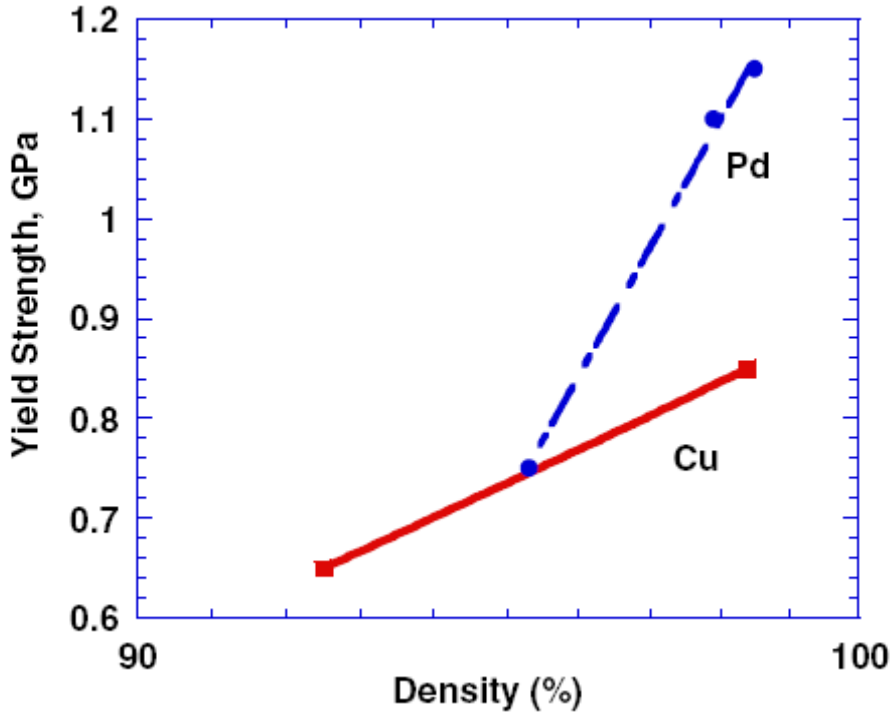

Fig 10 Compressive yield strength of Cu and Pd as a function of consolidation density [38].

2.7.2 Ductility

In conventional coarse grained materials, as we decrease the grain size, the strength and ductility increases. However the nanocrystalline materials exhibit, in the majority of the studies, poor ductilities (1-2% elongations) [39]. Hence, initially it was thought that it is an inherent property of these materials. However, Koch [40], after reviewing the available experimental data, identified three possible reasons for the limited ductilities observed in nano materials. They are 1) artifacts from the processing, 2) force instability in tension and 3) crack nucleation or propagation instability.

However, the recent advances in material processing led to the development of artifact free materials in a few material systems and thereby significant increases in strength as well as improved ductilities were observed in these materials. Available literature suggests that having bimodal grain size distribution results in high strength as well as good ductility in nanocrystalline materials [41, 42].

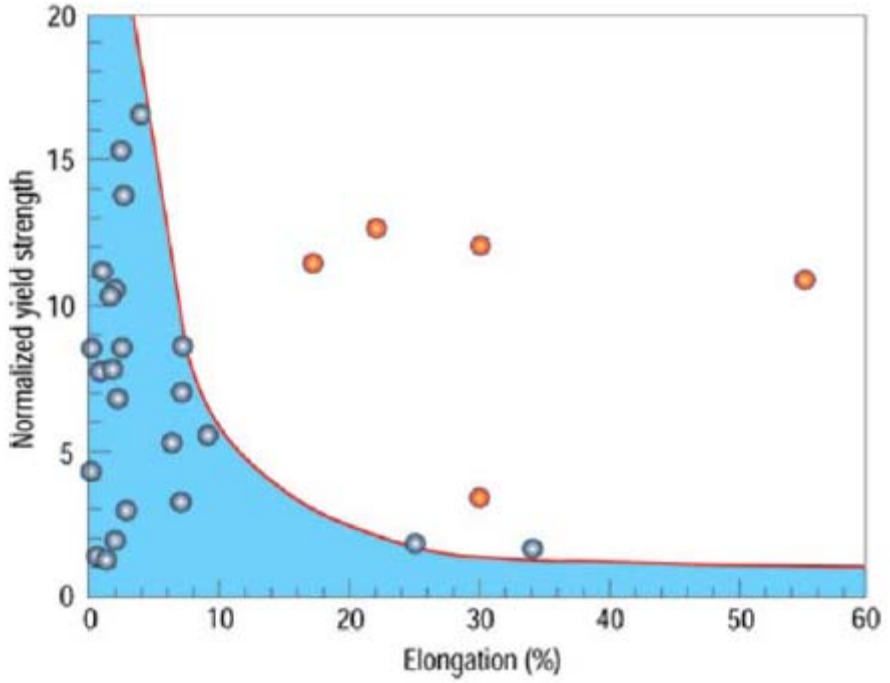

Fig 11. Normalized yield strength versus percentage elongation (ductility) for nanostructured metals. Measured yield strength has been normalized by dividing it by the yield strength of a material's coarse grained yield strength [43].

In Fig 11, normalized yield strength was plotted against percentage elongation for different nanocrystalline materials [43]. Most materials showed high strength accompanied by low ductilities. However few data points that are outside the shaded

region exhibit both high strength and good ductility, giving a ray of hope on retaining the ductility in nanomaterials to some extent.

2.7.3 Creep

Time dependant deformation characteristics of conventional coarse grained engineering materials were widely studied and the corresponding deformation mechanisms were identified [44]. However the creep studies of nanocrystalline materials have received very limited amount of attention from the research community because of the following possible reasons [45]:

1. Processing difficulties associated in obtaining the bulk samples (with uniform microstructure at nano scale) needed for the conventional creep testing.
2. Significant increase in interfaces (grain boundaries, triple lines and quadrupole junctions). The high amounts of these interfacial regions make the identification of the involved creep mechanism difficult.
3. Possible grain growth at low temperatures in comparison to coarse grained materials thus limiting the testing procedures to low homologous temperatures.

The high temperature deformation behavior of crystalline materials is given by the following Bird-Dorn-Mukherjee equation:

$$\dot{\varepsilon} = \frac{ADGb}{kT}\left(\frac{b}{d}\right)^{p}\left(\frac{\sigma}{G}\right)^{n} \tag{5}$$

Where $\dot{\varepsilon}$ is the strain rate, A is a dimensionless constant, G is the shear modulus, b is the magnitude of the Burgers vector, k is Boltzmann's constant, T is the absolute temperature, p is the grain size exponent and n is the stress exponent.

At very low stresses and small grain sizes, early theoretical considerations indicated that vacancies, rather than dislocations, may be responsible for the production of creep strain. Two models, Nabarro-Herring creep and Coble creep, have been formulated to account for such plastic flow. Nabarro-Herring creep involves the diffusion of vacancies through the grain volume. In Coble creep, vacancies diffuse along the grain boundaries. These two processes represent two independent mechanisms, so that faster process controls the creep behavior.

In coarse grained materials, the diffusion controlled creep occurs via two mechanisms; one is Nabarro-Herring creep where the diffusional flow of vacancies occurs through the lattice and the governing equation is given by:

$$\dot{\varepsilon}_{\mathrm{NH}} = \frac{A_{\mathrm{NH}} D_{\mathrm{L}} Gb}{kT}\left(\frac{b}{d}\right)^{2}\left(\frac{\sigma}{G}\right) \tag{6}$$

Where A_{NH} is about 28 and D_L is the coefficient of lattice diffusion; the exponent p=2 and n=1. And the other one, coble creep involves the flow of vacancies through the grain boundaries and the associated equation is:

$$\dot{\varepsilon}_{CO} = \frac{A_{CO} D_{gb} G b}{kT} \left(\frac{b}{d}\right)^3 \left(\frac{\sigma}{G}\right) \tag{7}$$

Where A_{CO} is about 50, Dgb is the grain boundary diffusion coefficient and the exponents p=3 and n=1.

Since the nanocrystalline materials possess significant fraction of grain boundaries and other interfaces, it was suggested that coble creep is the dominant deformation mechanism in these materials even at ambient temperatures.

2.7.4 Time dependant deformation characteristics of different nanocrystalline materials

In recent years, creep and superplasticity in nanocrystalline materials have been the subject of a number of studies [46]. More precisely, experimental studies have been focused to investigate (a) whether grain boundary diffusion creep, which is expected to be dominant in coarse-grained materials at moderate temperature(0.4-0.6 Tm) and low stresses, becomes significant at low temperatures (or at room temperature) and (b) whether the superplastic behavior of coarse grained materials, which has been observed at high temperatures (T > 0.5 Tm) and moderate strain rates (10^{-5} to 10^{-2} per sec) can be

observed at low temperatures and high strain rates. A review of these studies by Mohamed and Li [46] shows that data obtained by different investigators are either not consistent in trend or too limited in scope to draw any reasonable/meaningful conclusions. Various aspects characterizing these inconsistencies and limitations are identified. It is suggested that a number of issues need to be fully addressed in order to provide a better understanding of the deformation processes which control the behavior of nanocrystalline materials.

Nanostructured materials are believed to show poor creep resistance. However Weertman's group [47] showed that there were no differences between the creep behaviors of nanocrystalline Pd and Cu in comparison to their microcrystalline counterparts. In their work, it was found that the measured creep rates were several orders of magnitude slower than the values predicted from Coble creep. Their studies resulted in the following conclusions, (a) grain boundary diffusional creep does not account for the creep behavior of nanocrystalline Cu and Pd at both low and moderate temperatures, and (b) grains in the nanocrystalline range do not result in creep rates which are faster than those associated with grains in the microcrystalline range. They attributed the very low creep rates measured in their experiments to two factors that are related to the microstructural characteristics of nanocrystalline Cu and Pd and that do not favor the occurrence of creep by diffusional flow and/or by dislocation processes. These two factors are (a) the presence of twin boundaries and low angle boundaries that resist boundary sliding and that are poor paths for vacancy diffusion and (b) the limitation on dislocation activity due to the small grain sizes characterizing nanocrystalline materials.

The creep behavior of cryomilled and extruded ultra fine grained- 5083 Al alloy was investigated at two different temperatures, namely 573 K and 623 K [48]. The creep resistance of this nano alloy was found to exceed that of conventional 5083 Al alloy and it was attributed to the presence of nano scale precipitates and impurities. The creep behavior was manifested by three regions; (a) a low stress region with a stress exponent of 1.1, (b) an intermediate stress region with a very high stress exponent and (c) a high stress region with a stress exponent of 9. They observed that the microstructure is very stable at elevated temperatures even after prolonged exposures. The existence of second phases (nano scaled aluminum oxide, nitride, carbide or precipitates) in combination with grain boundary segregation of solute and/or impurity elements is considered to play a significant role in stabilizing the microstructure.

Kottada and Chokshi [49] investigated the creep behavior of electrodeposited nanocrystalline Ni under compressive conditions. The experimental data do not follow the predictions of Coble creep, since the stress exponent n is substantially greater than 1. The activation energies determined in their study are ~ 90-120 kJ/mole and are close to the value for grain boundary diffusion. The conclusion is that grain boundary sliding/rotation/migration accompanies the intragranular dislocation creep.

Yin et al [50] studied the creep characteristics of nano Ni at 290 K and 373 K. Their experimental results showed that significant creep deformation occurred even at room temperature at an initial applied stress of 600 MPa or higher. The creep resistance was

very sensitive to the test temperature. The activation energy for creep which was obtained from the plot of the threshold stress versus 1/T was found to be 0.72 eV. This value 0.72 eV is similar to that of the grain boundary diffusion in a coarse grained Ni, 1.08 eV, but deviates from that of the lattice diffusion, 2.0 eV. In their investigation, room temperature creep tests did not result in any grain growth as evidenced from the TEM of post deformation samples. However, the creep tests carried out at 373 K resulted in a slight grain growth and that was evidenced during their TEM studies. Grain size distribution exists in their material. In larger grains, a dislocation pile-up may occur at a much slower stress level whereas dislocations may not occur in sufficiently smaller grains. If this is the case, a new question arises as to the source of plastic deformation beyond yield stress. The idea is that the grain boundary migration is a competing mechanism against dislocation mechanism. It has been suggested that there is no hardening effect in nanocrystalline materials at room temperature deformation. This indicates that the dislocation pile-ups necessary for strain hardening may be absent or negligible in this material. Consequently, the grain boundary migration is the main mechanism for plastic deformation in such a material. The stress exponent is unity for room temperature creep while it is 6.5 for creep at 373 K. Their experimental data show that the governing creep mechanism is not the Coble creep mechanism but the dislocation mechanism. The calculated creep rate at room temperature, based on the Coble creep mechanism, is in agreement with the experimental results. However, the creep deformation mechanism might change from a diffusion-controlled process at room temperature to multiple mechanisms at 373 K. Above ambient temperature, lattice dislocation gliding and grain boundary sliding may play an important role in deformation.

The creep behavior of a cryomilled and extruded UFG Al-Mg alloy was studied [51]. The grain size ranged from 300-400 nm. The stress exponents ranged from 7.2 to 7.4. The apparent activation energy for creep, 83.7 kJ/mol at 27.5 MPa and 77 kJ/mol at 38 MPa, agreed well with the activation energy for grain boundary diffusion in aluminum. TEM analysis following creep at 300 deg C to approximately 0.2% strain in 1411 h revealed that the grain size was unchanged from its as extruded grain size indicating significant thermal stability of this material at relatively high fractions of melting temperature. The creep resistance of the Al-Mg alloy was rationalized in terms of an attractive interaction between grain boundary dislocations and incoherent particles within the boundary region, which suppressed grain boundary deformation. The grain boundary particles also led to high thermal stability by exerting a Zener pinning force on the grain boundaries, thus inhibiting grain growth at high temperatures.

The creep behavior of this Al-4%Mg alloy exhibits creep behavior very similar to that of the dispersion strengthened aluminum alloy within a similar stress-temperature regime. The stress exponent was found to be independent of temperature and stress level indicating that a single mechanism is responsible for creep under present experimental conditions. It is suggested that detachment controlled diffusional creep is the most likely mechanism responsible for the creep behavior of the cryomilled Al-4%Mg alloy.

Currently the available creep data do not allow us to come up with a concrete conclusion whether they exhibit improved/deteriorated creep properties. The preliminary results

suggest that grain boundary diffusion creep is dominant in a nanocrystalline Ni-P alloy (28 nm) [52] and lattice diffusion is dominant in large grained Ni-P (257 nm), whereas the power law mechanism controls creep in an Al-Mg alloy [51] of submicrometer grain size. The dislocation creep rate is practically independent of grain size, while the diffusional creep rate is inversely proportional to the second power of mean grain diameter when the diffusion mass transport occurs via the lattice (Nabarro-Herring) and to the third power of mean grain diameter when it occurs through the grain boundaries (Coble). At low homologous temperatures and small mean grain diameters, the grain boundary diffusion dominates over the lattice diffusion. Consequently under these conditions the diffusional creep will occur by stress directed mass transport through grain boundaries.

2.7.5 Proposed/predicted deformation mechanisms in nanocrystalline materials

The nanomaterials are believed (based on experimental data as well as MD simulations) to deform by the following mechanisms:

(a) Grain boundary sliding

(b) Grain rotation and coalescence and

(c) Grain boundaries acting as sources as well as sinks for full dislocations/partial dislocations/stacking faults etc

2.7.5.1 Grain boundary sliding

Grain boundary sliding was suggested as one of the dominant deformation mechanisms in nano grained materials (grain size <50 nm). In this, one layer of grains slides w.r.t other, producing shear strain in the process [Fig 12]. The process is shown in the schematic [45]. This is believed to be the dominant mode of deformation at finer grain sizes where the operation of conventional dislocation generating sources is doubtful.

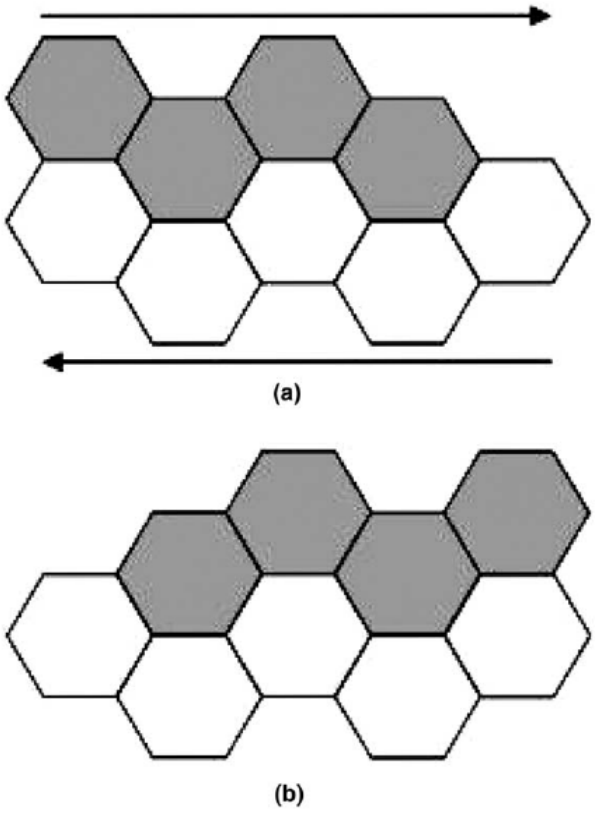

Fig 12. Grain boundary sliding model: (a) initial position of grains and (b) position after top layer has slid to right [45].

Conrad [53] analyzed the existing data and identified three regimes based on the grain size:

Regime 1 ($d>10^{-6}$):

In this regime, materials deform plastically by dislocation controlled slip mechanism and the rate controlling mechanism is given by

$$\tau = M\alpha Gb\left[(\rho_0(T,\gamma,\dot{\gamma}))^{1/2} + \frac{\beta(T,\dot{\gamma})\gamma}{bd^{1/2}}\right] \tag{8}$$

Where M is a parameter and α =0.3-0.5, ρ_0 is dislocation density. The first term contains the thermal component while the second term contains the grain size dependence.

Regime 2 ($d = 10^{-8}$ m-10^{-6} m):

In this regime, grain boundary shear promoted by the dislocation pile up is considered to be the deformation mechanism and the governing equation is given by

$$\tau = \alpha Gb\rho^{1/2} + \left[\left(\Delta F^* - kT\ln\left(\frac{\dot{\gamma}_0}{\dot{\gamma}}\right)\right)^{1/2}\left(\frac{Gb}{\pi V}\right)^{1/2}\right]d^{-1/2} \tag{9}$$

Where ΔF^* is the Helmholtz free energy, V is the activation volume and ρ is the dislocation density

Regime 3 ($d < 10^{-8}$ m):

In this regime, grain boundary shear is considered to be the dominant deformation mechanism and the governing equation is given by

$$\tau - \tau_0 = \left(\frac{kT}{V} \ln \left(\frac{\delta v_D}{\dot{\gamma}} \right) + \frac{\Delta F^*}{V} \right) + \frac{kT}{V} \ln d \qquad (10)$$

Where τ_0 is threshold stress for shearing, Δ is the grain boundary width, υ_D is the vibration frequency ($\sim 10^{13}$ s^{-1}), ΔF^* is the Helmholtz free energy.

2.7.5.2 Grain boundary rotation or grain coalescence

A recent interesting observation [54, 55] suggests another mode of plastic deformation in nano grained materials i.e., nano sized grains can rotate during plastic deformation and subsequently coalesce along the directions of shear. This leads to the larger paths for dislocation movement. During plastic deformation, two neighboring grains can rotate w.r.t. each other in a way such that the degree of misorientation between them approaches zero. This eliminates the boundaries between the grains and provides a path for more extended dislocation motion. This kind of mechanism leads to the softening of the material. The stages involved in this mechanism are schematically shown in Fig 13.

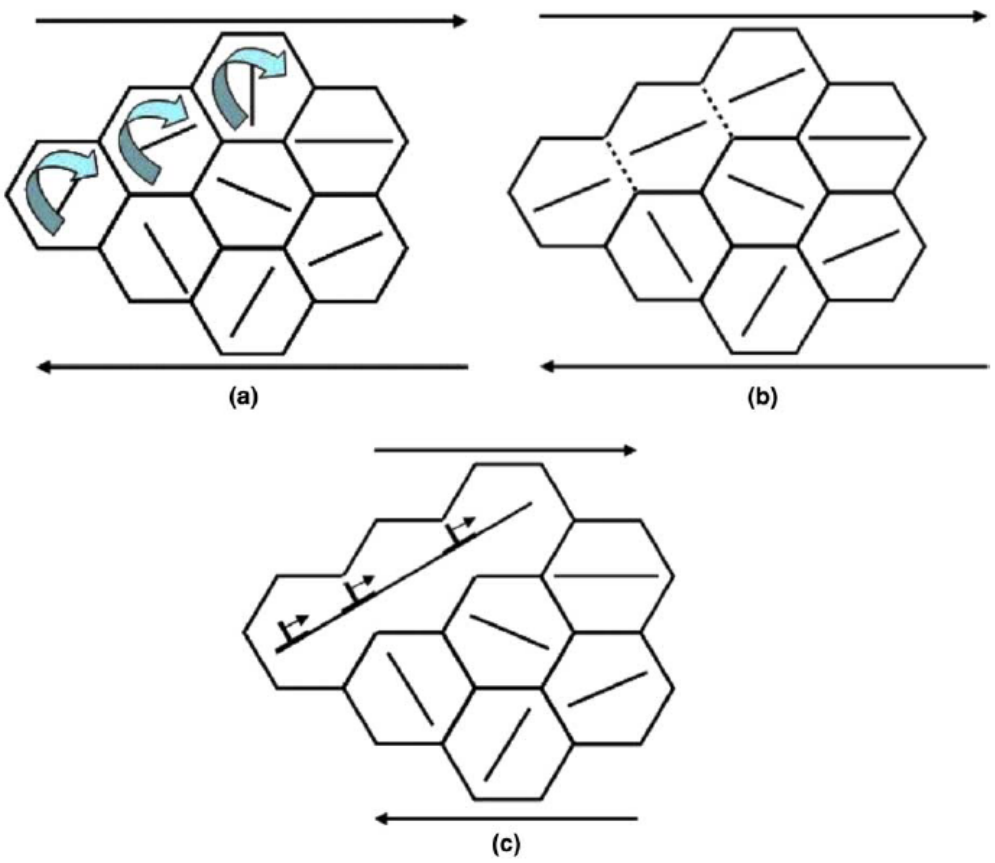

Fig 13. Rotation of neighboring nano grains during plastic deformation and creation of elongated grains by annihilation of grain boundary [45].

2.7.5.3 Grain boundaries as sources and sinks of dislocations

Molecular dynamics simulations helped a great deal in understanding the deformation mechanism in nanocrystalline materials. The deformation mechanisms operative mainly in the grain boundaries in nanostructured materials were realized by these simulations. Van Swygenhoven et al [56] with the aid of molecular dynamics simulations and Asaro and Suresh [57, 58] predicted that the defect (full dislocation/partial dislocation/stacking fault) generation mechanism is fundamentally different in nanocrystalline materials in comparison to their coarse grained counter parts. In nano sized grains, during plastic

deformation, the grain boundaries acts as the sources of dislocations. The generated dislocations sweep through the grains without any cross slip and get absorbed by the boundary on the other side of the grain. Hence there will not be any strain hardening in the material because of the low dislocation density and thereby absence of the dislocation pile ups. These processes are schematically shown in Figs 14 & 15.

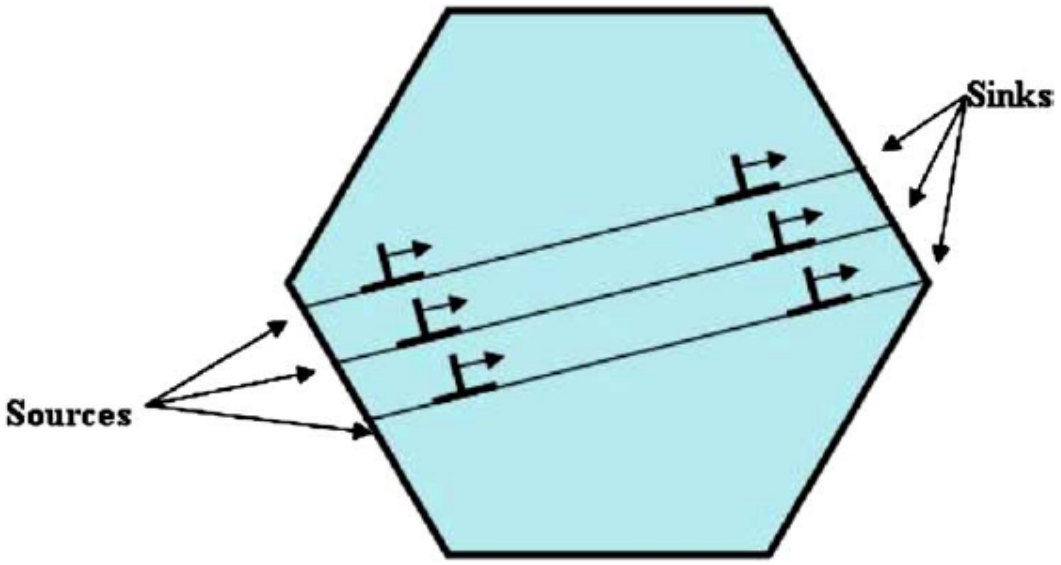

Fig 14. Schematic showing the grain boundaries as sources and sinks of dislocations in nanocrystalline materials [45].

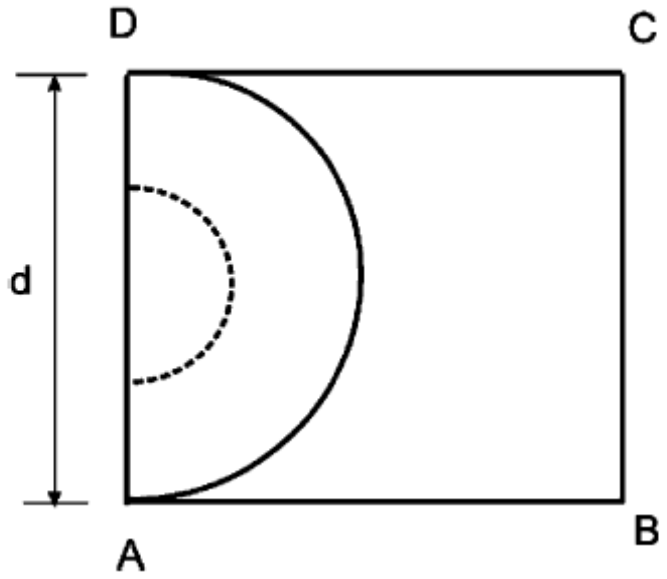

Fig 15. Perfect dislocation emitted from the grain boundary as a dislocation loop [45].

The above mentioned deformation mechanisms were experimentally observed/predicted using simulations in single phase nanomaterials. However, influence of a nano sized second phase on these mechanism is yet to be established.

2.8 Effect of alloying on the mechanical properties of nanomaterials

Improved mechanical properties in nanomaterials by refining the grain size was demonstrated in several single phase materials [45]. However, to date, very little attention was paid to the influence of alloying on the mechanical properties of single phase nanomaterials. Shen and Koch [59] observed solid solution hardening as well as softening in several nanocrystalline solid solutions made by ball milling. They concluded that the influence of alloying elements in nanocrystalline materials is different from that

of coarse grained materials. Both solid solution hardening and grain boundary hardening contributes to the strength of the nanocrystalline solid solutions. However the grain boundary hardening contributes more to the observed strength. Recently nanocrystalline Al-Mg alloy with ultrahigh strength and good ductility was synthesized [60] using in situ consolidation technique by ball milling.

Mechanical properties can also be enhanced via dispersion strengthening mechanism [61] by dispersing the second phase particles in a polycrystalline matrix. These second phase particles acts as the obstacles to the dislocation motion during plastic deformation. The size, volume fraction and distribution of these particles greatly influence the mechanical properties. In nano grained materials the presence of dislocations is doubtful. And it is predicted that plastic deformation occurs by fundamentally different mechanisms other than the traditional dislocation slip. Therefore it is intriguing to explore the new deformation mechanisms with real time experimental data. There are few reports on improvement of the mechanical properties in nanocrystalline multi phase materials made by controlled crystallization of amorphous materials [62]. However the governing deformation mechanisms are not well understood.

Despite all these, the still unanswered questions are:

1. Explanation for the softening at smaller grain sizes (i.e., inverse Hall-Petch effect)
2. Deformation mechanisms in these nanocrystalline materials in general.
3. Although the MD simulations offer some help in this area, the predictions still need to be verified by real time experimental data.

4. Deformation mechanisms in multi phase materials, to look for probable Orowan mechanism as it is the dominant deformation mechanism in multi phase coarse grained materials.

References:

1. R. Feynman, Engineering and Science- Caltech's issue of February 1960.
2. H. Gleiter, Prog. Mater. Sci., 33 (1989) 223.
3. H. Gleiter, Acta Mater., 48 (2000) 1.
4. G. Palumbo, S. J. Thorpe, K. T. Aust, *Scripta Metallurgica Et Materialia*, **24** (1990) 1347.
5. R. Birringer, H. Gleiter, H.P.Klein, and P. Marquardt, Phys. Lett. A., 102 (1984) 356.
6. C. C. Koch., Nanostruct. Mater., 2 (1993) 109.
7. R. O. Hughes, S. D. Smith, C. S. Pande, H. R. Johnson and R. W. Armstrong., Scripta Metall., 20 (1986) 93.
8. K. Lu, W. D. Wei and J. T. Wang, Scripta Metall. Mater., 24 (1995) 2319.
9. R. Z. Valiev, R. K. Islamgaliev and I. V. Alexandrov, Prog. Mater. Sci., 45 (2000) 103.
10. H. Wang, A. Sharma, A. Kvit, Q. Wei, X. Zhang, C.C.Koch and J. Narayan, Journal of. Mater. Res., 16 (2001) 2733
11. J. S. Benjamin, 234 (1976) 40.
12. B.S.Murty, S. Ranganathan, Int. Mater. Rev., 43 (1998)101.
13. C. Suryanarayana, Prog. Mater. Sci., 46 (2001) 1

14. H. J. Fecht, Nanostruct. Mater, 6 (1995) 33.
15. C.C.Koch, O. B. Cavin, C. G. McKamey and J. O. Scarbrough, Appl. Phys. Lett, 43 (1983) 1017.
16. C. Suryanarayana, Mechanical alloying and milling, CRC press publications (2004), ISBN: 082474103X.
17. H. Fecht in Nanostructured materials: Processing, Properties and Potential applications, edited by C. C.Koch (2002), Noyes publications, ISBN: 0815514514, p.73
18. G. Sakai, Z. Horita and T. G. Langdon, Mater. Sci. Engg, A393 (2005) 344.
19. V. A. Zhorin, D. P. Shashkin, N. S. Yenikoponyan, DAN SSSR 278 (1984) 144.
20. J. Bridgeman In : Processing of metals under high pressure conditions. Techizdat M, 1936, Moscow: P.230
21. N. A. Smirnova, V. I. Levit, V. I. Pilyugin, R. I. Kuznetsov, L. S. Davydova, V. A. Sazonova, Fiz Met Metalloved, 61 (1986) 1170.
22. N. A. Smirnova, V. I. Levit, V. I. Pilyugin, R. I. Kuznetsov, M. V. Degtyarov, Fiz Met Metalloved, 62 (1986) 566.
23. Zhilyaev AP, Oh-ishi K, Lagdon TG, McNelly TR, Mater Sci. Eng A 410-411 (205) 277.
24. Lee Z, Zhou F, Valiev RZ, Lavernia EJ, Nutt SR, Scripta mater, 51 (2004) 209.
25. J. Sort , A. Zhilyaev , M. Zielinska , J. Nogués , S. Suriñach , J. Thibault and M. D. Baró, Acta Materialia, 51 (2003) 6385.
26. R. Z. Valiev,R. S. Mishra, J. Grosa ,A. K. Mukherjee, Scripta Mater 34 (1996) 1443.

27. W. J. Botta Filho, J. B. Fogagnolo, C. A. D. Rodrigues, C. S. Kiminami, C. Bolfarini and A. R. Yavari, Mater. Sci. Engg A375-377 (2004) 936.
28. Ultra Fine grained Materials III, edited by Y. T. Zhu, T. G. Langdon, R. Z. Valiev, S. L. Semiatin, D. H. Shin and T.C.Lowe, TMS annual meeting, March 14-18, 2004, Charlotte, NC, USA.
29. Ultra Fine grained Materials IV, edited by Y. T. Zhu, T. G. Langdon, Z. Horita, M. J. Zahetbauer, S. L. Semiatin and T.C.Lowe, TMS annual meeting, March 12-16, 2006, San Antonio, TX, USA.
30. E. O. Hall, Proc. Roy. Soc., London, B64 (1951) 474.
31. N. J. Petch, J. Iron Steel Inst., 174 (1953) 25.
32. D. Tabor, JOM, 79 (1951) 465.
33. A. V. Sergueeva , V. Stolyarov, R. Z.Valiev, A. K. Mukherjee, Scripta Mater, 45 (2001)747.
34. Narayan J, Koch CC, Zhang X, and Venkatesan R. Unpublished results, 2000.
35. P.G. Sanders, J. A. Eastman, J. R. Weertman, Acta Mater, 45 (1997)4019.
36. J. B. Wachtman In: J.B.Wachtman, editor. Mechanical and thermal properties of ceramics. NBS Washington: NBS Special Publication; 1963. p. 139.
37. MacKenzie JK. Proc Phys Soc B 63 (1950) 2.
38. J. Youngdahl, P. G. Sanders, J. A. Eastman, J. R.Weertman, Scripta Mat 37 (1997)809.
39. C. C. Koch, D. G. Morris, K. Lu and A. Inoue, MRS Bulletin 24 (2): 54-58 Feb 1998

40. C. C. Koch, Journal of metastable and nanocrystalline materials: 2003: 18:9

41. Y. M. Wang, M. W. Chen, F. H. Zhou and E. Ma, Nature 419 (2002) 912.

42. X. Zhang, H. Wang, R. O. Scattergood, J. Narayan, C. C. Koch, A.V. Sergueeva and A. K. Mukherjee, Acta Mater 50 (2002) 4823.

43. Y. T. Zhu and X. Liao, Nature materials 3 (2004) 351.

44. G. E. Dieter, Mechanical metallurgy, 3rd edition, Boston: McGraw-Hill; 1986.

45. M. A. Meyers, A. Mishra and D. J. Benson, Prog. Mater. Sci, 51 (2006) 427.

46. F. A. Mohamed, Y. Li, MSE A, 298 (2001) 1.

47. P. G. Sanders, M. Rittner, E. Kiedaisch, J. R. Weertman, H. Kung and Y. C. Lu, Nanostuct. Mater. 9 (1997) 433.

48. B.Q.Han, Z. Zhang and E. J. Lavernia, Phil. Mag. Lett., 85 (2005)97.

49. R. S. Kottada and A. H. Chokshi, Scripta mater. 53 (2005) 887.

50. W. M. Yin, S. H. Whang, R. Mirshams, C. H. Xiao, Mater. Sci. Engg. A301 (2001) 18.

51. R. W. Hayes, V. Tellkamp, E. J.Lavernia, Jour. Mater. Res., 15 (2000) 2215.

52. D. L. Wang, Q. P. Kong, J. P. Shui, Scripta Metallurgica et Materialia, 31 (1994) 47.

53. H. Conrad, Met. Mater. Trans 35A (2004) 2541.

54. D. Jia, Y. M.Wang, K. T. Ramesh, E. Ma, Y. T. Zhu, R. Z. Valiev, Appl. Phys. Let., 79 (2001) 611.

55. D. Jia, K. T. Ramesh, E. Ma, Scripta Mater., 42 (2000) 73.

56. Van Swygenhoven H, Derlet PM, Hasnaoui A, Phys rev B 66 (2002) 024101.

57. Asaro RJ, Suresh S, Acta mater, 53(2005) 3369.

58. Asaro RJ, Krysl P, Kad B, Phil mag lett, 83(2003)733.

59. T. D. Shen and C. C. Koch, Acta mater, 44 (1996) 753.

60. K. M. Youssef, R. O. Scattergood, K. L. Murty, C. C. Koch, Scripta mater., 54 (2006) 251.

61. G. E. Dieter, Mechanical metallurgy, 3rd edition, Boston: McGraw-Hill; 1986. p.212.

62. J. Eckert in Nanostructured materials: Processing, Properties and Potential applications, edited by C. C.Koch (2002), Noyes publications, ISBN: 0815514514, p. 482

Chapter 3

Experimental Methods

3.1 Outline

- Materials used and their basic properties
- Processing parameters used during High energy ball milling
- Processing parameters used during warm compaction
- Processing parameters employed during High Pressure Torsion (HPT)
- Measuring grain size and lattice strain using X-ray peak broadening analysis
- Transmission electron microscopy with STEM-Z contrast imaging
- Hardness measurement using Vickers micro indentation
- Evaluation of time dependant mechanical properties using impression creep testing

3.2 Materials used and their basic properties

The starting materials are aluminum, tungsten and lead powders procured from Alfa Aesar with purity greater than 99.9 %. The fundamental properties of the materials used in the current investigation (Al, Pb and W) are given in Table 1. The aim of the current study was to investigate the effect of a nano scaled second phase (soft/hard) on the mechanical properties of nano scaled FCC matrix. Aluminum was chosen as the matrix material owing to its industrial importance. Pb was chosen as a soft phase which is of the similar crystal structure (FCC) where as W was chosen as the hard phase which is of different crystal structure (BCC). As the binary phase diagram of Al-Pb [Fig 1] suggests, both aluminum and lead are highly immiscible in each other under equilibrium

conditions. However, W forms some intermetallics with aluminum on the aluminum side under equilibrium conditions and the equilibrium phase diagram of Al-W is shown in the Fig 2.

Table 1 Fundamental properties of Al, W and Pb

Properties	Aluminum (Al)	Lead (Pb)	Tungsten (W)
Atomic Number (Z)	13	82	74
Mass Number (A)	27	207.21	183.84
Atomic radius (Å)	1.43	1.75	1.37
Crystal Structure	FCC	FCC	BCC
Melting Point (K)	933	600	3643
Density (gm/cc)	2.6999	11.34	19.3
Lattice Parameter (^{o}A)	4.0494	4.9506	3.1648
Hardness (MPa)	147	49	3038
Poisson's Ratio	0.33	0.42	0.28

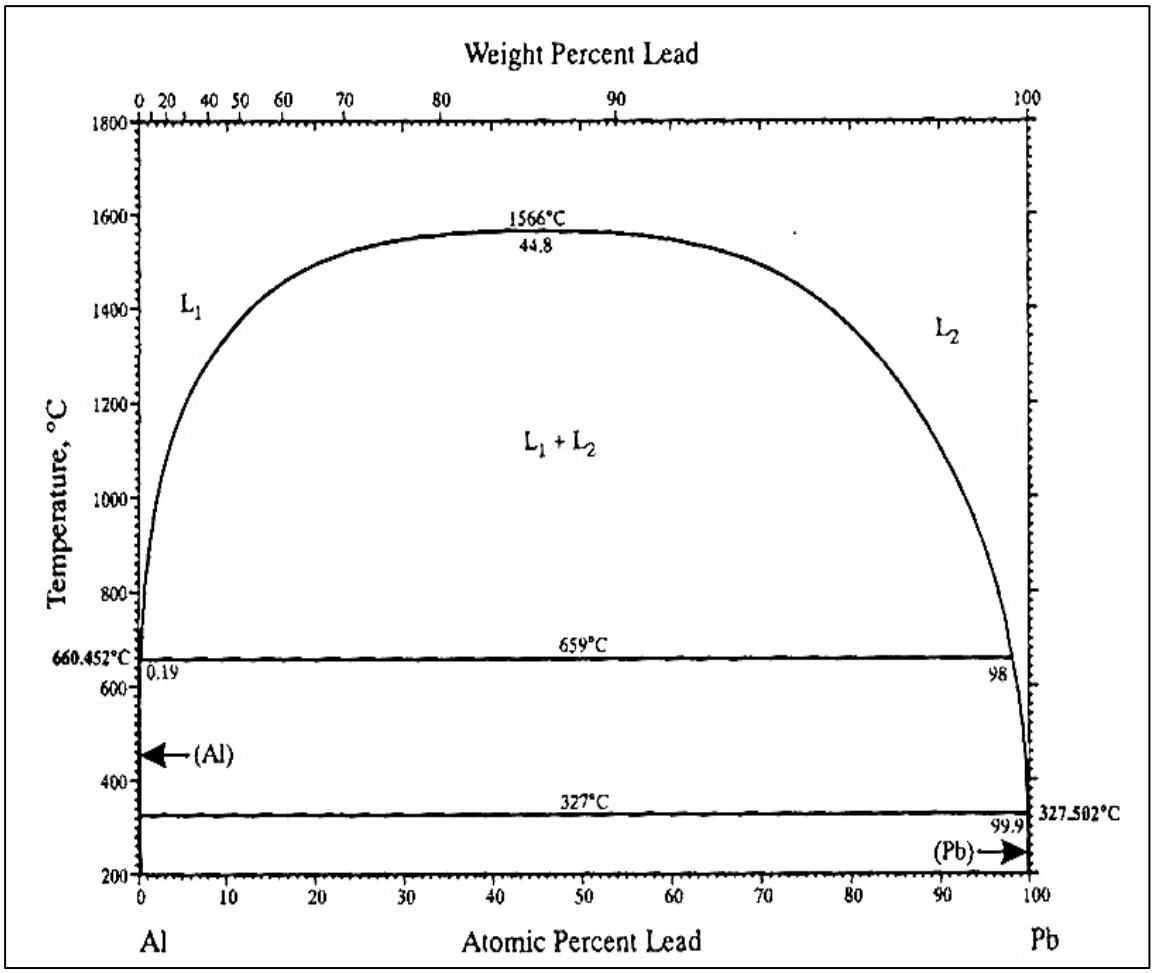

Fig 1 Binary alloy phase diagram of Al and Pb [taken from ref. 1]

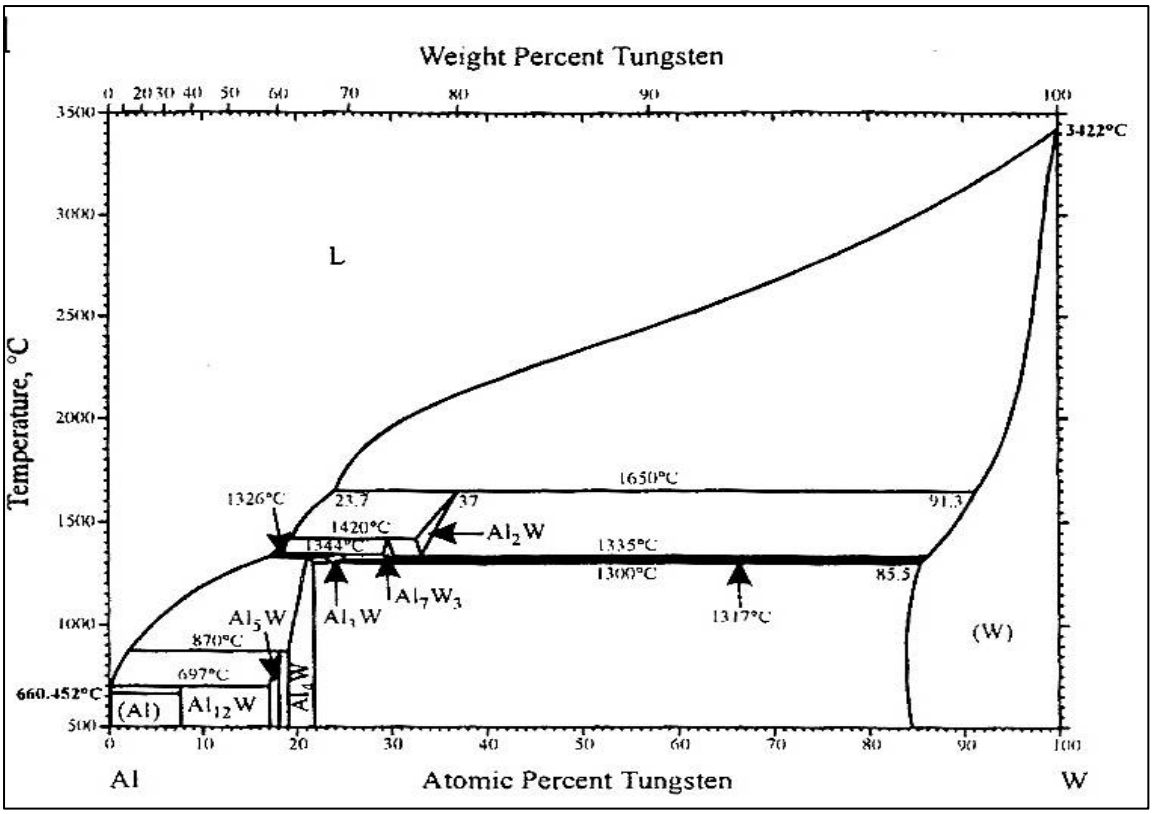

Fig 2 Binary alloy phase diagram of Al and W [taken from ref. 1].

3.3 Processing parameters during high energy ball milling

- SPEX 8000 Shaker mill.
- Hardened steel vial and martensitic steel (440C) balls of 6.4 mm and 7.9 mm diameter.
- Ball to Powder weight ratio (BPR): 5:1
- Surfactant used: Stearic acid ($CH_3(CH_2)_{16}COOH$)
- Temperatures used: 300 K and 77 K
- Atmosphere inside the vial: High purity argon (<3 ppm oxygen)

3.4 Processing parameters used during warm compaction

- Atmosphere: Argon
- Pressure: 1.8 G Pa
- Temperature: 573 K
- Holding time: 30 min
- Die set: tungsten carbide die set of 6.35 mm diameter

3.5 Processing parameters used during HPT

- Sample thickness: 0.8 mm
- Sample diameter: 10 mm
- Load: 2.5 G Pa
- Number of revolutions: 5
- Rotation speed: 1 revolution per minute
- Temperature: 300 K

3.6 X ray diffraction for structural characterization and grain size estimation

X ray diffraction is one of the most common and basic techniques that is used to characterize the solids to (a) determine their crystal structure, (b) measure the lattice constant, (c) identify the phases, (d) estimate the crystallite size and induced lattice strain and (e) detect the preferred orientation if there is any.

The working principle of this non destructive characterization technique is based on the well known Bragg's law:

$$n\lambda = 2d\sin(\theta) \tag{1}$$

Where λ = the wavelength of X-ray radiation, d is is is the interplanar spacing and θ is the angle.

A crystal lattice is a regular three-dimensional distribution of atoms in space. These are arranged so that they form a series of parallel planes separated from one another by a distance d (interplanar distance), which varies according to the nature of the material. For a given crystal, planes exist in a number of different orientations, each with its own specific d spacing. When a monochromatic X-ray beam with wavelength λ is projected onto a crystalline material at an angle theta, diffraction occurs only when the distance traveled by the rays reflected from successive planes differs by a complete number *n* of wavelengths or when it satisfies the Bragg condition [Fig 3]. For polycrystalline materials, the angle theta is varied to satisfy the Bragg condition for different d spacing.

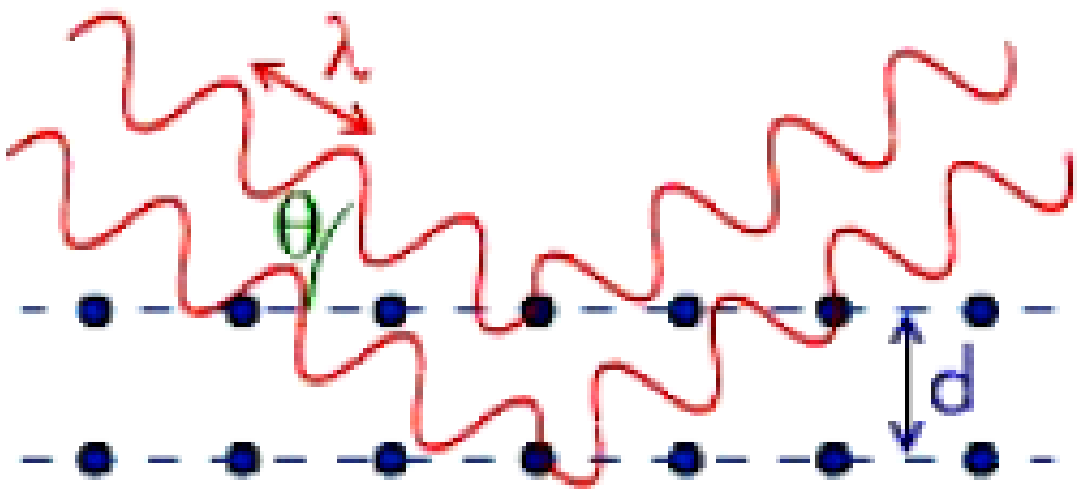

Fig 3. Schematic showing the interaction of X-rays with atoms in two different, parallel planes.

3.6.1 Methods to estimate the grain size and lattice strain

X ray diffraction peaks broaden when 1) the beam is not parallel and not monochromatic 2) the crystallite size is very small and 3) the material contains lattice defects, for example dislocations, stacking faults etc. The peak broadening from the instrument can be avoided / estimated by aligning the beam and using a standard large grained annealed (defect-free) sample. The broadening contributions from the small crystallite size and the strain coming from the defects can be estimated on the basis of different diffraction order dependence of peak broadening. Two classical methods have been developed over the last five decades: the Williamson-Hall [2] and the Warren-Averbach [3-4]. Later these two methods were modified to estimate the grain size and to convert the strain into the defect density [5]. The most widely used methods to estimate the grain size and lattice strain in nano grained materials are described below.

3.6.1.1 Scherrer method [6]

This is the simplest and well known equation that is being used to readily estimate the grain size of nanocrystalline materials.

$$t = K\lambda/(B\cos\theta) \quad (2)$$

Where t is the volume averaged dimension of the crystallites, K is Scherrer constant, often assumes values of either 0.9 or 1.0; λ is the wavelength of the x ray radiation, B is the full width half maximum (FWHM-2θ) converted to radians, θ is the position of peak maximum. This Scherrer analysis of estimating the grain size often suffers from a limitation in separating the contribution of lattice strain to the peak broadening.

3.6.1.2 Williamson-Hall Method [2]:

Using this method, one can estimate the grain size and separate the lattice strain as well. This approach assumes that

$$\beta\ (\text{sample}) = \beta\ (\text{size}) + \beta\ (\text{strain})$$

$$\beta = \lambda/D\cos\theta + 4\varepsilon\tan\theta$$

$$\beta\cos\theta = \lambda/D + 4\varepsilon\sin\theta$$

Here β is the integral breadth of the peak (or in other words FWHM). By plotting broadening ($\beta\cos\theta/\lambda$) on Y axis versus the scattering vector ($\sin\theta/\lambda$) on X axis, the

grain size and lattice strain can be measured. The slope of the linear fit gives the strain and inverse of the y-intercept yields the grain size.

3.6.1.3 Warren-Averbach Method [3]:

This method requires more rigorous approach than the earlier two methods. In this, instead of the breadth of the diffraction peak, knowledge about the shapes of the peaks is required. Here the peak profile is described by a Fourier series. The cosine Fourier coefficients are used for further analysis. The peak shape of a standard sample with no broadening will be used to deconvolute the instrumental and sample broadening effects. Atleast two reflections are needed to perform this analysis. In practice, two orders of one reflection can't be obtained. Hence only cubic crystals can be analyzed using this method. The grain size distribution can also be estimated in addition to the length averaged grain size using this analysis. In this method, instrumental broadening and sample broadening can be separated more precisely.

While characterizing the nanomaterials for grain size, transmission electron microscopy is always performed in conjunction with non-destructive and readily available X-ray diffraction.

3.7 Transmission Electron Microscopy for structural characterization

The properties of materials are dependant on their microstructural features and the chemistry. Hence while establishing the structure-property correlations; one should characterize the structure and composition to the highest accuracy possible. This characterization often involves the use of sophisticated methods of analysis with the aid of microscopy, diffraction and spectroscopy.

Light microscopy serves the purpose to image the structural features of the materials in the micro regime. However in order to reveal the finer features down to the atomic scale, electron microscopy is needed where an electron beam of much lower wavelength (0.00251 nm) in comparison to light (λ=0.4-0.75 nm) and X-rays (e.g., Cu K_{α}, λ=0.1541 nm) is used. Louis de Broglie (1925) was the first who postulated that an electron can behave both as a particle and a wave and this concept of wave particle duality of an electron is an important concept of the quantum mechanics. This concept is exploited in electron microscopy where the small wavelengths associated with the electron can be used to view the objects much smaller than can be resolved using visible light. Today, since a major fraction of the materials research deals with nanotechnology and low dimensional materials, electron microscopy is often required and has become an integral part of materials characterization.

3.7.1 Interaction of electrons with matter

When an energetic electron beam is incident on the specimen, several processes occur as shown in the Fig 4. There will be production of X-rays, backscattered electrons,

secondary electrons, Auger electrons etc. In addition, some part of the beam gets transmitted and the remaining part gets scattered elastically as well as inelastically. A fraction of the beam gets absorbed by the material too depending on the absorption characteristics of the material under investigation.

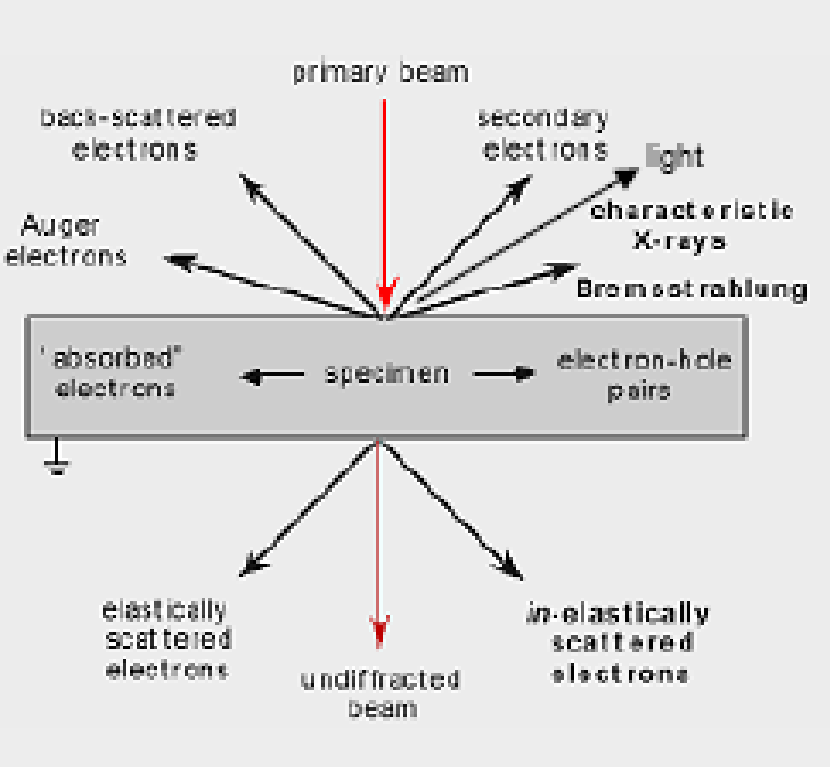

Fig 4. Schematic showing the different processes that occur when an electron beam interacts with a specimen.

Electron microscopes are basically of two types; 1) Scanning electron microscope (SEM) and 2) Transmission electron microscope. The working principle of SEM assumes that an electron is a particle while that of TEM assumes an electron both as a particle (scattering) and a wave (diffraction).

The different operating modes available in TEM are:

a) TEM mode and b) Scanning Transmission Electron Microscopy (STEM) mode.

3.7.2 Resolution and Rayleigh criterion [7]

Resolution (or resolving power) is defined as the closest spacing of two points which can be resolved by the microscope to be separate entities. The smallest distance between two points that human eyes can resolve is 0.1-0.2 mm. The different resolution limits of various characterization techniques are shown in Table 2. According to the Rayleigh criterion, the resolution is directly proportional to the wavelength of the radiation used. In other words, to achieve the best resolutions, radiations of shorter wavelengths are needed.

$$R = \frac{1.22\lambda}{2n \sin \alpha}$$

Where R=resolving power

λ= wavelength

n = refractive index of the viewing medium

α = semi angle of collection of the magnifying lens

n sin α is often called the numerical aperture.

Table 2. Resolution limits of different characterization techniques [taken from [7]].

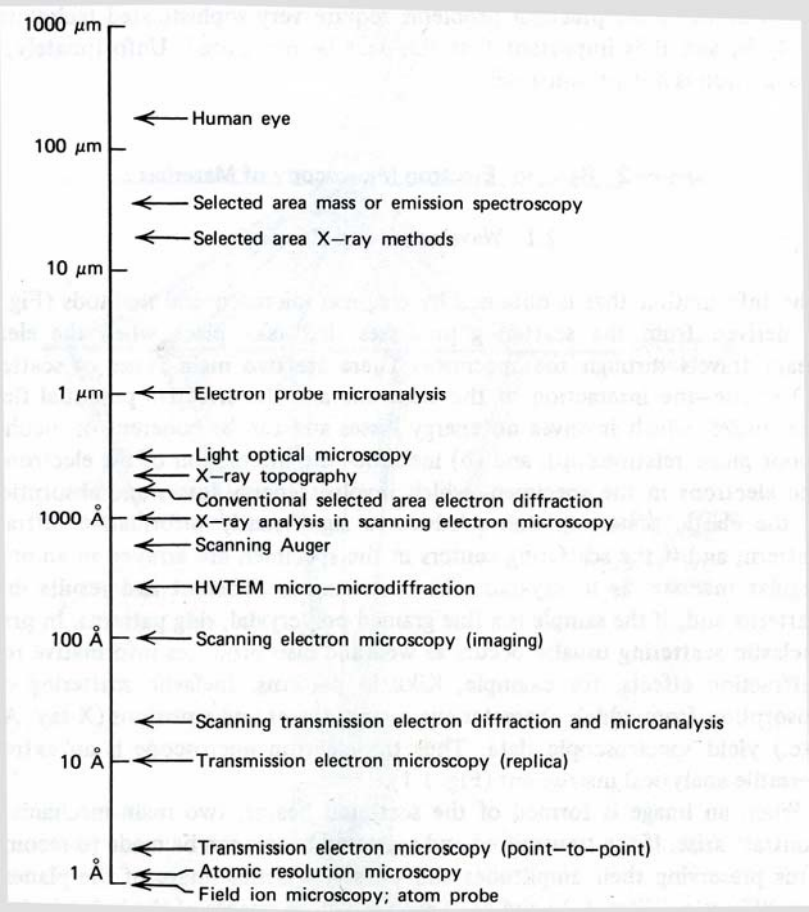

3.7.3 Imaging [8]

Contrast is defined as the intensity difference between two adjacent regions:

$$C = (I_2 - I_1)/I_1$$

As the electron wave traverses through the specimen, it can change both its amplitude and phase because of the scattering. These changes give rise to image contrast (amplitude contrast + phase contrast). Again, the amplitude contrast involves two major types, a) mass thickness contrast and b) diffraction contrast.

In TEM, the uniform electron intensity in the incident beam is transformed into a non uniform intensity after scattering by the specimen. When this variable electron intensity

hits the viewing screen or electron detector, one can see the regions of different contrast on the viewing screen. These regions of variable contrast are also observed in the diffraction pattern as the intensity of the direct beam (or Zero beam) and diffracted beam will be different.

Bright filed (BF) and dark field (DF) are the two basic ways of forming amplitude contrast images and they are complementary to each other. In order to translate the electron scatter into interpretable amplitude contrast we select either the direct beam or some of the diffracted beams (using the objective aperture) in the selected area diffraction (SAD) patterns to form bright filed (BF) or dark field (DF) images respectively. In scanning transmission electron microscope (STEM) mode, selection of direct or diffracted beams is done using detectors in stead of apertures.

3.7.4 Mass thickness contrast

The thinning process does not yield electron transparent regions of uniform thickness in the majority of the cases. Therefore these variations in mass and thickness result in mass thickness contrast.

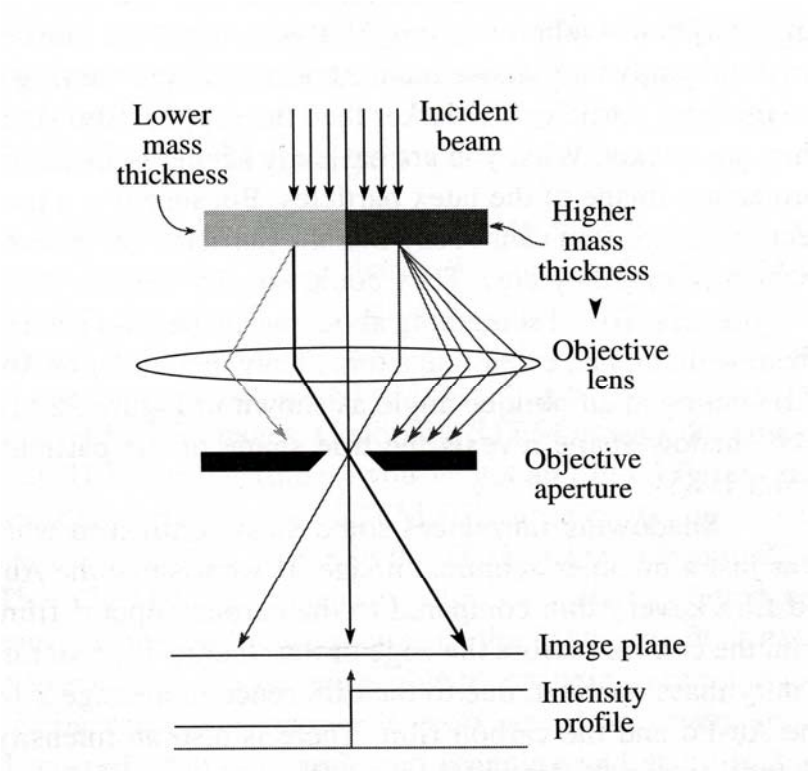

Fig 5. Schematic showing the working principle of mass thickness contrast [taken from ref. 8].

The cross section for elastic scattering is a function of Z (atomic number). As the thickness of the specimen increases, there will be more elastic scattering because the mean free path remains fixed. Therefore, high Z (i.e., high mass) regions of a specimen scatter more electrons than low Z regions of the same thickness. Similarly, thicker regions will scatter more electrons than thinner regions of the same average Z, all other factors being constant. Hence, in many a times, mass thickness contrast images are interpreted qualitatively. In BF image mode, thicker and/or higher mass areas appear darker than thinner and/or lower mass areas [Fig 5]. The reverse is true for the case of DF image mode.

3.7.5 Theory of diffraction contrast

Diffraction contrast is simply a special from of amplitude contrast because the scattering occurs at special Bragg angles. Incoherent elastic scattering produces mass-thickness contrast whereas coherent elastic scattering produces diffraction contrast. The contrast in BF and DF images is usually the diffraction contrast and it represents the variations in the intensities of diffraction across the sample.

The Laue condition is written as

$$\Delta \mathbf{k} = \mathbf{g}\text{-}\mathbf{s}$$

Where g is a reciprocal lattice vector of the crystal, s is the deviation parameter; and Δk is adjustable by tilting. Diffraction contrast and appearance of features in BF and DF images depend sensitively on how the Laue condition is satisfied. In other words, it depends on the active diffraction and the value of the deviation parameter, s.

To get good strong diffraction contrast in both BF and DF images, the specimen is tilted in order to produce a two beam condition in which only one diffracted beam (hkl) is strong. The direct beam (000) is the other strong spot in the diffraction pattern. The electrons in the strongly excited hkl beam have been diffracted by a specific set of hkl planes and so the area that appears bright in the DF image is the area where the hkl planes are at Bragg condition. Hence the DF image contains specific orientation information. In order to make certain diffraction spot/ring strong, the specimen can be tilted. While imaging, either the strong diffracted beam can be centered by making it zero beam (on-axis) or the objective aperture can be centered on the strong beam (off-axis).

3.7.6 High Resolution imaging (phase contrast imaging) in TEM

High-Resolution TEM (HRTEM) is the ultimate tool in imaging the lattice defects down to the atomic scale. The HRTEM image is a two-dimensional projection of the crystal with defects and all. The basic principle of HRTEM is as follows:

Consider a very thin slice of crystal that has been tilted so that a low-index direction is exactly perpendicular to the electron beam (or in other words in zone). All lattice planes about parallel to the electron beam will be close enough to the Bragg position and will diffract the primary beam. The diffraction pattern is the Fourier transform of the periodic potential for the electrons in two dimensions. In the objective lens all diffracted beams and the primary beam are brought together again; their interference provides a back-transformation and leads to an enlarged picture of the periodic potential. This picture is magnified by the following electron-optical system and finally projected on a screen at magnifications of typically 10^6. The images formed in HRTEM are due to differences in the phase of electron waves scattered through a thin specimen.

3.7.7 STEM mode and Z contrast imaging

An electron penetrating into the electron cloud of an atom is attracted by the positive potential of the nucleus (Coulombic interaction), and its path is changed as a result. The closer the electron comes to the nucleus, the higher is the force and consequently the scattering angle. In some cases, even complete backscattering can occur (back scattered electrons). These interactions can be treated as elastic, which means that no energy is

transferred from the scattered electron to the atom. The interaction of electrons with heavy atoms is stronger than with light atoms so that areas in which heavy atoms are localized appear with darker contrast than such with light atoms (mass contrast). In thick areas, more electrons are scattered of course; these areas appear dark (thickness contrast). In particular, the mass-thickness contrast is important in bright and dark field imaging.

The strong Coulomb interaction of the electrons with the potential of atom core, which leads to high angle scattering (designated as Rutherford scattering), is employed by Z-contrast imaging in STEM. By this method, small clusters (or even single atoms) of heavy atoms can be imaged in a matrix of light atoms since the contrast is proportional to Z^2 (Z: atomic number). Like TEM, the STEM system can also be used for both dark field imaging and bright field imaging.

In TEM mode, DF images are usually formed by permitting only a fraction of the scattered electrons to enter the objective aperture. But in STEM mode, the microscope is operated in similar fashion to a scanning electron microscope (SEM). A fine, highly focused beam of electrons [Fig 6] is scanned over a thin specimen (~100 nm). In STEM mode, images are formed by collecting most of the scattered electrons on the annual dark field detector (ADF). Since the STEM mode involves detectors unlike lenses in TEM mode, the STEM images are free from aberrations.. STEM offers unique imaging modes and enhanced microanalysis capabilities.

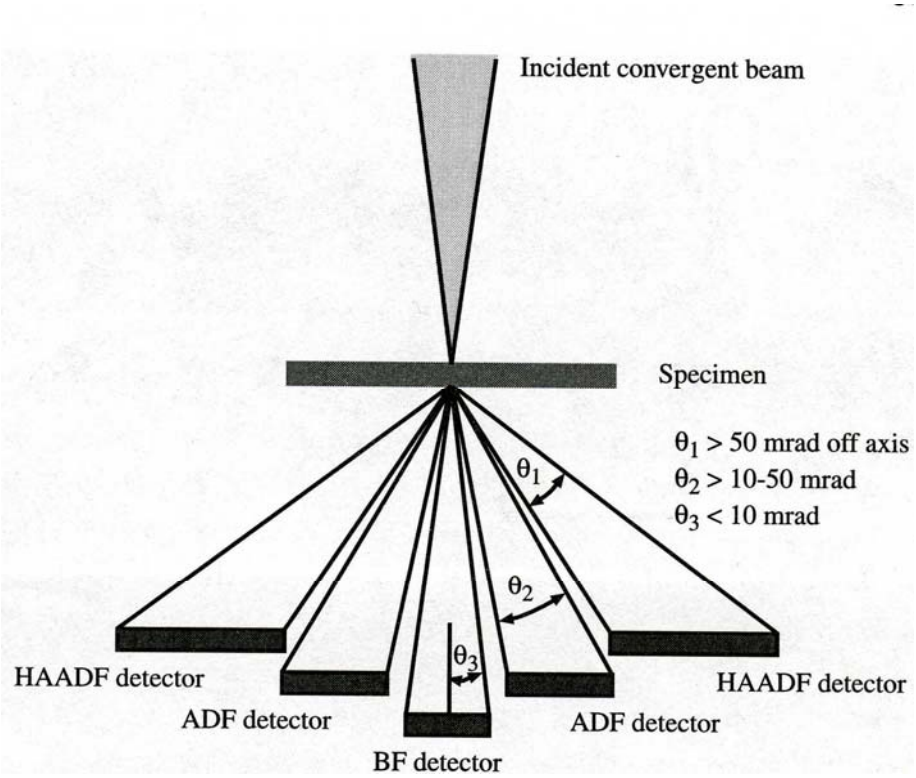

Fig 6. Schematic showing the working principle of Z contrast (STEM mode) [taken from ref. 8]

3.7.8 Limitations of a TEM

There are some limitations to the TEM. They are

1. Sampling

   The information that is obtained using TEM is from a small electron transparent region of a bulk sample. Depending on the processing history of the sample, the data obtained may or may not be the representative microstructure of the whole sample.

2. Interpretation of images:

   Interpretation of TEM images is not a trivial practice. Hence one should be careful while interpreting them. If needed, taking an expert's opinion is highly recommended.

In some cases such as HRTEM, simultaneous simulation work is needed to interpret the images which involve additional work.

3. Electron beam damage:

Because of the impingement of a high energy electron beam on a very small region of the sample, there is a danger of local microstructural changes that may occur or the sample itself may get destroyed. Hence the current day instruments are equipped with cooling stages around the specimen area.

4. Specimen preparation

Getting an electron transparent region in a bulk sample is a tedious, destructive and time consuming practice. However one has to go through the regular practice to get a thinner region (electron transparent).

In the current study, the microscopes used were TOPCON 002B EM and JEOL 2010F with a point to point resolution of 0.16 nm. These two instruments were operated at 200 kV.

3.8 Vickers microhardness [9]

Microhardness is one of the readily available and most used techniques to characterize the mechanical properties of nanostructured materials and most notably Vickers microhardness. The schematic of the Vickers micro indenter is shown in the above Fig 7. The indenter is of pyramid shape with a square base. The included angle between opposite faces of the pyramid is 136^0.

A predetermined load based on the material and its thickness is applied for certain amount of time. After releasing the load, the diagonals (d_1, d_2) of the square shaped impression are measured with the aid of a microscope attached to the instrument.

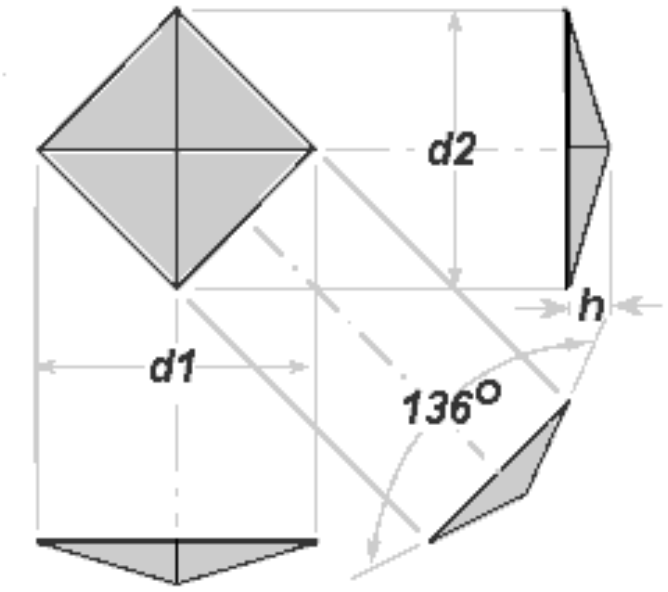

Fig 7. Schematic showing the two diagonals (d_1, d_2) of the square impression formed using the diamond indenter. The angle between the opposite faces of a diamond is 136^0 [taken from ref. 10].

The Vickers microhardness, H_v (in MPa) is evaluated using the following formula:

$$H_v = 1.854 * P/d^2$$

Where P = Load applied during the test in SI units

$d = (d_1+d_2)/2$ in SI units

In the current study, the instrument that was used was a Buehler Micromet microhardness tester with a diamond indenter.

3.9 Impression creep testing

Conventional creep testing is a time consuming process and requires large sample sizes. Processing techniques that are established to date to synthesize nanostructured materials often yield samples in very limited quantities and conventional mechanical testing is not feasible. Hence in order to study the mechanical properties of nanostructured materials, several small specimen testing techniques [11-12] have been developed including miniaturized tensile testing [13]. Therefore, on the similar lines, this indentation (impression) creep test is a potential and attractive method to evaluate the time dependant deformation characteristics of these nanostructured materials where the material availability is scarce.

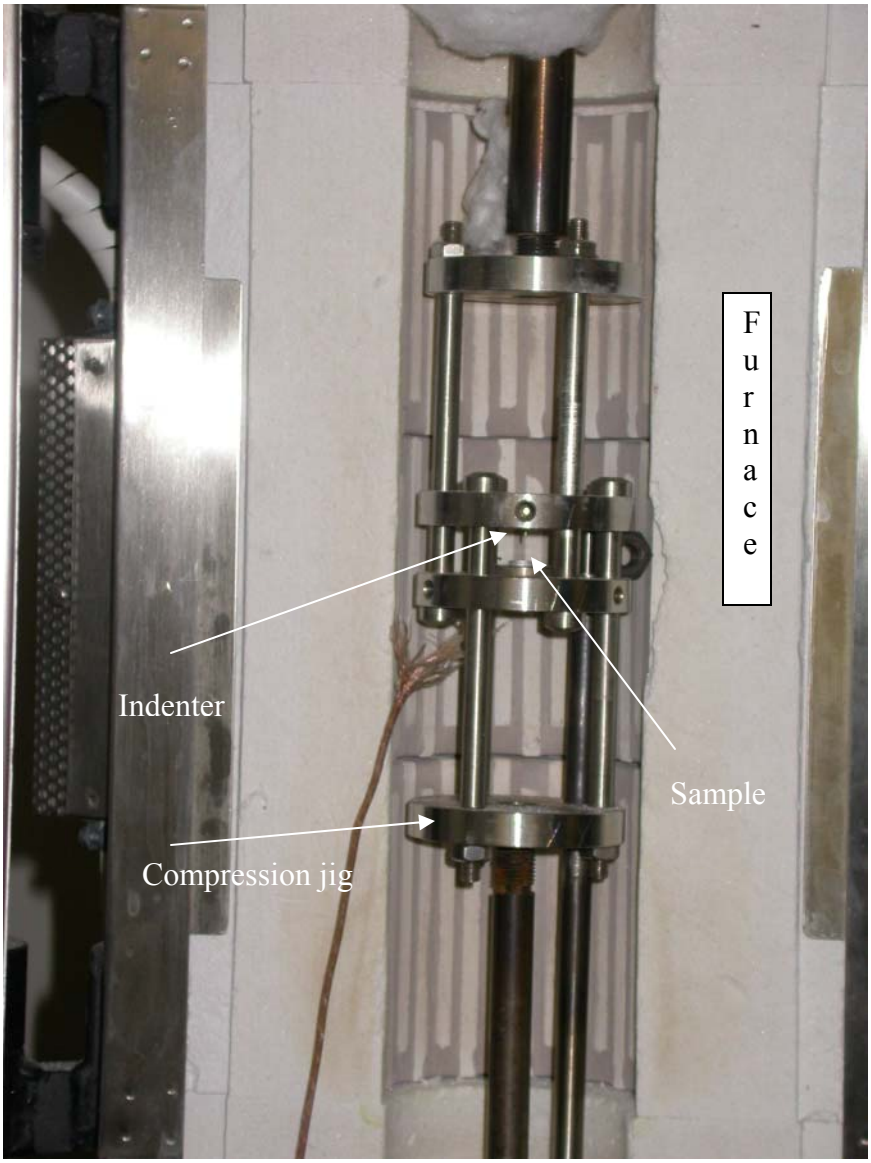

Fig 8 Impression creep testing setup used in the current study.

Several researchers have performed indentation creep tests with indenters of different shapes, namely pyramidal, conical and spherical [14]. But none of these indentation creep tests show the attainment of steady state creep. However, indentation tests with a flat cylindrical indenter do show the steady state at a constant load. The setup of impression

creep testing used in the current study is shown Fig 8. This technique was first developed and used by Chu and Li in 1977 [15]. This technique has been used to evaluate the creep properties of several metals [16], alloys [17], glasses [18], ceramics [19], ionic crystals [20], polymers [21] and thin films [22]. This technique was also used to study the superplasticity [23], stress relaxation [24] and impression fatigue [25].

In the previous studies, both the stress exponent and the activation energy values evaluated using this method agreed well with the results from the conventional compression tests using bulk specimens. When compared with the conventional tests, the punching stress must be divided by 3.3 to change to the compressive stress and the impression velocity must be divided by the punch diameter to convert to compressive strain rate.

References

1. Phase diagrams for binary alloys, edited by Hiroaki Okamoto (2000), ISBN 0871706822.
2. G. K. Williamson, W. H. Hall, Acta Metall., 1 (1953) 22.
3. B. E. Warren, B. L. Averbach, J. Appl Phys, 21 (1950) 595.
4. B. E. Warren, Prog. Met. Phys, 8 (1959) 147.
5. T. Ungar, J. Gubicza, G. Ribarik, A. Borbely, Appl Cryst., 34 (2001) 298.
6. Elements of X ray diffraction by B.D. Cullity (1978), 3rd edition,Addison-Wesley series.
7. Transmission electron microscopy of materials by G. Thomas and M. J. Goringe (1979), ISBN 1878907158

8. Transmission electron microscopy: A text book for materials science, 4 vol. set (1996) by D. B. Williams and C. B. Carter, ISBN 030645324X.
9. Mechanical Metallurgy by G. E. Dieter, 3rd edition (1986), ISBN 0071004068.
10. http://www.gordonengland.co.uk/hardness/microhardness.htm.
11. T. R. Malow and C. C. Koch, Acta Mater, 46 (1998) 6459.
12. T. R. Malow, C. C. Koch, P. Q. Miraglia, K. L.Murty, Mater Sci Eng, A 252 (1998) 36.
13. X. Zhang, H. Wang, C. C. Koch, Rev. Adv. Mat. Sci, 6 (2004) 53.
14. J.C.M Li, Mater. Sci Engg, A 322 (2002) 23.
15. S. N. G. Chu, J. C. M. Li, J. Mater. Sci., 12 (1977) 2200.
16. P. S. Godavarti and K. L. Murty, J. Mat. Sci. Lett., 6 (1987) 456.
17. M. Yamaguchi, Y. Umakoshi, T. Yamane, Trans. Iron Steel Inst. Japan, 25 (1985) B367.
18. N. Q. Chinh, P. Tasnadi, A. Juhasz, P. Szommer, E. Szep-Kiss, I. Kovacs, Key Engg Mater.,97-98 (1994) 159.
19. J. J. Petrovic, M. I. Pena, I. E. Reimanis, M. S. Sandlin, S. D. Conzone, H. H. Kung, D. P. Butt, J. Amer. Cera. Soc., 80 (1997) 3070.
20. Y. I. Golovin, A. I. Tyurin, Phys. Sol. Stat., 38 (1996) 1000.
21. D. Y. Chiang, J. C. M. Li, Ploymer, 35 (1994) 4103.
22. D. M. Shinozaki, Y. Lu, J. Electronic mater., 26 (1997) 852.
23. P. Tasnadi, A. Juhasz, N. Q. Chinh, I. Kovacs, Res. Mechan. 24 (1998) 335.
24. P. L. Larsson, S. Carlsson, Ploym. Test, 17 (1998) 49.
25. J. C. M. Li, S. N. G. Chu, Scr. Met. 13 (1979) 1021.

Chapter 4

Microstructure and microhardness of ball milled and high pressure torsioned bulk nanostructured aluminum

4.1 Introduction

Processing of fully dense nanostructured metals and alloys and establishing their structure-property correlation has been the focus of interest among the research community in the recent years [1]. Studying the mechanical behavior of these novel materials vis-à-vis their microstructure is the subject of widespread research and in the recent past, there have been several review articles, summarizing the unique deformation mechanisms observed/predicted at the nano scale [2-6]. Often the experimental studies have been hampered by the lack of theoretically dense samples to evaluate the meaningful/reasonable mechanical properties and thereby making the identification of the associated inherent deformation mechanisms difficult. Hence there is a pressing need to synthesize fully dense nanocrystalline materials. Several processing procedures were employed to produce bulk ultra fine grained/nanostructured materials; These procedures can broadly be classified into two categories; a) starting from the coarse grained bulk materials and then refining the microstructural features using high shear strains by subjecting them to equal channel angular pressing (ECAP) [7-10], high pressure torsion (HPT) [11-13] etc. Many times this has resulted in ultra fine grained structures instead of nanostructures in several metals and alloys ; b) obtaining the nano scaled microstructures either by mechanical milling of elemental powders or inert gas condensation of vapors and subsequently consolidating them into bulk solids. The methods involved in the later approach results in nanostructures but compacting them to their theoretical densities with

good inter particle bonding and simultaneous retaining the original nanostructure has been a grand challenge. There are very few reports, highlighting the efforts on synthesizing bulk nc aluminum via several routes [14-16]. However, Owing to the technological importance, synthesizing nanocrystalline aluminum and its alloys with high end mechanical properties is highly demanding and thereby is the continued focus of the intensive research studies.

4.2 Experimental

Coarse grained Al powders (-325 mesh) with a purity of 99.97 % were procured from Alfa-Aesar. The powders were loaded into a tool steel vial in a glove box under a high purity argon atmosphere (<3ppm oxygen). Martensitic stainless steel balls (440C) were used as milling media with a Spex 8000 shaker mill. Initially Al was milled for several durations up to a maximum of 25 h at room temperature. In order to avoid the cold welding of powders, stearic acid (1.5 wt %) was used as a surfactant. The resultant powders were consolidated into 6.35 mm diameter disks at 300 K and 573 K using a compressive load of 1.8 GPa under an argon atmosphere. The density of all the samples was measured using the Archimedes principle method. The hardness measurements were taken using a Buehler Micromet microhardness tester at 100 gm load. Before taking the hardness readings, samples were metallographically polished to a mirror-like surface. In this case, the value of each datum point is the average of 10 readings taken at various points over the surface of the sample. The as milled powders were compacted at room temperature into pellets of 10 mm diameter. These samples were subjected to high pressure torsion at room temperature at Kyushu University, Japan. The HPT parameters were 2.5 GPa load, 5 revolutions and 1 revolution per minute. The microhardness

measurements of the HPT samples were done at a load of 20 gm. XRD experiments were carried out, to estimate the grain size and lattice strain of the milled samples, using a Rigaku Geigerflex diffractometer with CuK_α radiation (λ = 0.1541 nm). In order to estimate the grain size and lattice strain of HPT samples at various positions along the diameter, XRD experiments were performed using a 4 circle Bruker AXS D-5000 diffractometer with a CuK_α radiation. The grain size was computed using the Scherrer equation [17] from broadened X-ray line spectra after accounting for instrumental broadening. The lattice strain was determined using Stokes-Wilson formula. Samples for transmission electron microscopy studies were electrolytically thinned with 20% perchloric acid and 80% methanol at 243 K using a Fischione twin jet electropolisher and observed in JEOL 2010F TEM operated at 200 kV.

4.3 Results and discussion

Fig 1 shows the crystallite size and lattice strain accumulated/induced in aluminum during mechanical milling. The crystallite size decreased with the increase in milling time to a minimum of 23 nm. The lattice strain increased during the initial stages of milling, suggesting the creation of defects like dislocations, stacking faults etc. On prolonged milling, the lattice strain decreased continuously to 0.15 %. This could be because of the dynamic recovery processes that might have taken place during milling and thereby reducing the defect densities. These crystallite size and lattice strain values were in good agreement with the values reported in the literature for the nc aluminum synthesized by ball milling [15-16].

The compaction of as milled aluminum powders at room temperature yielded a density of 97 % whereas the consolidation at 573 K resulted in a density value of 98.5 % of its bulk value. In an effort to produce, fully dense bulk nc aluminum, the as milled powders were compacted at room temperature in 10 mm diameter WC die to a thickness of 0.8 mm and then subjected to high pressure torsion at room temperature using a pressure of 2.5 GPa and five revolutions. The rotation speed of the lower anvil is one revolution per minute. The density measurements, made on the samples after HPT using Archimedes principle method, resulted in 100% of their bulk value.

High pressure torsion is an established and a potential process to produce bulk ultra fine grained/nanostructured materials and is well described in the literature [7]. A thin disc shaped specimen is deformed by simple shear under heavy compressive loads. The sample is pressed with the upper anvil and the lower anvil is simultaneously rotated. The sample dimensions remain unchanged under ideal processing conditions. The amount of load and the number of revolutions can be varied as per the requirements and those parameters are dictated by the material under study. The bulk sample obtained after high pressure torsion is shown in Fig 2.The high pressure torsion which involves high loads as well as large amount of strains could have resulted in heavy shearing among the powder particles leading to the improved mechanical interlocking among the particles. Prior to this, cryomilled nc Al-7.5%Mg alloy [18-22] was successfully consolidated to its theoretical density using high pressure torsion.

In the earlier studies, high pressure torsion was used as a technique to refine the microstructure of the coarse grained bulk materials, whereas in the current investigation it

is used as one of the processing steps to consolidate the ball milled powder materials. The X ray diffraction studies were carried out on the as milled and high pressure torsioned materials and the corresponding diffractograms were shown in Fig 3. The grain size computed from the Scherrer equation yielded a value of 23 nm in the milled condition and it remained the same even after subjecting to extensive plastic deformation during HPT. The constancy of grain size even after extensive plastic deformation by HPT suggests that there were not notable microstructural changes in HPT. The lattice constants calculated from the Nelson-Riley extrapolation function are 4.0465 Å and 4.0443 Å in as milled and HPTed conditions respectively. The standard lattice constant for aluminum is 4.0495 Å.

The HPT samples were metallographically polished to mirror like surface and then hardness measurements were taken at several positions (the spacing between these positions is 1 mm) of the sample along several diameters (angled at 45^0 to each other). Each datum point is the average of atleast 5 data points taken from the vicinity of the respective positions. In total, 5 samples were tested and the microhardness data presented here is the representative of 5 samples. These hardness studies are summarized in Fig 4. The hardness values measured during different stages of compaction were also shown for comparison. The commercial purity aluminum in annealed condition possesses a hardness of 210 MPa [23]. The ball milled and cold compacted sample has a hardness of 885 MPa and the hot compacted sample has 925 MPa. The microhardness values after HPT increases to 970 MPa in the center and 1200 MPa in the edge region. This is because of the larger strains in the edge region that were imposed during HPT might have resulted in the increase in defect densities. In the end, the microhardness was enhanced

by nearly 6 times in comparison to the coarse grained aluminum. This trend is consistent with the microhardness values on different metals and alloys reported in the literature that are synthesized by high pressure torsion [24].

In an effort to investigate the microstructural uniformity of the HPT samples, micro XRD experiments were performed by collimating the X-ray beam to a diameter of 0.8 mm and then directing it to different positions along the diameter of the disk sample. The obtained X-ray diffraction data were analyzed. The results were a uniform grain size of 23 nm throughout the sample. However, the lattice strain is low in the central region and it increased as we move towards the circumference [Fig 5]. This trend in lattice strain mirrors that of microhardness [Fig 4], suggesting that the increase in hardness is because of the rise in internal stresses as one moves towards the edge.

The HPTed samples were further characterized by TEM and the corresponding data is shown in Figs 6 (a), 6 (b) & 7. In the central region (Figs 6 (a) & 6 (b)), the mean grain size computed from 320 grains yielded a value of 30 nm (based on number fraction). The calculations performed based on volume fraction resulted in a mean grain size of 58 nm. In the edge region (Fig 7), there exist regions where several smaller grains are clustering. This is because of the very large strains imposed in this region during HPT. However several grains that are in the range of 20-30 nm can be seen. Hence it appears that the grain size is nearly uniform through out the sample. The shear strain induced during HPT processing is directly related to the radius of the sample i.e., the shear strain induced will be minimum at the center and will be the maximum near the circumference. This variation in applied strain may cause slight microstructural variations in the edge region

in comparison to the central region. The TEM micrographs obtained from the edge region reveals the presence of smaller grains of less than 50 nm in size in addition to some regions containing large density of grains.

It is still an existing debate on the attainment of uniform microstructure in HPT processed samples if the starting material is of coarse grained microstructure [25]. Some researchers have shown differences in microstructures in longitudinal and torsion directions as well [26]. In the present case, the initial milled powders were of nano sized microstructural features and HPT is used as a means of consolidation and not as the processing step for grain refinement, the large differences in mean grain size values are not expected. However the lattice defect densities appears to be varying with the position. The micro XRD confirms the uniform grain size of 23 nm at all positions along the diameter of the HPT sample. The grain size analysis computed from the TEM micrographs gives 30 nm as the mean grain size which is slightly larger than that obtained from X ray analysis. This is because of the X ray line broadening used in Scherrer analysis that involves the contribution of dislocations and other lattice defects to it. The hardness variation between central region and the edge region is about 200 MPa. Since the grain size of aluminum is relatively uniform from the center to the edge, the only apparent reason for this hardening is the combined effects of dislocation density. Twin formation was observed during deformation in nanocrystalline aluminum [27]. These deformation twins will also contribute to the strength increment.

Identifying the new routes for nanostructure synthesis that are based on sequentially combining different non equilibrium processing methods is one of the primary foci of the

research community. In the current investigation, it is successfully demonstrated that combination of ball milling and high pressure torsion can be used to produce bulk nanostructured materials with improved properties. The obtained high hardness values in the current study can be attributed to 1) the attainment of full density 2) smaller grain size 3) defects (dislocations) induced during high pressure torsion straining.

4.4 Summary and Conclusions

High strength bulk nanostructured aluminum with a grain size of 30 nm (from TEM) is synthesized using combined processing steps of ball milling and high pressure torsion. Our investigation highlights that high pressure torsion is a viable and potential technique to compact the ball milled nanostructured materials to their full density. The bulk nanocrystalline aluminum produced in the current investigation has a hardness of 1200 MPa. The high hardness observed could be because of three factors, (a) obtaining of full density, (b) having the microstructural features in the nano regime and (c) lattice strain induced during the extensive plastic deformation of high pressure torsion.

References

1. J. R. Weertman in "Nanostructured Materials: Processing, Properties and applications, ed. C. C. Koch (Noyes Publishing/William Andrew Publishing, Norwich, NY 2002).
2. K. S. Kumar, H. Van Swygenhoven, S. Suresh, Acta mater 51 (2003) 5743.
3. M. A. Meyers, A. Mishra, D. J. Benson, Prog. Mat.Sci 51 (2006) 427.

4. V. Yamakov, D. Wolf, S. R. Phillpot, A. K. Mukherjee, H. Gleiter, Nature mat. 3 (2004) 43.
5. D. Wolf, V. Yamakov, S. R. Phillpot, A. K. Mukherjee, H. Gleiter, Acta mater 53 (2005)1.
6. H. Van Swygenhoven, J. R. Weertman, Materials Today, 9 (2006) 24.
7. R. Z. Valiev, R. K. Islamgaliev, I. V. Alexandrov, Prog Mat Sci, 45 (2000) 103.
8. R. Z. Valiev, Mater. Sci. Eng. A 234–236 (1997) 59.
9. T. G. Langdon, M. Furukawa, M. Nemoto, Z. Horita, J. Met. 52 (2000) 30.
10. V. V. Stolyarov, Y. T. Zhu, I. V. Alexandrov, T. C. Lowe, R. Z. Valiev, Mater. Sci. Eng. A299 (2001) 59.
11. Furukuwa M, Horita Z, Nemoto M, Langdon TG, Mat Sci. Eng., 2002
12. Z. Horita, T. G. Langdon, Mater Sci Eng. A 410-411 (2005) 386.
13. P. Kumar, C. Xu, T. G. Langdon, Mater Sci Eng A (in press).
14. E. Bonetti, L. Pasquini, E. Sampaloesi, Nanostruct mater, 9 (1997) 611.
15. J. Eckert, J. C. Holzer, C. E. Krill III, W. L. Johnson, J Mater Res, 7 (1992) 1751.
16. D. Oleszak, P. H. Shingu, J Appl Phys, 79 (1996) 2975.
17. Elements of X ray diffraction by B.D. Cullity (1978), 3rd edition,Addison-Wesley series
18. R. Z. Valiev Synthesis and processing of nanocrystalline powder, In: David L.Bourell, editors, The Minerals, Metals and Materials Society, 1996, p.153.

19. I. V. Alexandov, Y. T. Zhu, T. C. Lowe, R. K. Islamgaliev, R. Z. Valiev, Nanostruct. Mater, 10 (1998) 49.

20. Z. Lee, F. Zhou, R. Z. Valiev, E. J. Lavernia, S. R. Nutt, Scripta mater, 51 (2004) 209.

21. R. Z. Valiev, R. S. Mishra, J. Grosa, A. K. Mukherjee, Scripta Mater, 34 (1996) 1443.

22. H. Shen, Z.Li, B. Gunther, A. V. Korznikov, R. Z. Valiev. Nanostructured Mater 6 (1995) 385.

23. A. P. Zhilyaev, K. Oh-ishi, T. G. Langdon, T. R. McNelly, Mater Sci. Eng, A 410-411 (2005)277.

24. A. P. Zhilyaev, S. Lee, G. V. Nurislamova, R. Z. Valiev and T. G. Langdon, Scripta Mater, 44 (2001) 2753.

25. A. Vorhauer, R. Pippan, Scripta mater, 51 (2004) 921.

26. X. Huang, A. Vorhauer, G. Winther, N. Hansen, R. Pippan, M. Zehetbauer, Proceedings of UFG III, edited by Y. T. Zhu et al., TMS (The Minerals, Metals and Materials Society) 2004, p. 235.

27. M. W. Chen, E. Ma, K. J. Hemker, H. W. Sheng, Y. M. Wang, X. M. Cheng, Science 300 (2003) 1275.

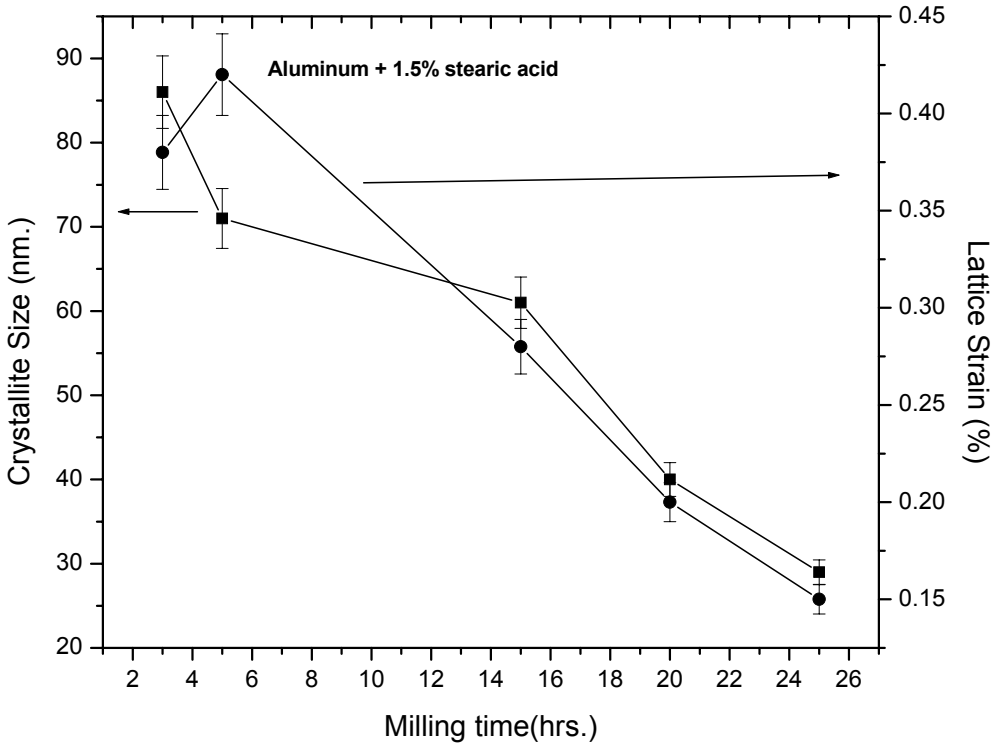

Fig 1. Variation of crystallite size and lattice strain in ball milled aluminum with milling time

Fig 2. Fully dense bulk nanocrystalline aluminum sample obtained after high pressure torsion of ball milled powders.

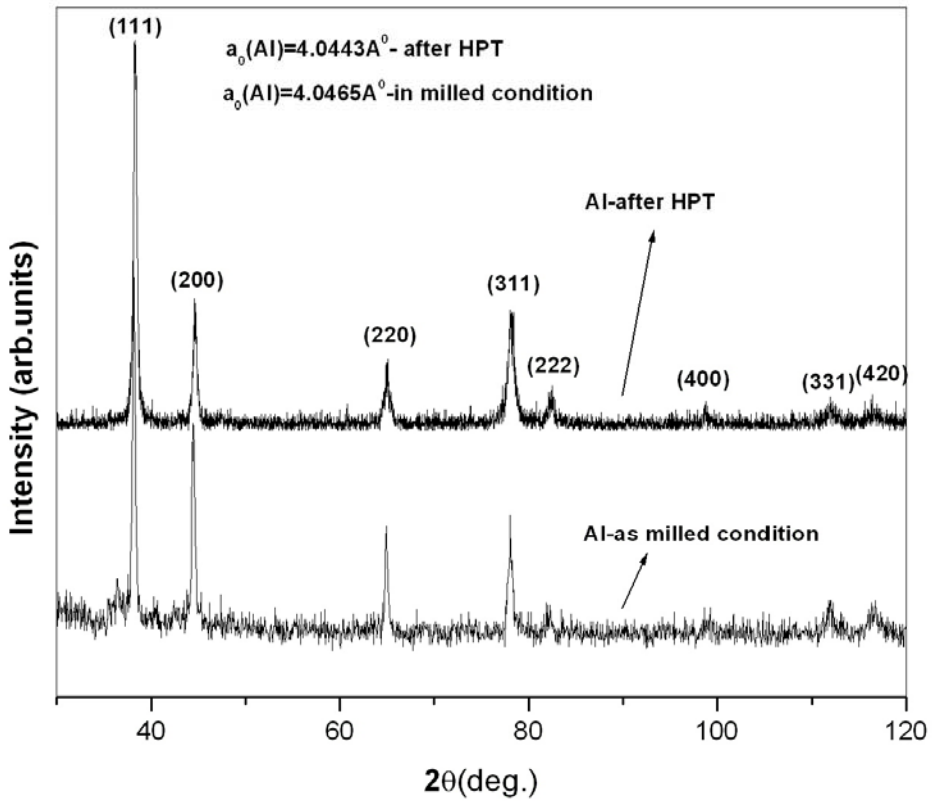

Fig 3. X ray diffractograms of ball nanocrystalline aluminum in as milled and HPTed condition.

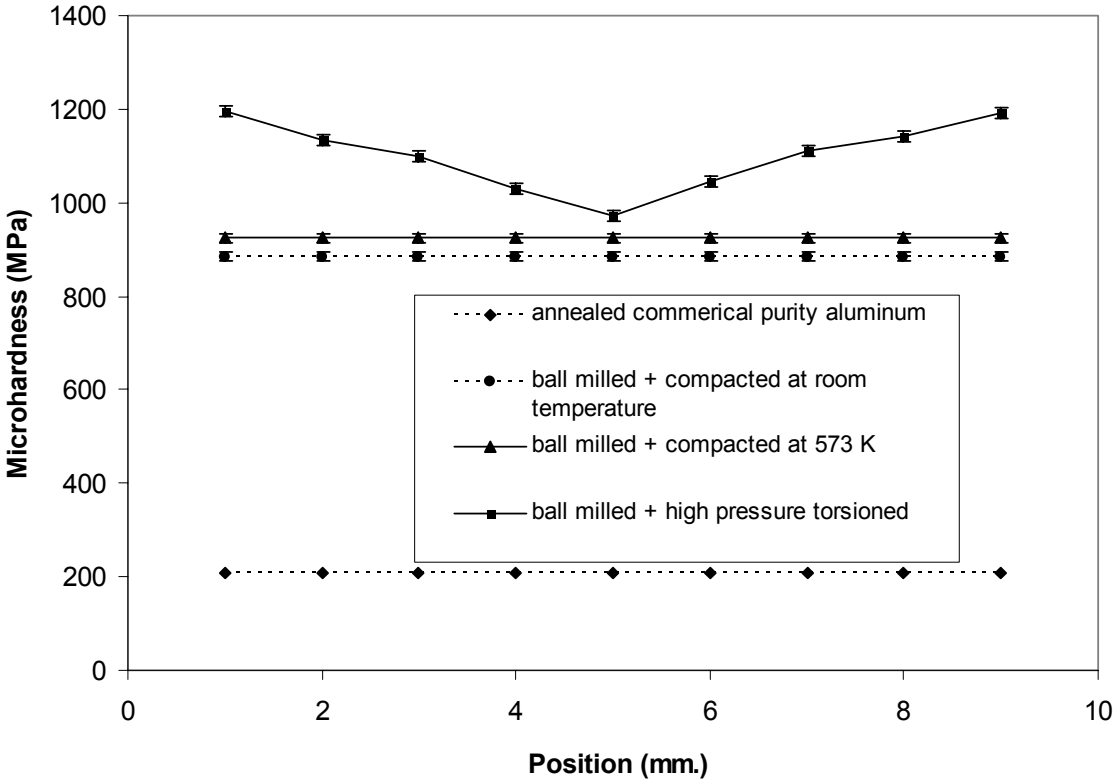

Fig 4. Variation of hardness in nanostructured aluminum.

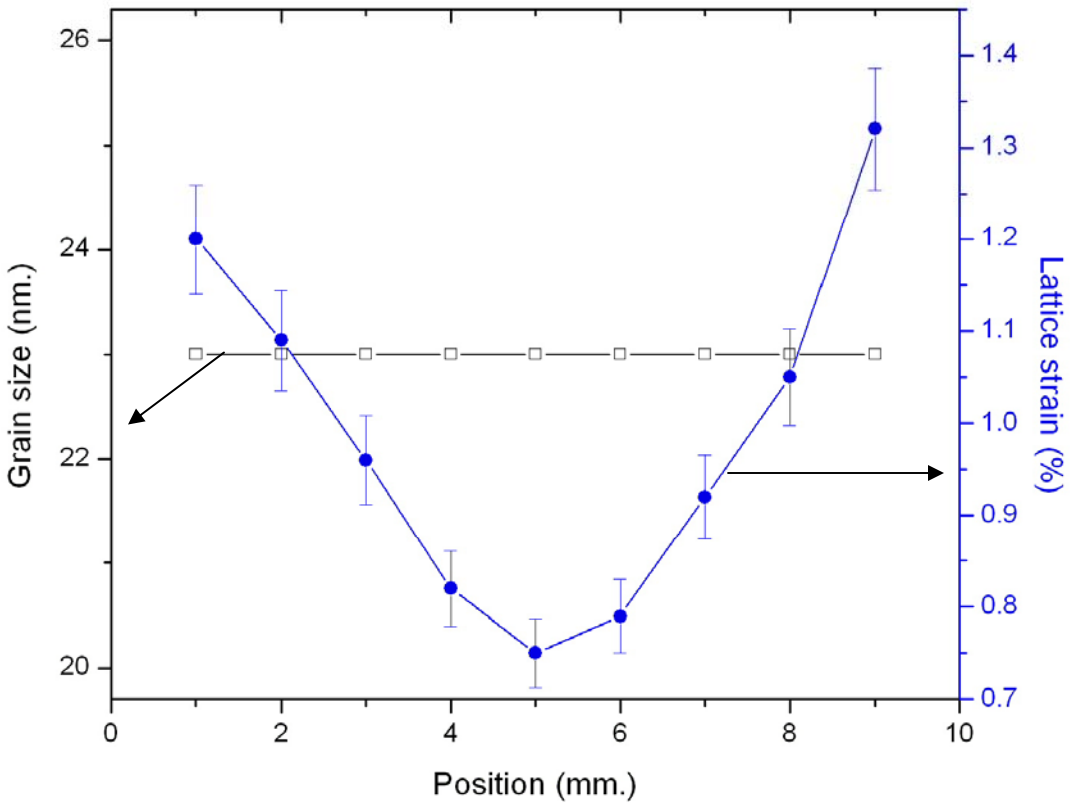

Fig 5.Variation of grain size and lattice strain in HPTed nanocrystalline aluminum sample w.r.t .position along the diameter.

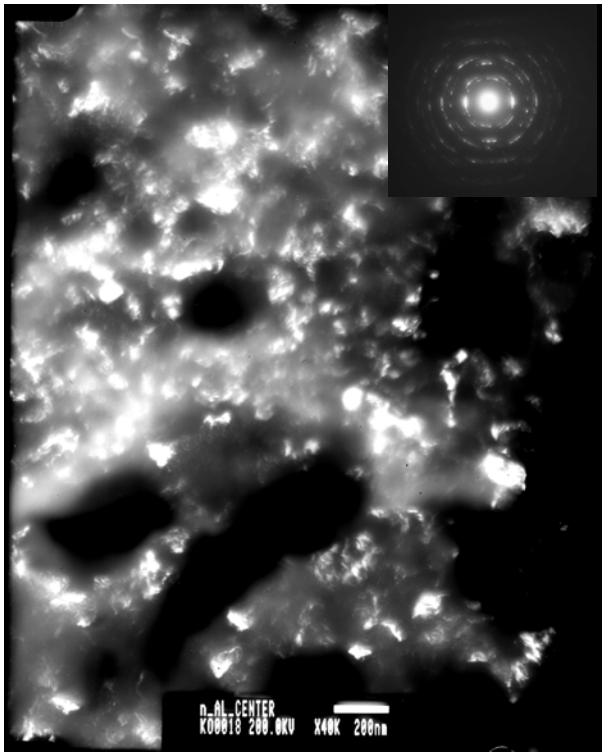

Fig 6 (a) TEM dark field image showing the grain size distribution in the central region of bulk nc Al sample. The corresponding diffraction is shown in inset.

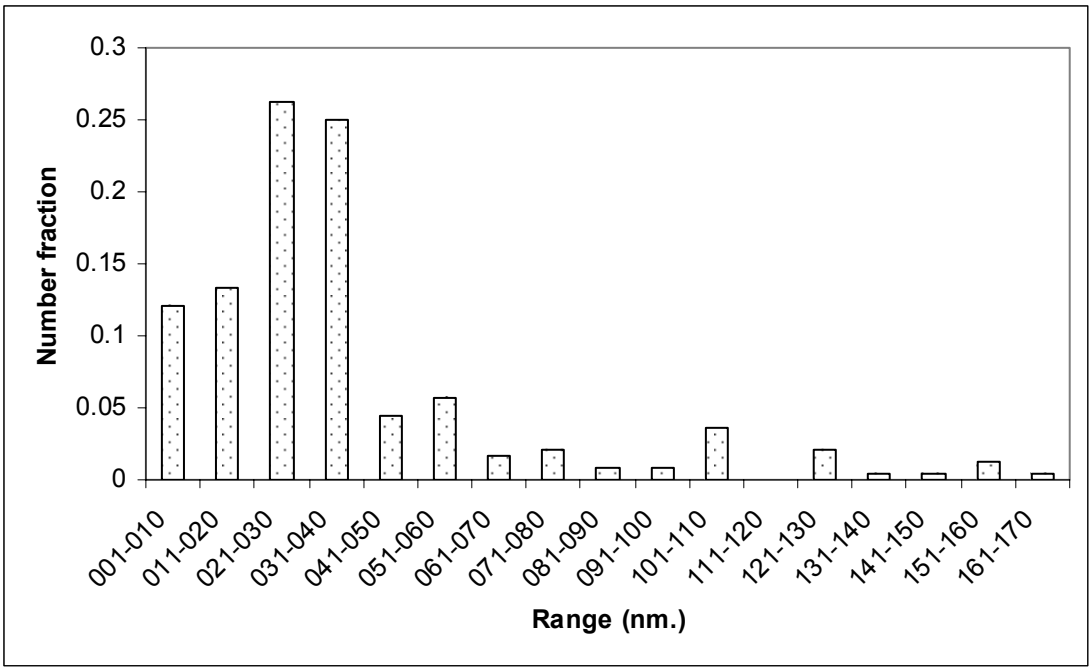

Fig 6 (b) Grain size distribution in nanocrystalline aluminum. The mean grain size computed using number fraction yielded a value of 30 nm.

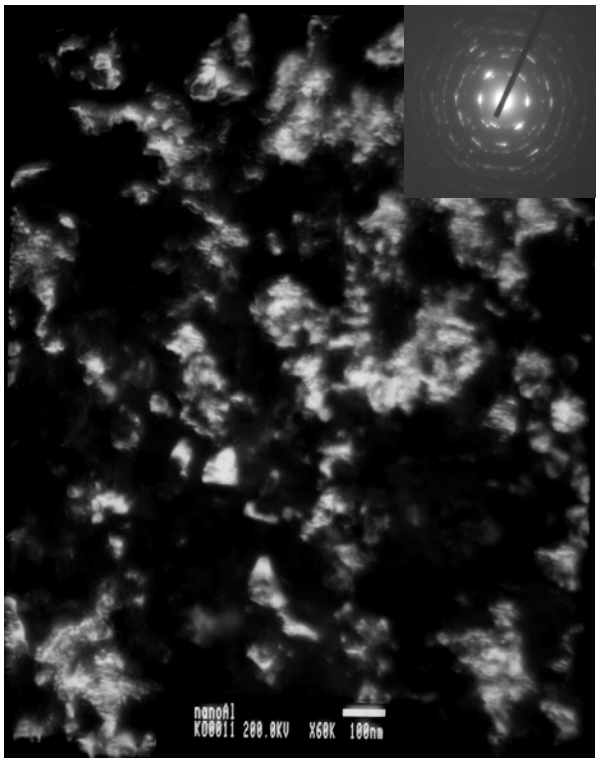

Fig 7 TEM dark filed image obtained from the edge region of the bulk nanocrystalline aluminum sample. The corresponding diffraction pattern is shown in inset.

Chapter 5

Effect of a nanocrystalline W phase on the mechanical properties of bulk nanostructured aluminum processed by high energy ball milling and high pressure torsion

5.1 Introduction

The strength of the polycrystalline materials can be enhanced by several routes;

(a) Refining the grain size

(b) Strain hardening

(c) Solid solution hardening

(d) Precipitation hardening

(e) Dispersion strengthening

In all the above mentioned procedures, the underlying theme is the making of dislocation movement difficult. Strength is dependent on dislocation mobility. If the dislocation mobility is easy, low forces are needed for plastic deformation. If the dislocations are pinned, higher stresses are needed for their progressive movement [1]. A special class of advanced materials, nanocrystalline materials (grain size < 100 nm) triggered an enormous amount of curiosity among the scientific community in the past two decades because of their novel, superior and unique physical, chemical and mechanical properties [2]. Many researchers have demonstrated that the refinement of grain size alone can result in the multifold enhancement of mechanical strength. It is a known fact that nano scaled dispersions will have a positive effect on the strength of coarse grained materials via Orowan strengthening [3]. The effects of the size, spacing and distribution of these particles on the mechanical properties of coarse grained materials are well established.

However the effects of nano dispersoids on the mechanical properties of nanocrystalline materials are not studied in detail.

There are many reports on development of high strength multi phase bulk nanocrystalline aluminum alloys with high strength and good ductility [4]. These materials were prepared by the controlled crystallization of amorphous materials. Hence, the second phase was either crystalline or quasicrystalline depending on the crystallization kinetics and/or the material system. Often the problem associated with the materials made by this method is the incomplete transformation of amorphous matrix into a fully nanocrystalline structure. Hence the left over amorphous phase will surely have an effect on the observed mechanical properties. Therefore having fully nanocrystalline matrix with fully nanocrystalline dispersions is always desirable to study the effects of nano scaled matrix and nano sized dispersions on the mechanical behavior of these multi phase materials. The current understandings (from both the experimental and theoretical considerations) on deformation mechanisms of single phase nanomaterials suggest that at finer grain sizes, the plasticity is controlled by some fundamentally different new mechanisms other than the traditional dislocation slip [5-9]. It is evidenced that the grain boundaries play a major role in dictating the nature of plastic deformation in these materials. It was emphasized with the aid of molecular dynamics simulations that, the mechanisms like grain boundary sliding, grain rotation, defect nucleation from the grain boundaries will come into picture. However the supporting experimental data is yet to be available. In addition to that a second phase with nano scaled microstructural features dispersed in a nanocrystalline matrix is expected to influence the inherent deformation mechanics of the

nano scaled polycrystalline matrix.

In view of all these, the thrust of the current study is to disperse nano sized hard particles (in this case it is W) in a nanocrystalline FCC matrix (aluminum) and thereby to investigate the influence of nanocrystalline W phase on the mechanical properties of nanocrystalline Al. Nanocrystalline aluminum is always softer than nanocrystalline W (at constant grain size). Al and W are of different crystal structures and therefore different slip systems will be active during plastic deformation.

5.2 Experimental

Here the process variables used during ball milling, warm compaction and high pressure torsion are exactly the same as those used to synthesize bulk nanostructured aluminum [chapter 3].

5.3 Results and discussion

Fig 1 shows the X-ray diffractograms of Al, Al-1.0%W, Al-2.0%W, Al-3.0%W and Al-4.0%W alloys milled for 25h at room temperature and compacted at 573 K to densities >98%. It is evident from the Fig 1 that, both Al and W reflections are present and thereby there is no equilibrium or metastable solid solution formation during milling. The indexing of the powder patterns depicts that there was not any formation of intermetallic compounds between Al and W. Therefore it is purely a two phase material consisting of Al and W. The grain size of Al estimated using Scherrer equation yielded a value of 29±3 nm in all the alloys in the as milled condition [Fig 2] and it increased to 34±2 nm after warm compaction at 573 K in an argon atmosphere. The grain size of W was 34±2 nm in

all the alloys in the as milled condition and it did not change on exposure to 573 K. The temperature used for warm compaction, 573 K might be too low to bring in any changes in the microstructure of W because of its higher melting point (3643 K). The precise lattice constants of Al in all these alloys, estimated using the Nelson-Riley extrapolation function analysis [10], were of 4.0445±0.0020 Å (the standard lattice constant of aluminum is 4.0494 Å). Therefore it can be concluded that the high energy ball milling of Al100-xWx (where x=1.0-4.0 atomic %) produced two phase Al and W structures at the nano scale.

In recent years, severe plastic deformation that involves the application of high shear strains under heavy imposed pressures was evolved as a potential technique to produce bulk nanostructured materials [11]. Bulk nanostructured aluminum with improved properties was successfully synthesized by high pressure torsion of ball milled powders [Chapter 3]. Therefore, in an effort to fabricate fully dense, bulk nanostructured Al-W alloys, the ball milled powders were compacted into disk shaped samples of 10 mm diameter and 0.8 mm thickness. These samples were further strained by high pressure torsion at room temperature. This additional extensive plastic deformation resulted in fully dense Al-W alloys. The X-ray diffractograms of different Al-W alloys in the HPT condition are shown in Fig 3. A closer observation of these powder patterns suggests that W did not form any intermetallic compounds with Al even after additional straining by HPT. The measured precise lattice parameters in this condition yielded a value of 4.0435 ± 0.0012 for aluminum. Therefore, Al and W are not forming any solid solutions among themselves.

Fig 4 summarizes the microhardness values obtained at various positions along the diameter in different nc Al-W alloys. It is evident that the hardness increases monotonically towards the edge of the sample. This trend is consistent with the several other studies on high pressure torsion of different metals and alloys including the one on nanostructured aluminum [Chapter 3]. In addition to that, the strength of these alloys increases with the increase in W content. In order to determine the variations in microstructural features (grain size, defect densities), micro X-ray diffraction experiments were performed on Al-2.0%W by collimating the X-ray beam to a diameter of 0.8 mm and then projecting it to the different positions on the sample. From the obtained, different position specific, X-ray diffraction patterns, grain size of both the Al and W were determined using a Scherrer equation and the lattice strain was evaluated using Stokes-Wilson formula and this data is shown in Table 1 and Fig 5 respectively. Interestingly, the grain size is relatively uniform at all the positions. However the lattice strain follows the same trend as that of the hardness [Fig 4], suggesting the variations in the hardness of these samples is because of the variations in lattice strain induced during HPT. The increase in strength in these alloys with increase in W content can also be evidenced.

TEM dark field image of nanocrystalline aluminum from the edge region of HPTed Al-2.0%W is shown in Fig 6 (a) and the corresponding diffraction pattern is given in Fig 6 (b). Indexing of the diffraction patterns suggests that both Al and W reflections are present and it is a purely two phase structure at nano scale. The mean grain size computed using number fraction yields a value of 30 nm [Fig 6 (c)]. The presence of

large W particles can be evidenced from Fig 6 (d) and the corresponding diffraction pattern is given in Fig 6 (e). Assuming that the degree of deformation in the center region of the disk is not as high as that in the edge region, the hardness values from the central region of all these alloys are compared with the hardness values of the warm compacted samples [Fig 7]. It shows that the samples after HPT possess higher strength. In the warm compacted condition itself, the hardness of these alloys increases monotonically with increase in W content. In the HPTed condition, the strength dependence of these alloys on W still holds good but with increased strength level. The improved densities could have resulted in improvement in strength levels. In high pressure torsioned condition, the nanocrystalline aluminum has a hardness of ~950 MPa. It shows that with the addition of 4.0 atomic percentage of W, the strength of the nanocrystalline Al-W alloys can be elevated to nearly 1600 MPa.

The non equilibrium processing procedures employed in the current study, namely high energy ball milling and high pressure torsion, are known to produce materials with a high density of lattice defects, grain boundaries, triple junctions etc [12-13]. These defect regions acts as paths of higher diffusivity in a given single/multi phase material. There are several experimental evidences showing the formation of metastable compounds, intermetallics, metastable or super saturated solid solutions in highly immiscible material systems by high energy ball milling [14]. In contrast to that, the equilibrium phase diagram of the material system in the current investigation Al-W [15] suggests the existence of several intermetallic compounds between Al and W. However, the

experimental investigations carried out in the current study [Figs 1, 3 & 6] results in a conclusion that W is dispersed as a second phase in a nanocrystalline aluminum matrix.

Ivanisenko et al [16] observed shear induced $\alpha \rightarrow \gamma$ transformation during high pressure torsion in nano scaled Fe-C composite. Straumal et al [13] decomposed the supersaturated solid solution in Al-Zn and Al-Mg alloys using high pressure torsion. However in the present study, there was no alloying effect in Al-W even after subjecting to extensive plastic deformation using HPT. It suggests that two phase structure obtained in Al-W via ball milling at room temperature is not disturbed during HPT. The reasons for this kind of abnormal characteristics in Al-W material system under non equilibrium conditions are unknown at this time.

In conventional coarse grained two phase materials, during plastic deformation, the dislocations bypass the hard particles. However, in nano grained materials, since the existence of dislocations is doubtful, either partial dislocations/stacking faults/twins may encounter the hard particles on their way. In the current investigation, these lattice defects might find it hard to shear the nano scaled W particles on their way during plastic deformation. Using molecular dynamics simulations [17-18] and mathematical models [19-20], it was suggested that there will be a change in deformation mechanisms in nanocrystalline FCC materials when the grain size is below 100 nm. They predicted that partial dislocations/stacking faults may be involved in the plastic deformation. In the current investigation since it is a two phase material at nano scale, the deformation mechanisms in nanocrystalline aluminum (of grain size 30 nm) are believed to get

influenced by the nanocrystalline W because of the operation of different slip systems in Al [{111}<110>] and W [{110}<111>] during plastic deformation.

The high strength of the nanocomposites, resulting from the smaller grain size and unique defect structure makes them very attractive for structural applications. For the second phase particles to effectively strengthen the matrix, they should be uniformly distributed inside the grains and/or along the grain boundaries. In the present nano scaled Al-W system, it is anticipated that a fraction of W is present along the nanocrystalline Al grain boundaries thereby increasing the interface cohesive strength. Since Al and W are forming a composite structure at the nano scale, hardness of different nc Al-W composites were evaluated using the rule of mixtures and is shown in Fig 8 along with the data obtained experimentally. Wile evaluating the hardness values using rule of mixtures, hardness values of 934 MPa and 14 GPa were considered for nc Al and nc W respectively. It shows that the obtained experimental hardness values by rule of mixtures are in good agreement with those predicted by rule of mixtures. Since the grain size is relatively uniform in these nanocrystalline Al-W alloys, the increase in strength levels with increase in W content [Fig 8] is attributed to the dispersion strengthening mechanism via rule-of-mixtures (composite model). The particle size of W is larger than the grain size of aluminum matrix. For the Orowan mechanism to be operative, the W particles should be dispersed in the nanocrystalline aluminum grains of size ~ 30 nm. Since the particle size of the dispersoids is larger than the aluminum grain size, operation of the Orowan mechanism is unlikely in the present case. On the other hand, it is clear

that in these nanocrystalline Al-W composite, the hardening with increase in W content is following the trend predicted by rule of mixtures [Fig 8].

5.4 Summary and Conclusions

Al and W composite structures at nano scale were obtained by high energy ball milling at room temperature. In one case, the obtained powders were warm compacted to a densities > 98%. In the other route, they were compacted to their full densities using high pressure torsion. In both the cases, the hardness of the nc Al-W composites were increased with the increase in W content. High pressure torsioned condition yielded a better hardness values in comparison to the warm compacted condition because of having full densities and the lattice strain induced during HPT. The aluminum matrix grain size was about 30 nm whereas the particle size of W is around 500 nm. Therefore strengthening by dislocation-particle interaction (Orowan mechanism), as is the mechanism when the size of the dispersoids is less than the grain size of the matrix, in the present case is unlikely. Finally, the hardness values follow the composite model based on the rule of mixtures.

References:

1. G. E. Dieter, Mechanical metallurgy, 3rd edition, Boston: McGraw-Hill; 1986. p.184.
2. C. C. Koch, Nanostructured Materials: Processing, Properties and applications, (Noyes Publishing/William Andrew Publishing, Norwich, NY 2002).
3. M. A. Meyers, K. K. Chawla, Mechanical behavior of materials, Prentice-Hall; Upper saddle river, New Jersey (1999), p. 484.
4. F. Schurack, J. Eckert, L. Schultz, Nanostruct. Mater, 12 (1999) 107.

5. K. S. Kumar, H. Van Swygenhoven, S. Suresh, Acta mater 51 (2003) 5743.
6. M. A. Meyers, A. Mishra, D. J. Benson, Prog. Mat.Sci 51 (2006) 427.
7. V. Yamakov, D. Wolf, S. R. Phillpot, A. K. Mukherjee, H. Gleiter, Nature mat. 3 (2004) 43.
8. D. Wolf, V. Yamakov, S. R. Phillpot, A. K. Mukherjee, H. Gleiter, Acta mater 53(2005)1.
9. H. Van Swygenhoven, J. R. Weertman, Materials Today, 9 (2006) 24.
10. Elements of X ray diffraction by B.D. Cullity (1978), 3rd edition, Addison-Wesley series
11. G. Sakai, K. Nakamura, Z. Horita, T. G. Langdon, Mater. Sci. Eng A406 (2005) 268.
12. G. Palumbo, S. J. Thorpe, K. T. Aust, *Scripta Metallurgica Et Materialia*, 24 (1990) 1347.
13. B. B. Straumal, B. Baretzky, A. A. Mazilkin, F. Phillip, O. A. Kogtenkova, M. N. Volkov, R. Z. Valiev, Acta Mater, 52 (2004) 4469.
14. C. Suryanarayana, Mechanical alloying and milling, CRC press publications (2004), ISBN: 082474103X.
15. Phase diagrams for binary alloys, edited by Hiroaki Okamoto (2000), ISBN 0871706822.
16. Yu. Ivanisenko, I. MacLaren, X. Sauvage, R. Z. Valiev, H.-J. Fecht, Acta Mater, 54 (2006) 1659.
17. H. Van Swygenhoven, P. M.Derlet, A. Hasnaoui, Phys rev B, 66(2002) 024101.
18. H. Van Swygenhoven, P. M. Derlet, Phys rev B, 64(2001) 224105.

19. R. J. Asaro, S. Suresh, Acta mater, 53 (2005) 3369.

20. R. J. Asaro, P. Krysl, B. Kad, Phil mag lett, 83 (2003) 733.

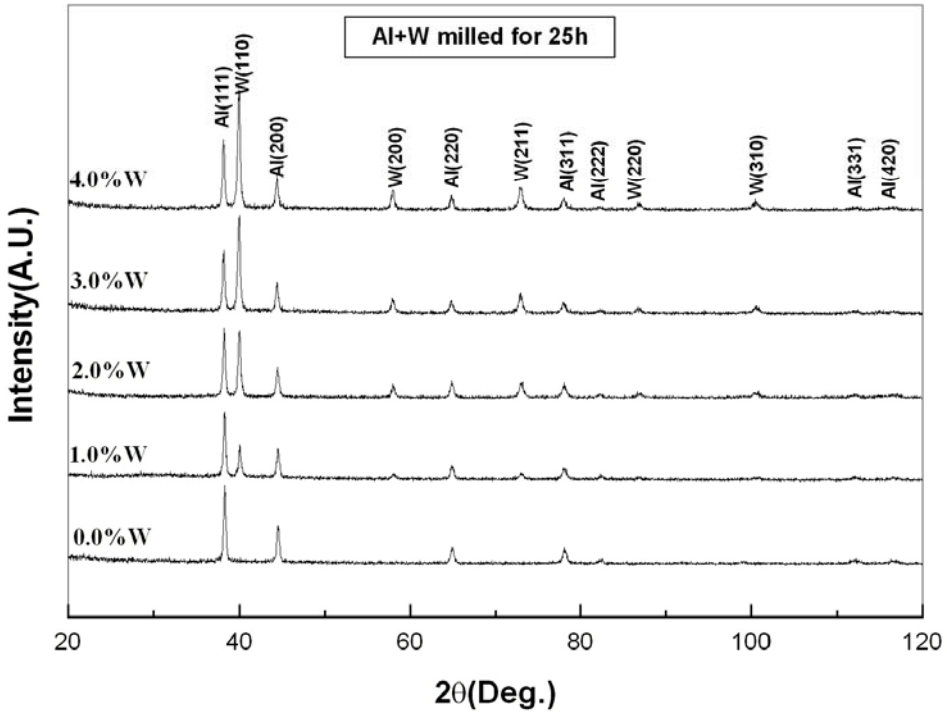

Fig 1. X ray diffractograms of ball milled (at room temperature for 25h) different nanocrystalline Al-W alloys.

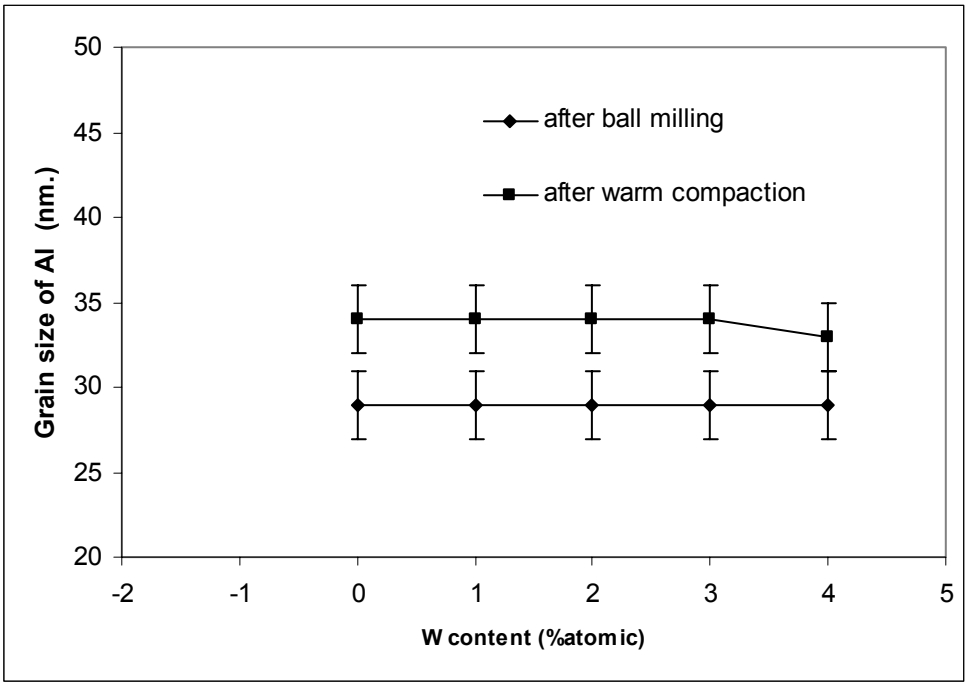

Fig 2. Grain size of ball milled and warm compacted different nanocrystalline Al-W alloys.

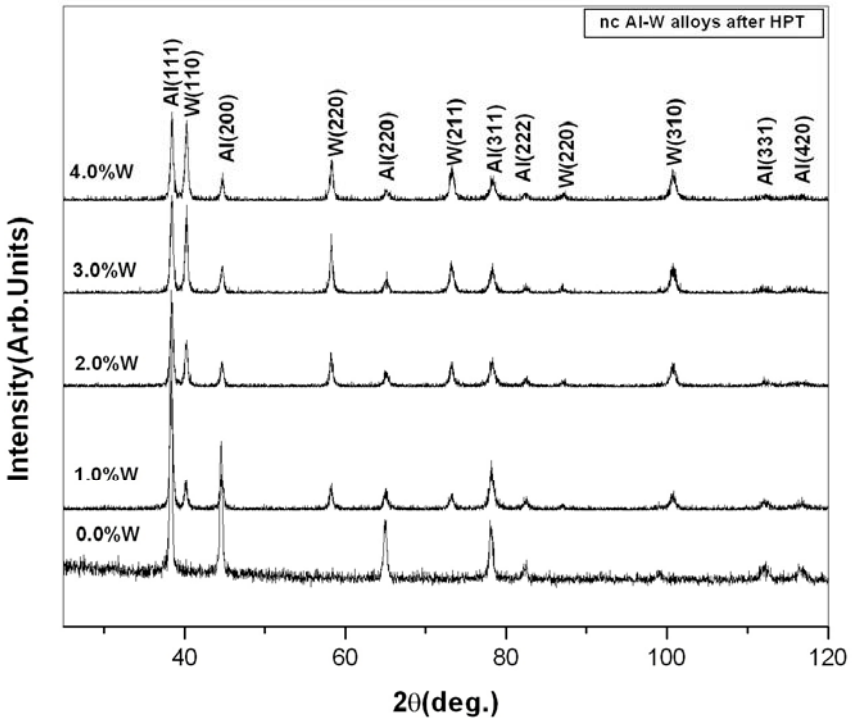

Fig 3. X ray diffractograms of different nanocrystalline Al-W alloys after high pressure torsion.

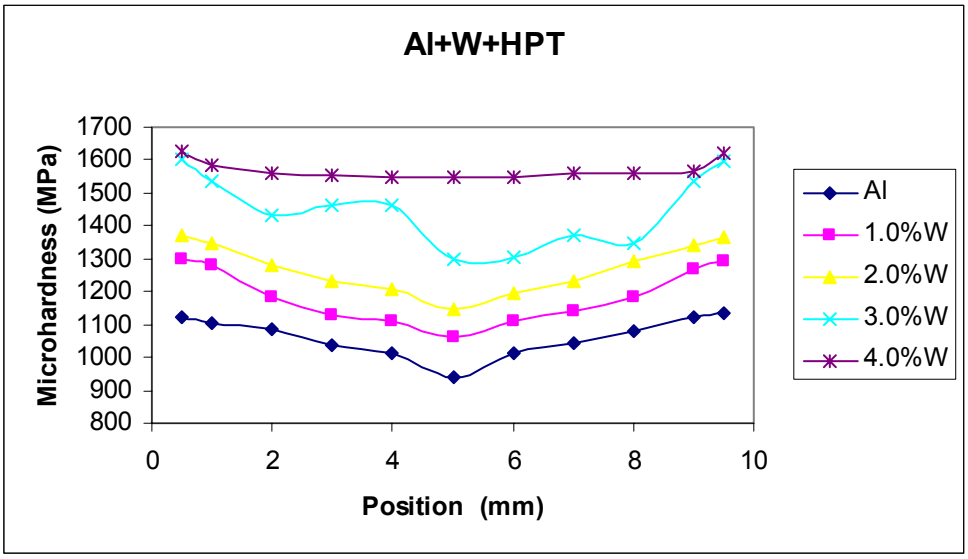

Fig 4. Microhardness of different nanocrystalline Al-W alloys in HPT condition.

Table 1 Variation in grain size values w.r.t position for nanocrystalline Al and nanocrystalline W after high pressure torsion.

Position	Crystallite size of Al (nm.)	Crystallite size of W (nm.)
2 mm	24±2	26±2
3 mm	24±2	26±2
4 mm	26±4	27±3
5 mm	26±3	29±4
6 mm	26±2	28±2
7 mm	25±3	29±2
8 mm	24±4	26±3

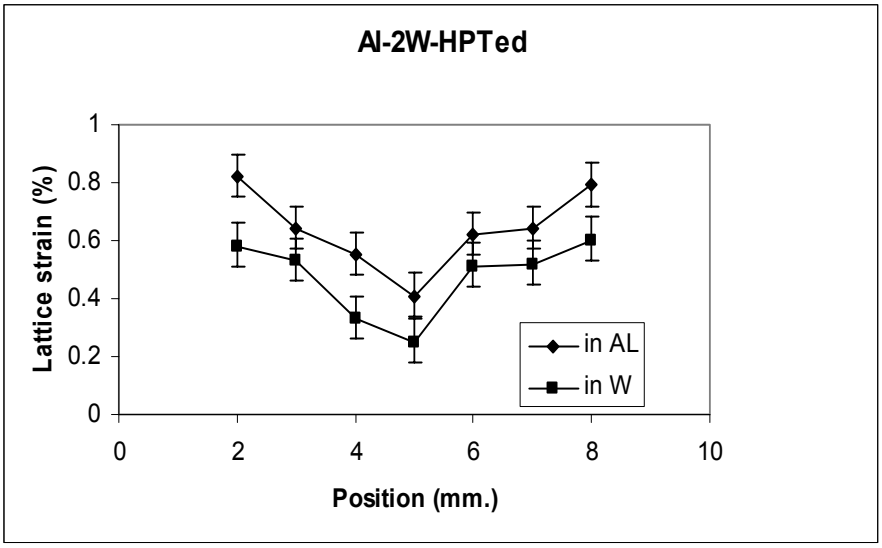

Fig 5. Lattice strain induced in nanocrystalline Al and nanocrystalline W during high pressure torsion of ball milled Al-2.0%W.

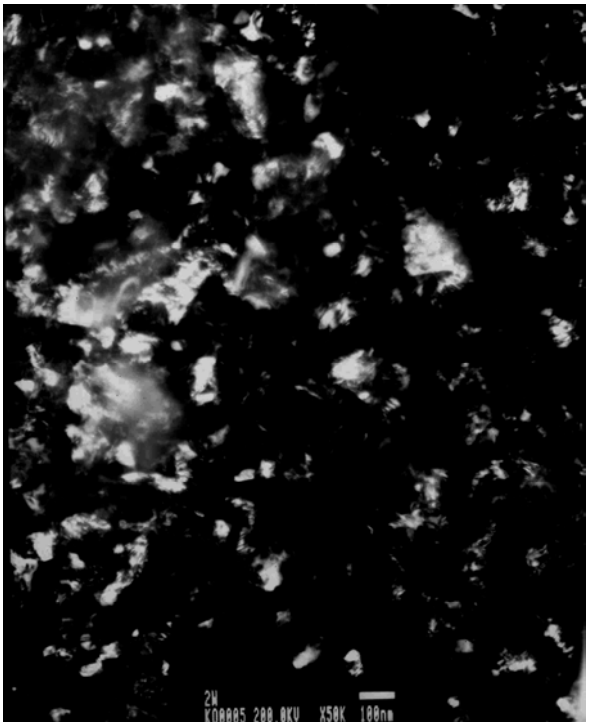

Fig 6 (a) TEM dark field image of nanocrystalline aluminum obtained from the edge region of high pressure torsioned Al-2.0%W.

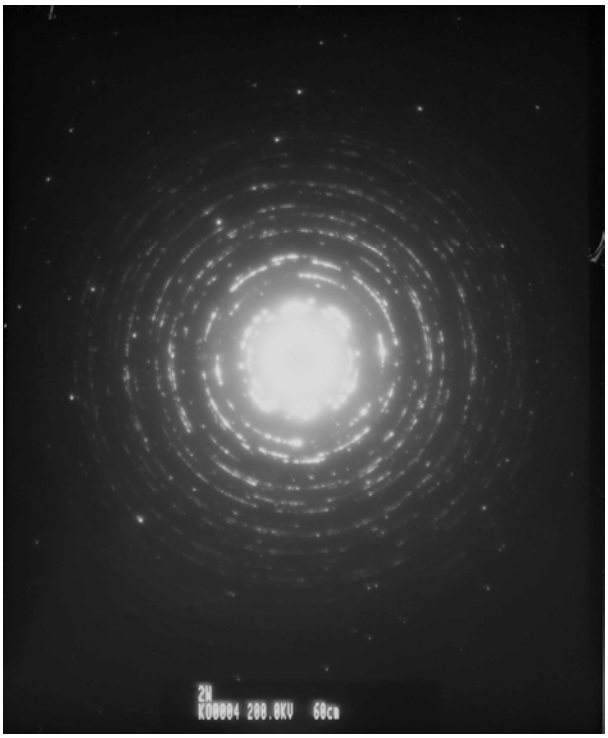

Fig 6 (b) Diffraction pattern corresponding to Fig 6 (a). The indexing of the diffraction pattern shows the presence of the following reflections: Al (111), W (110), Al (200), W (200), Al (220), W (211), Al (311), Al (222), W (220), Al (331), and W (222).

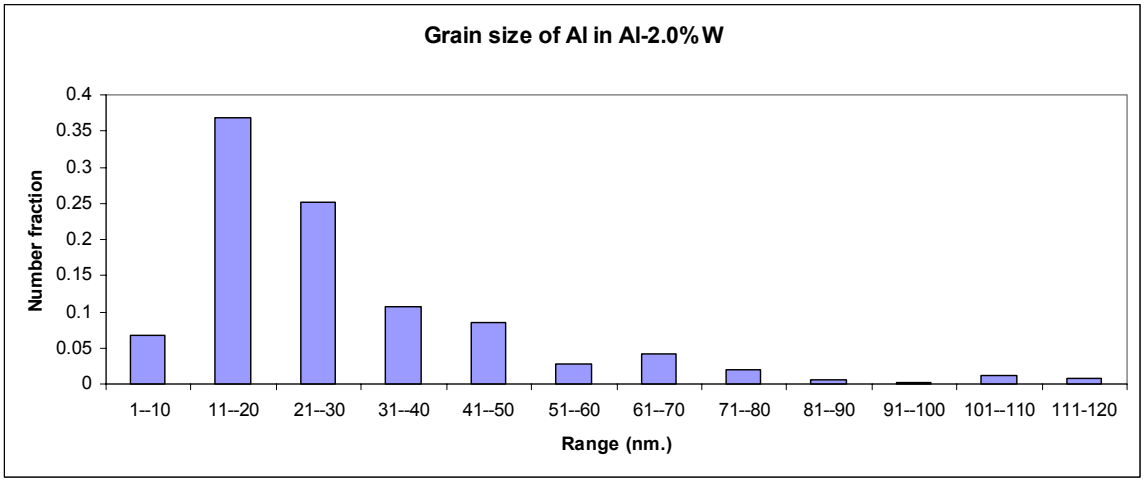

Fig 6 (c) Grain size distribution of nanocrystalline aluminum in HPTed Al-0.2%W. The mean grain size of Al calculated using number fraction is 30 nm.

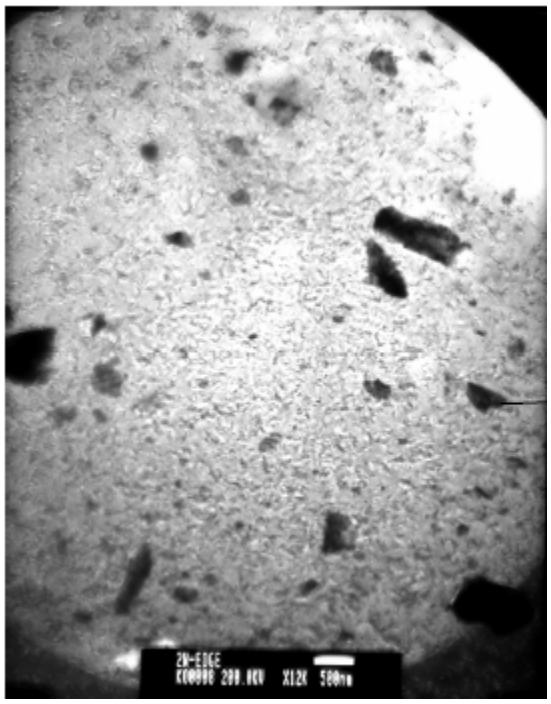

Fig 6 (d) TEM image showing the size variations among W particles.

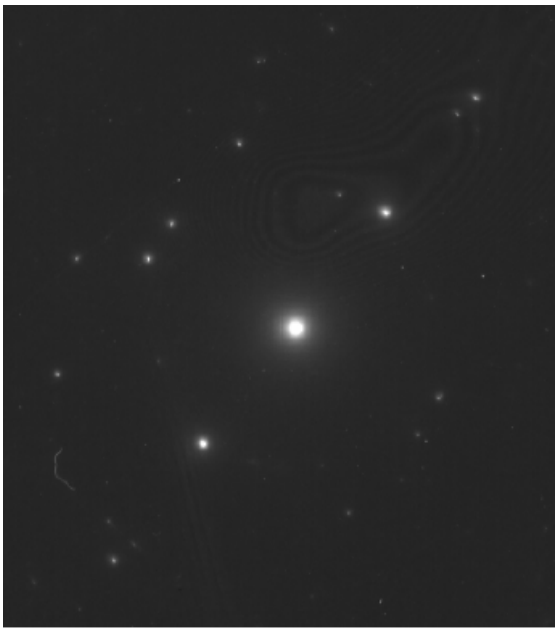

Fig 6 (e) The diffraction pattern obtained from one of the above particles. The measured d spacing values correspond to W.

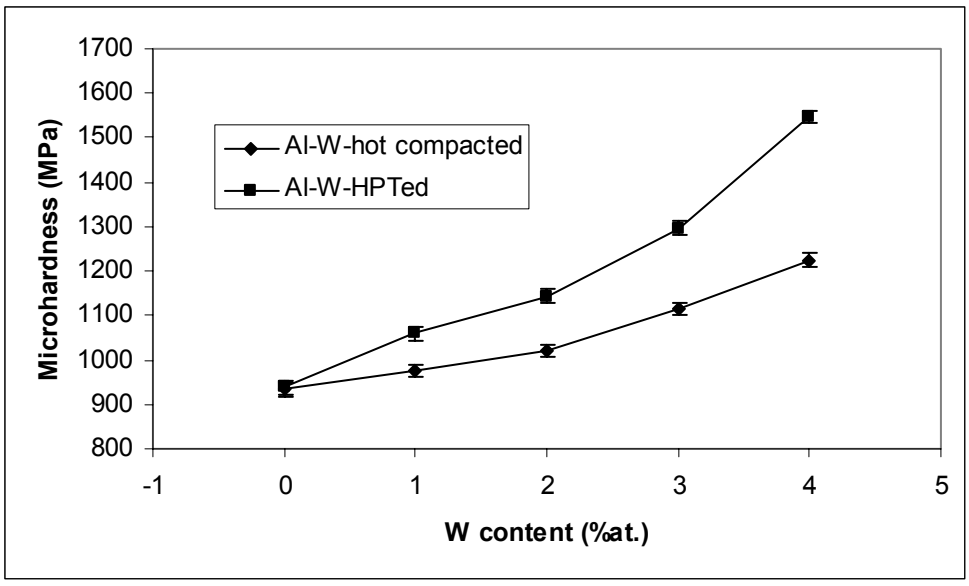

Fig 7. Comparison of hardness values in different nanocrystalline Al-W alloys in warm compacted condition and high pressure

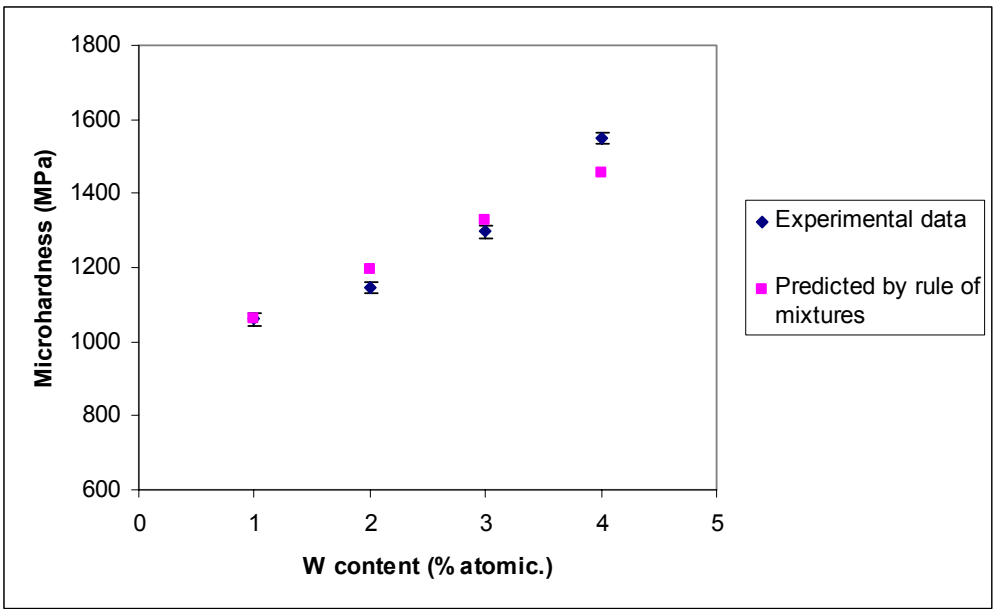

Fig 8. Correlation between the hardness values obtained after HPT (taken from the center of the disk) and the values predicted by rule of mixtures considering the respective volume fractions. A hardness value of 934 MPa for nanocrystalline Al and a hardness value of 14 GPa for nanocrystalline W were considered for the prediction of hardness values using rule of mixtures.

Chapter 6

Effect of Pb on the mechanical properties of nanocrystalline Al

6.1 Introduction

Although the mechanical behavior of nanocrystalline (nc) materials is being intensively investigated by the research community, there still exist uncertainties and unanswered questions on deformation mechanisms at the nano scale [1-3]. There have been several reports showing the novel and exciting properties of nc pure metals [4, 5]. However, detailed studies on the effect of a second phase on the mechanical properties of nc metals are lacking. In the current study efforts have been made to understand the effect of nc Pb on the mechanical properties of nc Al. Al-Pb is a binary alloy system that exhibits a positive heat of mixing and a large miscibility gap between liquid and solid states and hence is the ideal system to obtain two phase structures. Several researchers have discussed the size and shape dependant melting behavior of Pb nano crystals embedded in an Al matrix by both experimental and theoretical means [6-12]. It has been shown that the presence of nano sized Pb particles in an Al matrix can result in depression [8] or elevation [9, 12] of the melting point of Pb from its bulk value. The depression of the melting point was attributed to the presence of a disordered and incoherent interface between Pb/Al and the elevation to the presence of an ordered and coherent interface between Pb/Al. Nano sized dispersions in a coarse grained matrix will produce dispersion hardening and the effect of size and spacing between the particles on the mechanical properties are well documented [13]. However, the effects of dispersion hardening for a nanocrystalline matrix are still unknown.

6.2 Experimental

Al and Pb powders (procured from Alfa-Aesar) with a purity of 99.97% and 99.9% respectively were used as raw materials. The powders were loaded into a tool steel vial in a glove box under a high purity argon atmosphere (<3ppm oxygen). Martensitic stainless steel balls (440C) were used as milling media with a Spex 8000 shaker mill. Initially Al, Al-0.2%Pb, Al-0.7%Pb and Al-1.0%Pb alloys were synthesized at room temperature with the addition of 1.5 wt. % stearic acid as a surfactant in order to avoid cold welding. The resultant powders were consolidated into 6.35 mm diameter disks of near theoretical density at 573 K using a compressive load of 1.8 GPa under an argon atmosphere. In the second processing route, spherical balls (of 8mm maximum diameter) were consolidated *in situ* using a combination of milling at liquid nitrogen temperature and milling at room temperature. Consequently these spheres were transformed into disks. The density of all the samples was measured using the Archimedes principle method. The hardness measurements were taken using a Buehler Micromet microhardness tester at 100 gm load. Before taking the hardness readings, samples were metallographically polished to a mirror-like surface. The value of each datum point is the average of 10 readings taken at various points over the surface of the sample. Three samples were tested at each composition. XRD experiments were carried out using a Rigaku Geigerflex diffractometer with CuK_{α} radiation (λ = 0.1541 nm). The grain size was computed using the Scherrer equation from broadened X-ray line spectra after accounting for instrumental broadening. Samples for transmission electron microscopy studies were electrolytically thinned with 20% perchloric acid and 80% methanol at 233 K using a Fischione twin jet

electropolisher and observed in TOPCON EM 002B TEM and JEOL 2010F TEM both operated at 200 kV.

6.3 Results and discussion

Fig 1 shows the X-ray diffractograms of nanocrystalline Al-Pb alloys of different compositions ball milled for 25 hrs at room temperature with the addition of stearic acid as a surfactant and then compacted at 573 K. It is clear from the diffractograms that Pb is not forming a non-equilibrium solid solution. In addition to that, precise lattice parameter calculations using the Nelson-Riley extrapolation function were performed and there was no significant change in the lattice parameter of Al with the addition of Pb. The lattice parameter of Al assumed a value of 4.0442±0.0003 Å in all the nc Al-Pb alloys against a standard literature value of 4.0495 Å. Therefore, nanocrystalline Pb appears to be dispersed as a second phase in the nc Al matrix. The grain size of Al in nc Al-Pb alloys calculated from x-ray line broadening using the Scherrer equation gives a value of 29 nm after milling and it increases to 32 nm after hot compaction showing negligible grain growth during the compaction process [Fig 2]. The Pb phase in the grain boundaries could be restricting the growth of Al grains in this case. Nearly 100 % of theoretical density was achieved in all the samples. This could be because of the low melting point of Pb and thereby acting as a lubricant, supporting the previous results on ball milled and hot isostatically compacted Al-Pb samples [14, 15].

The same two phase mixtures were also produced by *in situ* consolidation of the Al-Pb powders into spheres during milling itself using the combination of milling at liquid nitrogen temperature and milling at room temperature. This is a relatively novel yet efficient technique developed in our laboratory to synthesize bulk nanocrystalline

materials. Prior to this, bulk nc Cu [5] and nc Zn [16] were successfully synthesized using the same technique. TEM dark field images [Figs 3 & 4] show the distribution of nano Al grains in *in situ* consolidated Al-0.2%Pb and Al-1.0%Pb respectively. The mean grain size of Al computed using number fraction from 400 grains in each case yields a value of 23 nm in Al-0.2%Pb and 28 nm in case of Al-1.0%Pb. The Pb particles of different sizes ranging from 5 nm to 400 nm are dispersed in the nc Al matrix. These are in good agreement with the grain size values of hot compacted samples estimated from X-ray analysis [Fig 2]. Prior to this, Sheng et al [14] reported the microhardness data on ball milled and hot isostatically consolidated nanocrystalline Al-Pb samples. In their report, they showed that hardness of Al-Pb increased with increase in Pb content and they concluded that dispersion hardening was the strengthening mechanism. Fig 5 shows the hardness data obtained on hot compacted samples as well as *in situ* consolidated samples in the current study. Ball milled and hot compacted pure Al has a hardness of 925 MPa whereas in situ consolidated Al has a hardness of ~900 MPa. An addition of 1.0% (atomic) of Pb results in drastic softening of nc Al matrix decreasing the strength by 35-37 %! The effect of stearic acid on the measured hardness values of hot compacted samples is minimal as the same hardness levels are observed in the hot compacted samples (synthesized with the addition of stearic acid) and in the *in situ* consolidated samples (synthesized without the addition of stearic acid).These results are at variance with the data of Sheng et al [14] where they have observed the hardening of the Al matrix of grain size 24 nm with the increased addition of Pb. Since the samples in the current study were of 100% theoretical density and with relatively uniform Al grain size, the only

apparent reason for this softening is the nc Pb, its distribution and its interaction with nc Al grain boundaries.

It is well documented that plastic deformation, in coarse grained materials, occurs via intragranular slip through dislocation motion. As we reduce the grain size to the nano regime, the increased volume fraction of grain boundaries becomes increasingly significant in dictating the mode of plastic deformation. It is well known that dislocation multiplication during plastic deformation in coarse grained materials occurs through the operation of Frank-Read sources. However, to date, operation of Frank-Read sources is not observed in nano grained materials. Using molecular dynamics simulations Van Swygenhoven et al [17] showed, in fcc metals at the nano scale, that a fundamentally different dislocation generation mechanism will be operative, involving partials. These new partial dislocations nucleate at the grain boundary, traverse through the grains and get absorbed by the boundary on the other side of the grain. It was further suggested that in nanocrystalline Ni of grain size 12 nm and 20 nm the emission of these partials occurs by local atomic shuffling and stress assisted free volume migration to or from a triple junction. It is reported that the emission of these grain boundary dislocations is affected by the intrinsic stacking fault energy, unstable stacking fault energy and stress concentrations at the grain facets [18]. Hence, while studying the deformation mechanisms at the nano scale, one needs to understand the nature of these grain boundaries as well as the type and densities of defects contained in these boundaries and ultimately the response of these defects to the applied strain. Asaro et al [19] argue that in fcc metals, there occurs a transition in deformation mechanisms when the grain size is below 100 nm. They propose that in nc fcc metals stacking faults are emitted from the

grain boundaries and they traverse through the nanocrystalline grains, reaching the other end of the boundary which is consistent with the mechanism proposed by Van Swygenhoven et al [17]. Recently Asaro and Suresh [18] described a model incorporating intrinsic stacking fault energy and unstable stacking fault energy and estimated the stress needed to nucleate a partial dislocation in nanocrystalline fcc metals. They tested the validity of their model using the available experimental data for pure fcc metals. However, the stress needed to nucleate such partial dislocation/stacking-fault from a grain boundary containing Pb atom segregates is unknown at this time.

Nanocrystalline Pb may harden the nc Al matrix via dispersion hardening or may soften it by reducing the stress needed to emit grain boundary dislocations. From the obtained hardness data [Fig 5], it is clear that Pb is softening the nc Al matrix well below the values predicted by the rule of mixtures. While evaluating the hardness values using the rule of mixtures [Fig 5], nanocrystalline Al of hardness 925 MPa and nanocrystalline Pb of hardness 80 MPa were used. Z contrast imaging in TEM is a technique to distinguish two phase structures even on the atomic scale especially if the atomic number (Z) difference of the two phases is large because the intensity (I) in Z-contrast imaging scales as Z^2 [20,21]. The Pb atom is of higher atomic number and larger in size in comparison to the Al atom. The Z-contrast image of *in situ* consolidated Al-1.0%Pb [Fig 6] shows that Al grain boundaries are coated with Pb atoms as the grain boundaries are of brighter contrast in comparison to the grain interior. The grain boundaries in nc Al-Pb [Fig 6] are of curved morphology unlike the polygonal morphology that one can see in coarse grained materials. This could be because of the processing technique employed in the

current study to produce nanostructured material as well as the higher free energy associated with these metastable grain boundaries. It is evident from the current study [Fig 3&4] and the past studies [22] that the high energy ball milling is known to produce grains (<100 nm) with curved and irregular shaped grain boundary morphology. The effect of Pb atoms in the grain boundary on dislocation emission is not clear at this time. However, based on the aforementioned discussion we could anticipate some changes in free volume and stress concentrations at triple points due to segregation of Pb to the grain boundaries [Fig 6]. Such changes could make the defect generation from grain boundaries easier and would be the mechanism for grain boundary softening observed in the current study. Grain boundary sliding is also related to the grain boundary dislocation emission [23] and the Pb present at the grain boundaries would also affect this process.

Sheng et al [13] observed the hardening of a nc Al matrix (of grain size 24 nm) by nc Pb particles via dispersion hardening. Presence of Pb in Al grain boundaries was not reported in their study whereas Al grain boundaries are covered with Pb atoms in the current study [Fig 6]. The Al-Pb in [13] was milled in a low energy type vibratory ball mill for 10 h at room temperature whereas in the current investigation, milling was carried out for 25 h in a high energy type Spex shaker mill at room temperature. Cryomilling was also employed for *in situ* consolidation. Different processing conditions may lead to different microstructures and may lead to different properties in the same material system. Hence, at this stage, we believe that Pb atoms are interacting with Al atoms in the grain boundaries, resulting in the decrease of critical resolved shear stress

needed for the plastic deformation i.e., decreasing the stress needed for the defect (dislocation/partial/stacking fault) generation from the grain boundary.

6.4 Summary and conclusions

Nanocrystalline two phase Al-Pb alloys were synthesized using high energy ball milling via two different routes. Nanocrystalline Pb phase appears to be softening the nanocrystalline Al matrix with increased addition of Pb content irrespective of the method of synthesis employed in the current study. The Pb atoms located at the Al grain boundaries are suggested as the cause of the dramatic decrease of strength levels observed in the current investigation. The applicability of the theoretically predicted deformation mechanisms involving nucleation and subsequent absorption of dislocations/partials/stacking faults to the obtained experimental data was discussed.

References:

1. Kumar KS, Van Swygenhoven H, Suresh S, Acta mater 2003; 51:5743
2. Weissmuller J, Markmann J, Adv engr mater 2005; 7:202
3. Wolf D, Yamakov V, Phillpot SR, Mukherjee A, Gleiter H, Acta mater 2005; 53:1
4. Wang Y, Chen M, Zhou F, Ma E, Nature 2002; 419:912
5. Youssef KM, Scattergood RO, Murty KL, Koch CC, Appl phys lett 2004; 85:929
6. Dahmen U, Xiao SQ, Paciornik S, Johnson E, Johansen A, Phys rev lett 1997; 78:471
7. Rosner H, Weissmuller J, Wilde G, Phil mag lett 2004; 84:673
8. Sheng HW, Ren G, Peng LM, Hu ZQ, Lu K, Phil mag lett 1996; 73:179
9. Sheng HW, Lu K, Ma E, Nanostruct mater 1998; 10:865

10. Shi Z, Wynblatt P, Srinivasan SG, Acta mater 2004; 52:2305

11. Rosner H, Scheer P, Weissmuller, Wilde G, Phil mag lett 2003; 83:511

12. Zhang DL, Cantor B, Acta metall mater 1991; 39:1595

13. Dieter GE, Mechanical metallurgy, 3rd edition, Boston: McGraw-Hill; 1986. p.212

14. Sheng HW, Zhou F, Hu ZQ, Lu K, J mater res 1998; 13:308

15. Zhou F, Sheng HW, Lu K, J mater res 1998; 13:249

16. Zhang X, Wang H, Scattergood RO, Narayan J, Koch CC, Sergueeva AV, Mukherjee AK, Acta mater 2002; 50:4823

17. Van Swygenhoven H, Derlet PM, Hasnaoui A, Phys rev B 2002; 66:024101

18. Asaro RJ, Suresh S, Acta mater 2005; 53: 3369

19. Asaro RJ, Krysl P, Kad B, Phil mag lett 2003; 83:733

20. Pennycook SJ, Boatner LA, Nature 1988; 336: 565

21. Pennycook SJ, Ultramicroscopy 1989; 30:58

22. Zhang X, Wang H, Narayan J and Koch CC, Acta mater 2001; 49: 1319

23. Van Swygenhoven H, Derlet PM, Phys rev B 2001; 64:224105

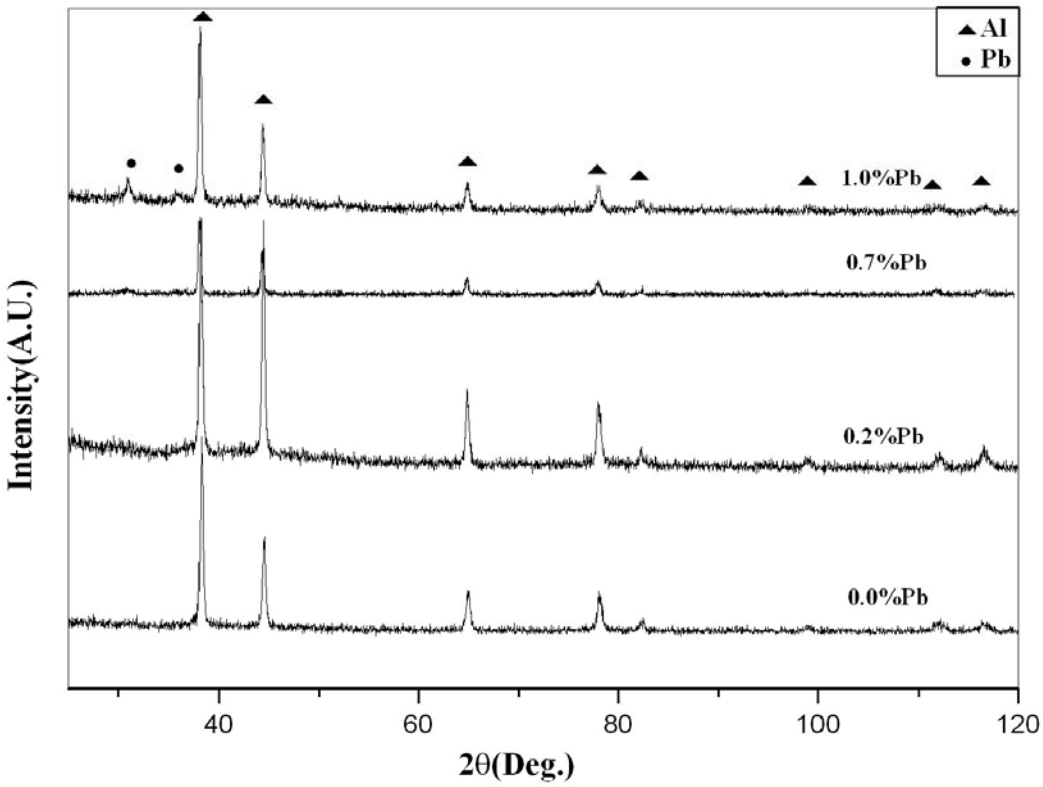

Fig 1. X-ray diffractograms of ball milled and hot compacted nanocrystalline Al-Pb alloys. The presence of Al and Pb peaks shows that there was not any formation of a non-equilibrium solid solution between Al and Pb.

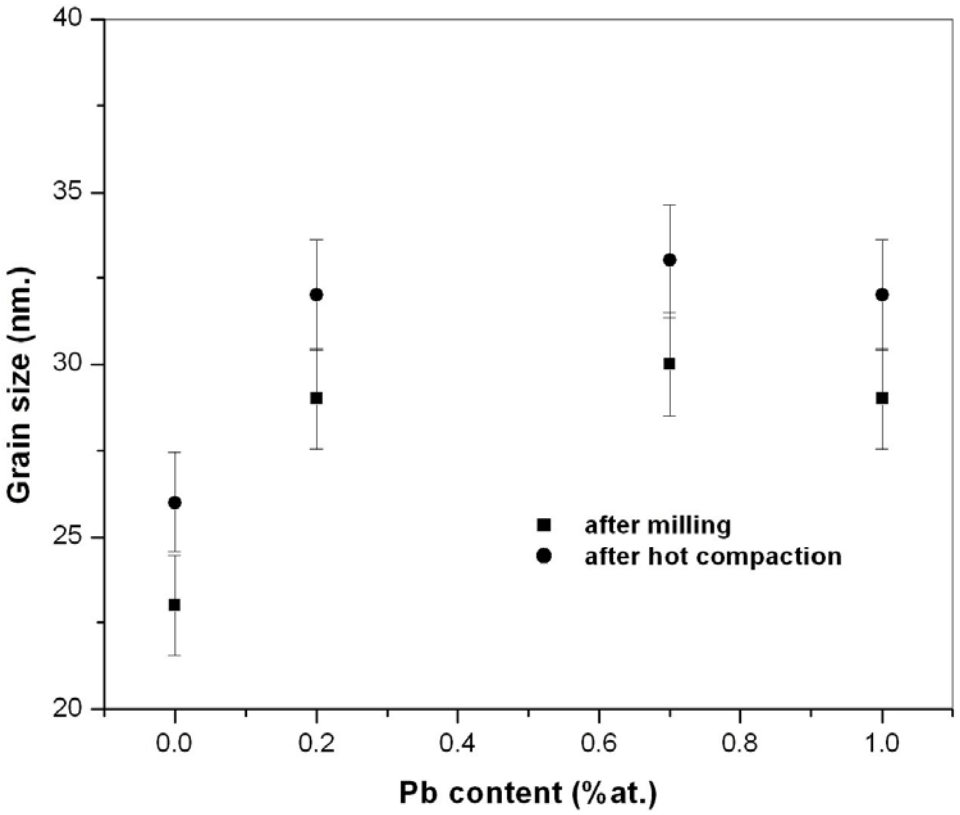

Fig 2. Grain size for Al in ball milled and hot compacted nanocrystalline Al-Pb alloys estimated from X-ray line broadening.

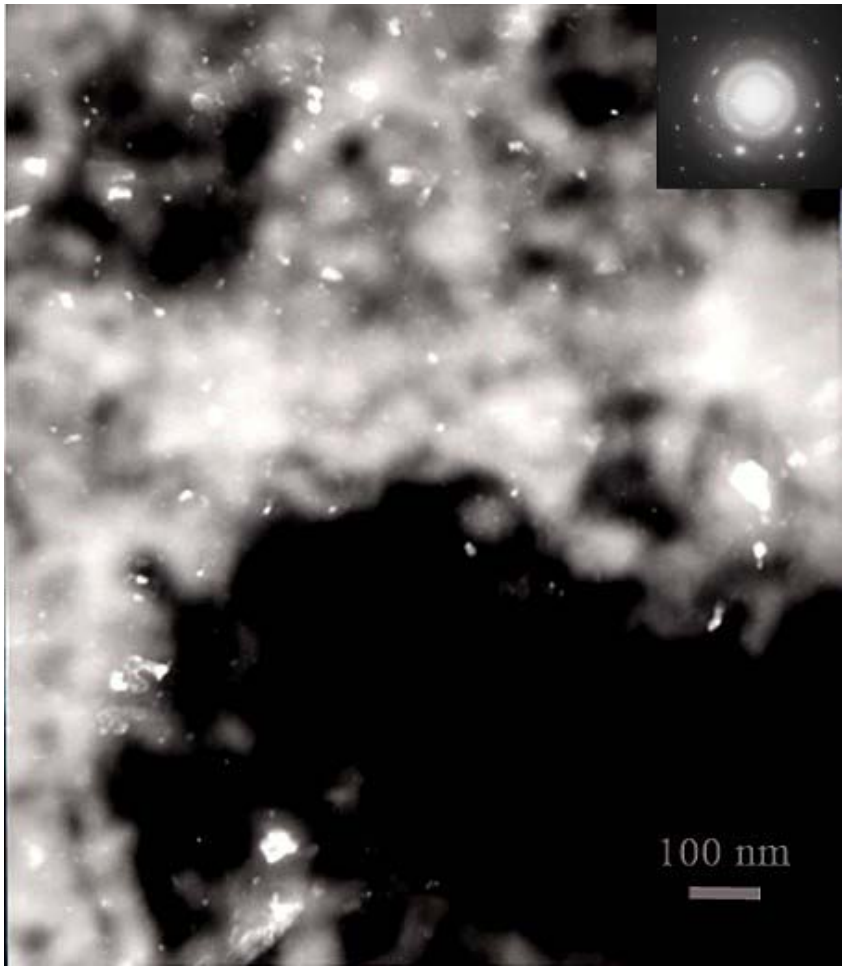

Fig 3. TEM dark field image of *in situ* consolidated nanocrystalline Al-0.2%Pb and the corresponding diffraction pattern (inset).

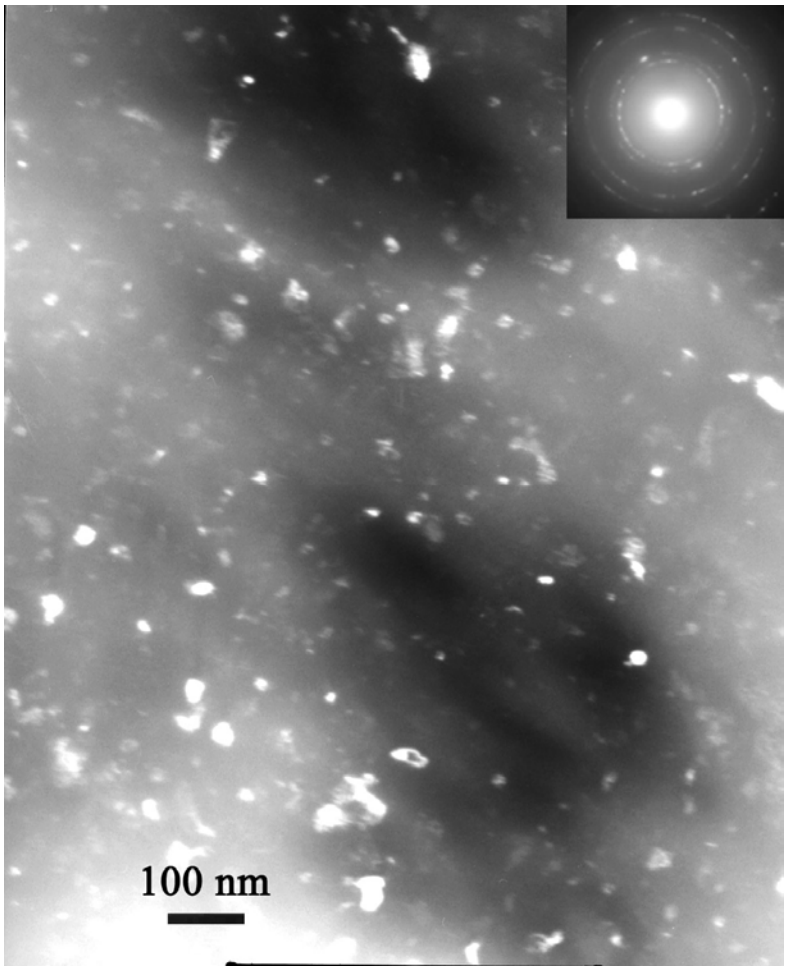

Fig 4 TEM dark field image of *in situ* consolidated nanocrystalline Al-1.0%Pb and the corresponding diffraction pattern (inset).

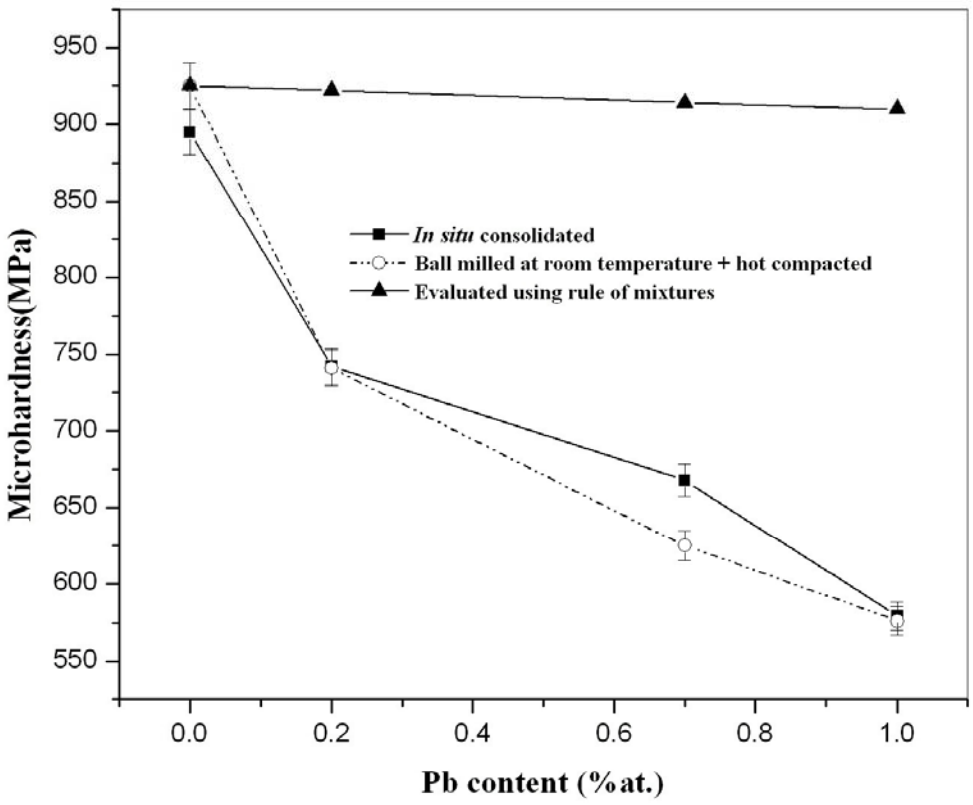

Fig 5 Variation of microhardness in *in situ* consolidated and hot compacted nanocrystalline Al-Pb alloys. The hardness values predicted by the rule of mixtures are also shown. Nanocrystalline Al with a hardness of 925 MPa and nanocrystalline Pb with a hardness of 80 MPa was used in evaluating the hardness values by the rule of mixtures based on the volume fractions of Al and Pb.

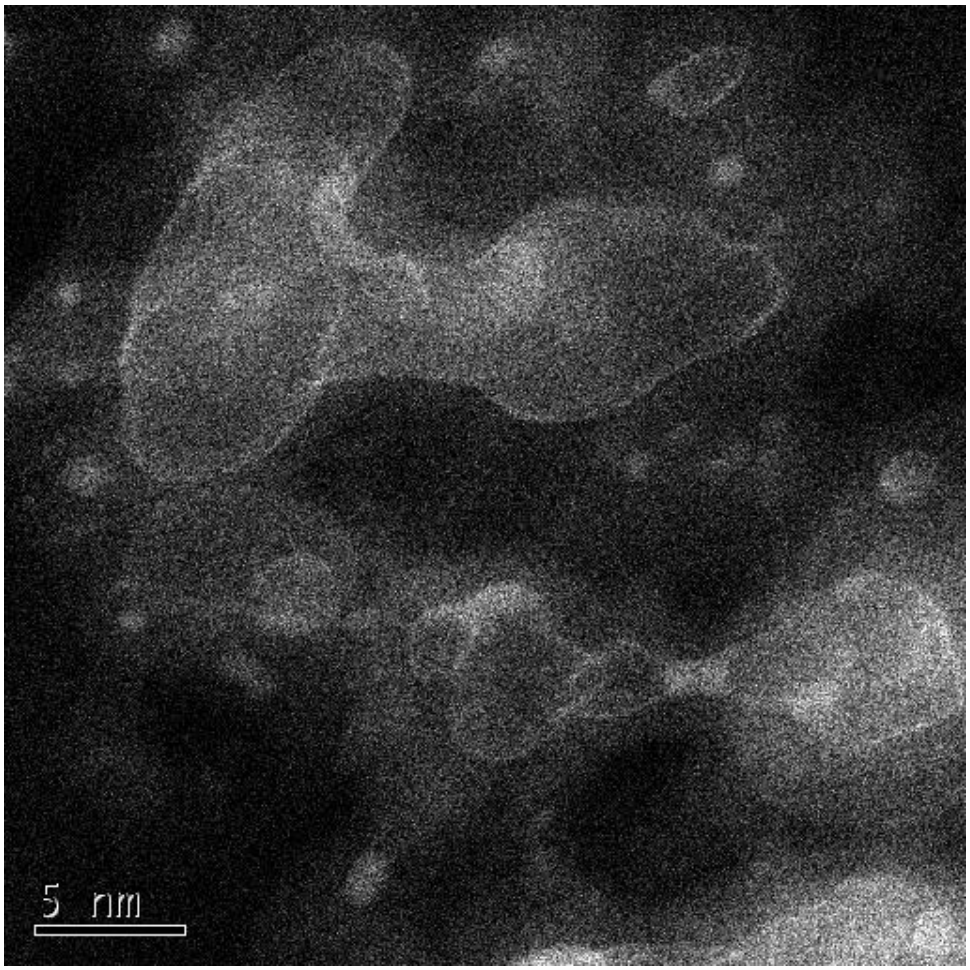

Fig 6 Z-contrast image of *in situ* consolidated Al-1.0%Pb showing the Al grain boundaries covered with Pb atoms. The brighter region represents Pb phase and darker region represents Al phase.

Chapter 7

Effect of additional strain induced by high pressure torsion on the microhardness of nanocrystalline Al-0.7%Pb composite.

7.1 Introduction

It is a well established fact that the nature of the interface (coherent/incoherent, ordered/disordered) between nano sized Pb particles and the Al matrix will dictate the melting characteristics of Pb in Al-Pb composites [1-7]. Recently [8], Al-1.0%Pb composite ribbons were produced by the melt spinning technique and were additionally strained by high pressure torsion [HPT] under a high uniaxial stress of 8 GPa. In as spun condition, the Pb particles that are within the Al grains had facetted morphology and exhibited elevation in the melting point of Pb. However, after additional straining by HPT, the Pb particles displayed curved morphology and a depression in the melting point of Pb was observed. These findings leads to a conclusion that, the original interfacial regions are getting disturbed and are rearranged during HPT and they led to the changes in the thermal properties of Pb in Al. Likewise, it can be argued that even the other properties, for example, mechanical properties may depend on the interfacial characteristics of nano sized Pb and aluminum, although it was not investigated so far. In view of this, the aim of the current study is to investigate the effect of induced strain during HPT on the mechanical properties of in situ consolidated nanocrystalline Al-0.7%Pb composite.

7.2 Experimental

Al and Pb powders (procured from Alfa-Aesar) with a purity of 99.97% and 99.9% respectively were used as raw materials. The powders were loaded into a tool steel vial in a glove box under a high purity argon atmosphere (<3ppm oxygen). Martensitic stainless steel balls (440C) were used as milling media with a Spex 8000 shaker mill. Spherical balls (of 8mm maximum diameter) were consolidated *in situ* using a combination of milling at liquid nitrogen temperature and milling at room temperature. Consequently these spheres were transformed into disks of 10 mm diameter and 0.8 mm thickness. These samples were further strained using HPT (using a Bridgman anvil type device) at room temperature using a pressure of 2.5 GPa, 5 revolutions and 1 revolution per minute. The density of all the samples was measured using the Archimedes principle method. The hardness measurements were taken using a Buehler Micromet microhardness tester at different loads ranging from 20 gm to 100 gm. Before taking the hardness readings, samples were metallographically polished to a mirror-like surface. The value of each datum point in case of as consolidated sample is the average of 10 readings taken at various points over the surface of the sample. In case of HPT samples, hardness was measured along different diameters angled at 45^0 to each other. XRD experiments were carried out using a Rigaku Geigerflex diffractometer with CuK_α radiation (λ = 0.1541 nm). Position dependant X-ray diffraction studies were performed (using a 4 circle Bruker AXS D-5000 diffractometer with a CuK_α radiation) on HPT samples by collimating the X-ray beam to a diameter of 0.8 mm and then projecting it to the several locations on the sample. The grain size was computed using the Scherrer equation from the broadened X-ray line spectra after accounting for instrumental broadening. Lattice

strain was calculated using the Stokes-Wilson formula. Samples for transmission electron microscopy studies were electrolytically thinned with 20% perchloric acid and 80% methanol at 233 K using a Fischione twin jet electropolisher and observed in TOPCON EM 002B TEM operated at 200 kV.

7.3 Results and discussion

Fig 1 shows the X ray diffractograms of as consolidated and HPTed samples. It is evident (from the presence of both Al and Pb reflections) that Pb is not forming any non equilibrium solid solution with Al during ball milling. This structure was not disturbed even after HPT. The grain size calculated from FWHM of X ray peaks yielded a value of 30 nm and 33 nm for aluminum in as consolidated condition and HPT condition respectively. This shows that there was not a significant change in the average grain size of aluminum after HPT. In the milled condition, the lattice strain induced in aluminum was 0.43 % and it increased to 0.8 % after HPT. This could be because of strain that was resulted by rearrangement of the structure and increase in dislocation density during HPT. In case of Pb, the average grain size in as consolidated condition was 11 nm and it was refined to 5 nm after HPT.

Fig 2 (a) is the dark field image of as consolidated Al-0.7%Pb sample showing the distribution of Al grains. The corresponding diffraction pattern was given in Fig 2 (b). The mean grain size calculated using number fraction [Fig 2(c)] yielded a value of 29 nm for Al. The size variation among Pb particles is shown in Fig 2 (d).The Pb particle size varies from 10 nm to 200 nm which is larger in comparison to the aluminum grain size.

Hence it appears that Al and Pb are forming a composite structure at the nano scale during ball milling.

Fig 3 (a) is the dark field image of HPTed nanocrystalline (nc) Al-0.7%Pb sample, showing the distribution of aluminum grains. The corresponding diffraction pattern is given in Fig 3 (b). The mean grain size evaluated using number fraction was 34 nm for Al [Fig 3(c)] although the grain size distribution is slightly larger that that in the as-consolidated condition [Fig 2 (c)]. This confirms that the mean grain size of aluminum was not changed during HPT. The presence of larger grains can be explained on the basis of coalescence of smaller grains via grain rotation that might have occurred during HPT. The size variation among Pb particles after HPT is shown in Fig 3(d). It shows that the size of the Pb particles was about 200 nm, although presence of still smaller Pb particles can be seen.

The microhardness values of nanocrystalline Al-0.7%Pb composite are shown in Fig 4. In as consolidated condition, the nc Al-0.7%Pb sample has a hardness of 685 MPa whereas nanocrystalline pure aluminum with a grain size of 30 nm has a hardness of 925 MPa [9]. This drastic softening in nanocrystalline aluminum with the minute addition of Pb was attributed to the presence of Pb atom segregates in nanocrystalline Al grain boundaries [9].

In the current study, the addition of 0.7 atomic % of Pb decreases the hardness of nanocrystalline aluminum by 25 % by decreasing the hardness to 685 MPa and an additional strain induced by HPT further softens the material to hardness of 520 MPa (i.e.

by another 24 %). The obtained experimental hardness values for these nc Al-Pb composites are far below the values predicted by rule-of-mixtures although Al and Pb form a two phase composite structure at the nano scale. Since the mean grain size of aluminum is nearly uniform (~30 nm) in the as consolidated sample and HPT sample, the only apparent reason could be the rearrangement of nanocrystalline aluminum grain boundaries during HPT and the interaction of Pb atom segregates with these grain boundaries. However, the atomistic mechanism responsible for this kind of scientifically interesting phenomenon in nanocrystalline Al-Pb composites is still under exploration.

7.4 Summary and conclusions

Al-0.7%Pb nano composite was synthesized by in situ consolidation technique using ball milling by milling at cryogenic temperature followed by milling at room temperature. The minute amount of Pb added caused a precipitous decrease in hardness of nanocrystalline aluminum. Additional strain induced using high pressure torsion further softened the Al-0.7%Pb composite. The invariant mean grain size suggests that the nanocrystalline aluminum grain boundaries and their interaction with Pb atom segregates could be the cause of this interesting softening effect.

References:

1. U. Dahmen, S. Q. Xiao, S. Paciornik, E. Johnson, A. Johansen, Phys rev lett., 78 (1997) 471.
2. H. Rosner, J. Weissmuller, G. Wilde, Phil mag lett., 84 (2004) 673.
3. H. W. Sheng, G. Ren,L. M. Peng, Z. Q. Hu, K. Lu, Phil mag lett., 73 (1996) 179.
4. H. W. Sheng, K. Lu, E. Ma, Nanostruct mater., 10(1998) 865.

5. Z. Shi, P. Wynblatt, S. G. Srinivasan, Acta mater., 52 (2004) 2305.
6. H. Rosner, P. Scheer, J. Weissmuller, G. Wilde, Phil mag lett., 83(2003) 511.
7. D. L. Zhang, B. Cantor, Acta metal. mater, 39 (1991)1595.
8. H. Rosner, G. Wilde, Scripta mater, 55 (2006) 119.
9. K. V. Rajulapati, R. O. Scattergood, K. L.Murty, G. Duscher, C. C. Koch, Scripta mater, 55 (2006) 155.

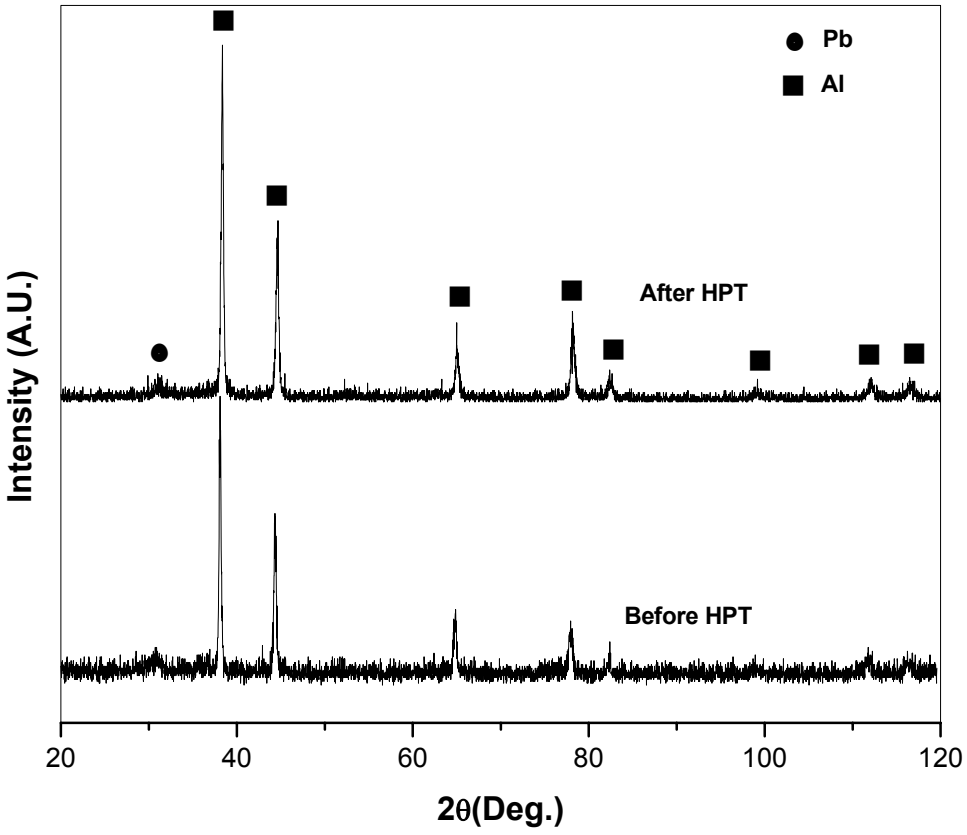

Fig 1. X ray diffractograms of as consolidated and high pressure torsioned nanocrystalline Al-0.7%Pb composite.

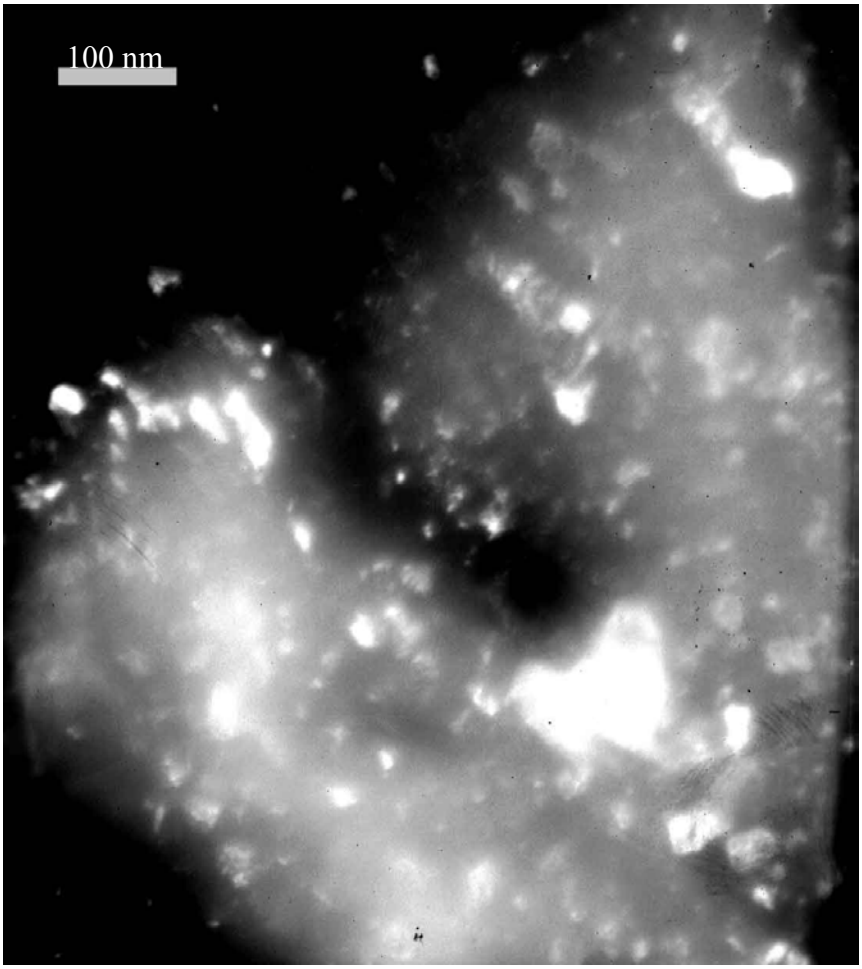

Fig 2 (a). TEM dark field image of as consolidated nanocrystalline Al-0.7%Pb sample showing the distribution of aluminum grains.

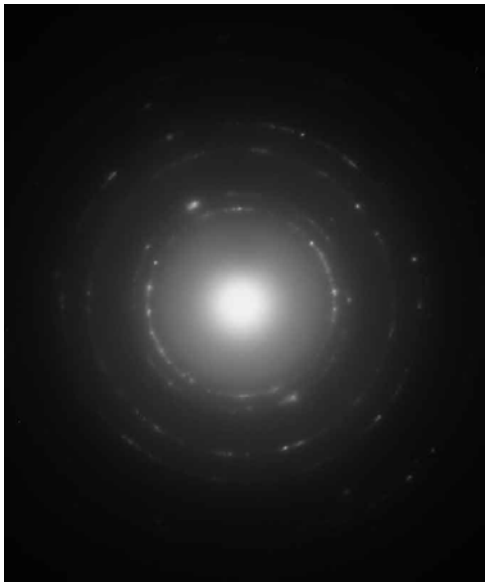

Fig 2 (b) Diffraction pattern corresponding to Fig 2 (a).

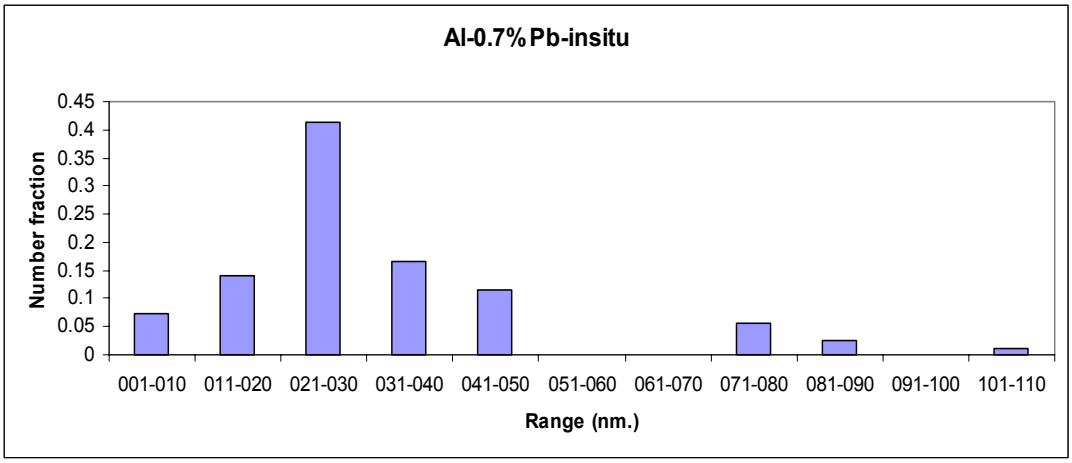

Fig 2(c) Grain size distribution of aluminum in nanocrystalline Al-0.7%Pb in as consolidated condition. The mean grain size was 29 nm.

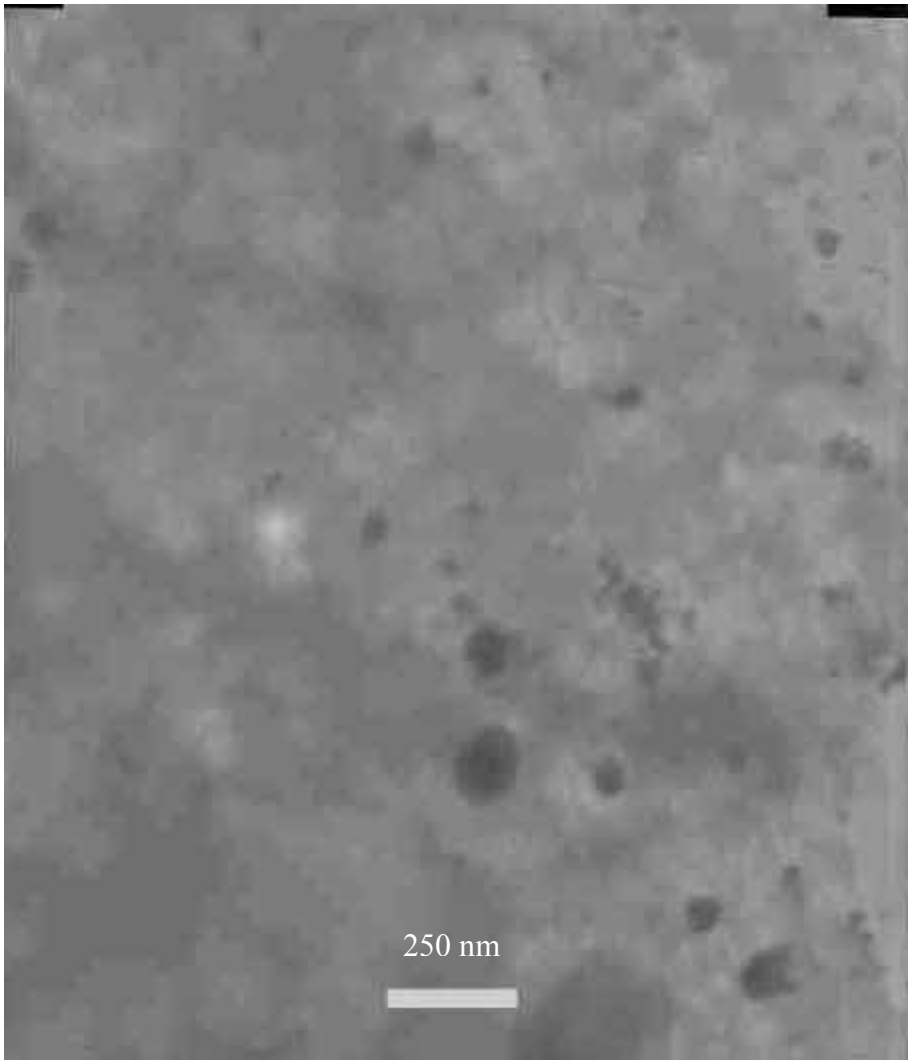

Fig 2(d) Size variations among Pb particles in nanocrystalline Al-0.7%Pb composite in as consolidated condition.

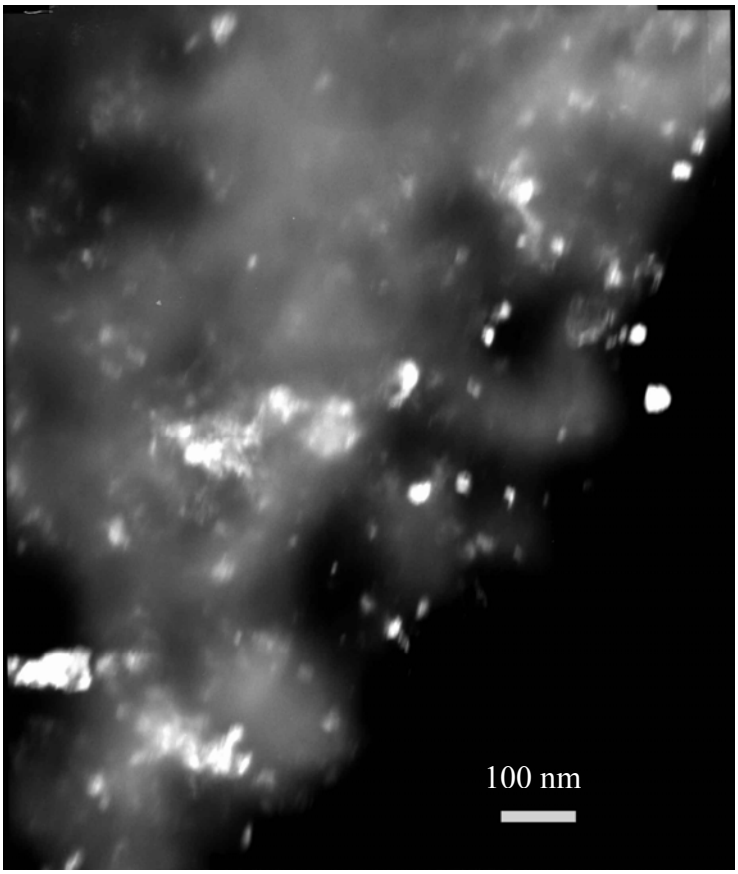

Fig 3(a) TEM dark field image of nanocrystalline Al-0.7%Pb sample after HPT showing the distribution of aluminum grains.

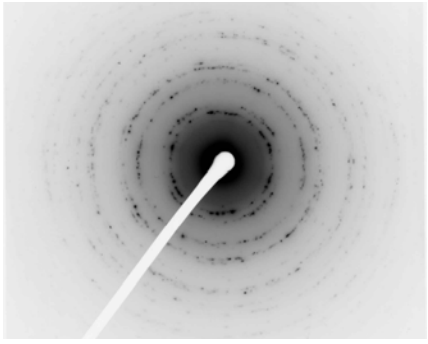

Fig 3(b) Diffraction pattern corresponding to Fig 3 (a).

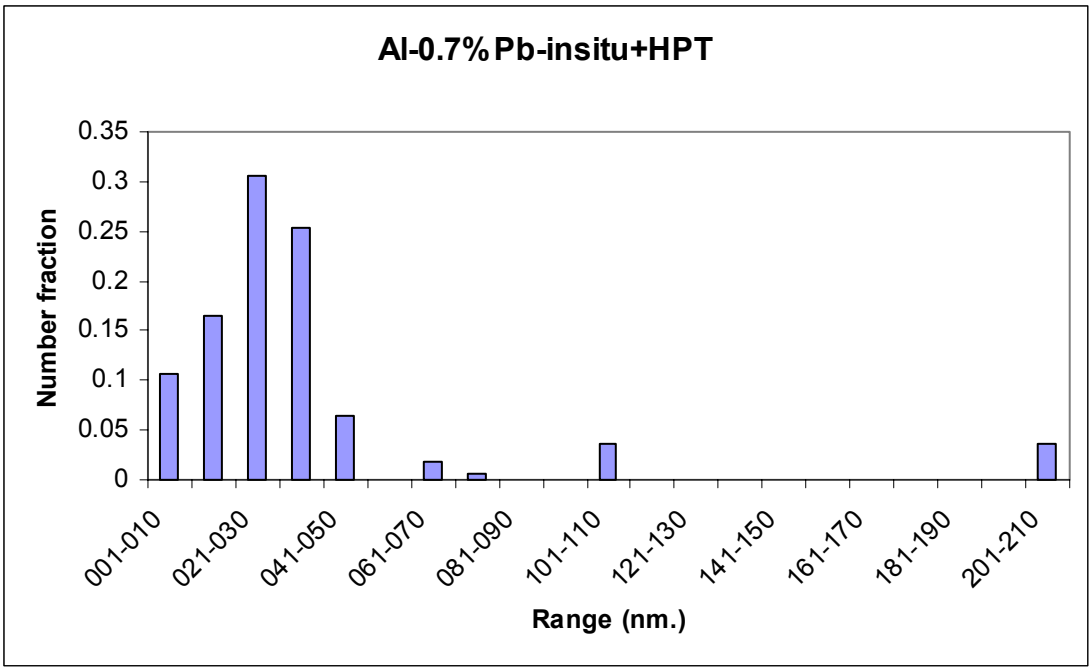

Fig 3(c) Grain size distribution of aluminum in nanocrystalline Al-0.7%Pb after HPT. The mean grain size was 34 nm.

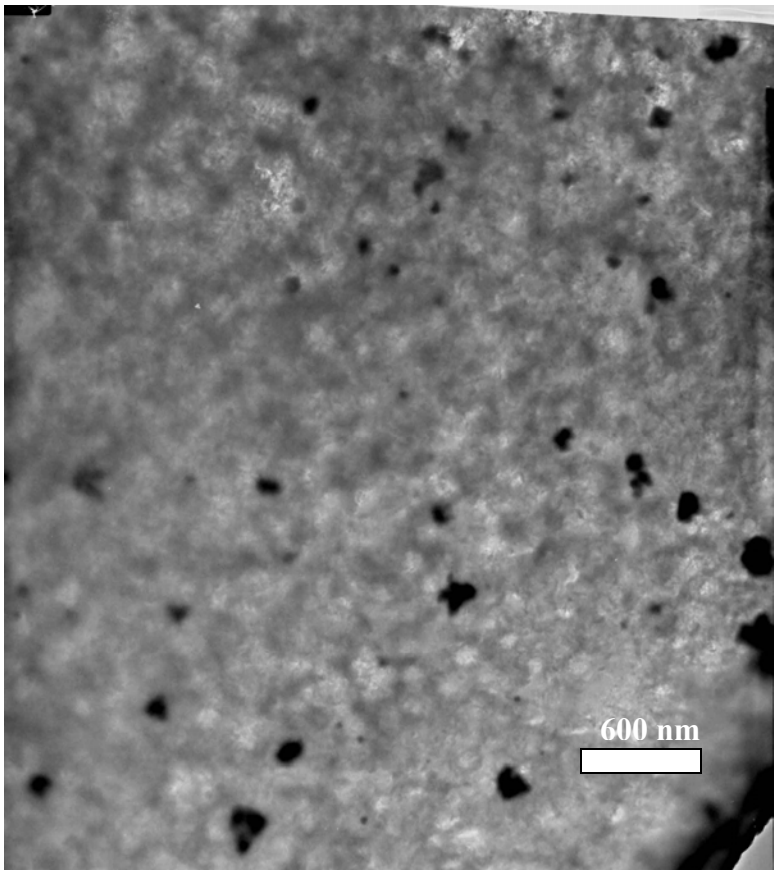

Fig 3(d) Size variations among Pb particles in nanocrystalline Al-0.7%Pb composite after HPT.

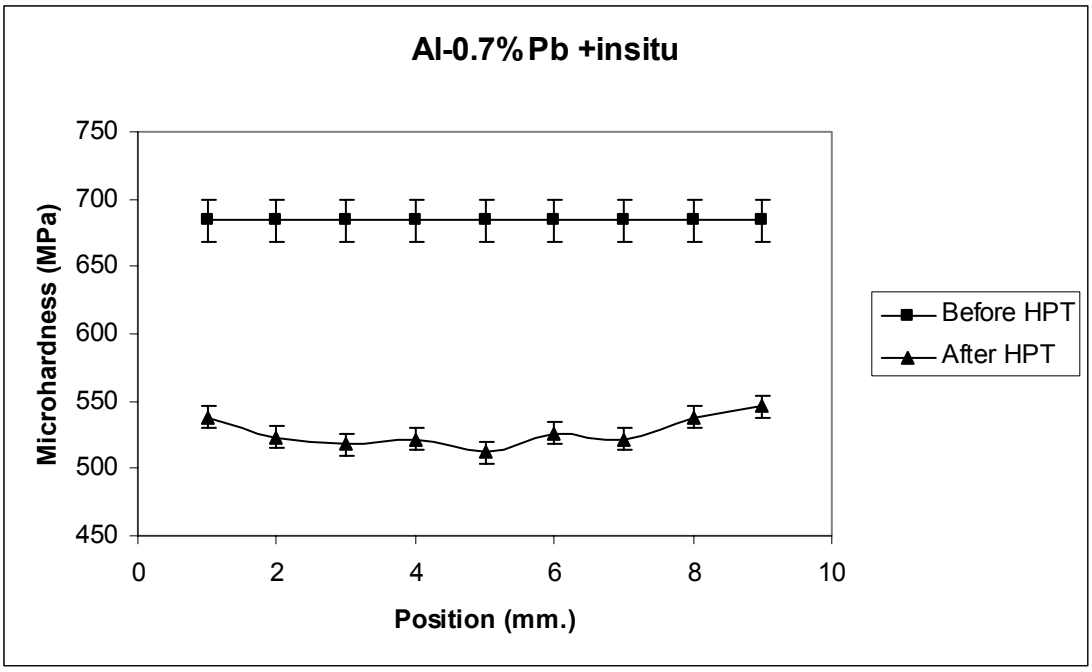

Fig 4 Variation of microhardness in nanocrystalline Al-0.7%Pb composite before and after HPT.

Chapter 8

Time dependant deformation characteristics of nanostructured aluminum

8.1 Introduction

Creep is defined as the time dependant plastic deformation under constant stress and temperature. There have been several studies on exploring the different mechanical properties of nanostructured materials [1-2]. However, creep of nanostructured materials received very little attention from the scientific community, mainly because of the difficulties in fabricating conventional specimens for creep testing. However, there have been several methods developed and validated to test the materials using very small quantities of samples using sub size specimens [3-5]. The mechanisms that control the plasticity of materials with nano scaled microstructural features are not clear, the creep mechanism being one of them.

Sanders et al evaluated the creep properties of nanocrystalline Cu, Pd and Al-Zr synthesized by inert gas condensation [6]. Creep tests were performed over a range of temperatures (0.24 – 0.64 Tm) and range of stresses. Their findings suggest that nanocrystalline materials are not inferior to their coarse grained counterparts in terms of creep resistance. They suggest that the creep behavior in those materials follows logarithmic creep. The creep rates observed are two to four orders of magnitude smaller than that predicted by Coble creep equation. The low angle grain boundaries and the smaller grains with negligible dislocation activity are suggested as the cause of smaller creep rates. Wang et al [7] studied the room temperature creep behavior of

electrodeposited nanocrystalline Ni. In their investigation, grain boundary sliding and the diffusion via the intercrystalline regions are suggested as the mechanisms responsible for the deformation. Cai et al [8] evaluated the creep properties of electrodeposited and cold rolled nanocrystalline copper in 20-50 ^{o}C range. They obtained activation energy of 0.82 eV and the corresponding n value was 2. It was suggested that the deformation was controlled by grain boundary sliding accommodated by grain boundary diffusion. The high temperature (0.5 Tm) creep behavior of nanocrystalline Ni-P, Fe-B-Si alloys indicates that the deformation was controlled by grain (and/or phase) boundary diffusion [9].

Therefore, the objective of the current study is two fold, 1) to check whether the small specimen testing technique, impression creep testing can be used to measure the time dependant mechanical properties of nanostructured materials or not and 2) to investigate the creep characteristics of nanocrystalline aluminum and thereby to identify the associated creep mechanisms.

8.2 Experimental

In the current study, time dependant deformation behavior of nanocrystalline aluminum (of grain size 32 nm) processed by ball milling and high pressure torsion is evaluated using impression creep testing technique. A cylindrical punch of diameter 150 microns was used to make the impression at constant stress at a given temperature. The variation of impression depth with time was measured using a LVDT. Data was obtained using a computer controlled data acquisition system. The experimental data between impression depths versus time was similar to conventional creep curves. The density of the sample

(evaluated using the Archimedes principle method) was 100% of its bulk density. Prior to testing, samples were metallographically polished to mirror like surface. The investigations were carried out over a range of temperatures (at 293 K, 323 K and 343 K) and range of stresses. Creep tests were performed at a new location on the sample surface for a given temperature and stress. The sample was heated to the required temperature before applying the load. Creep tests were carried out until steady state was attained. The impression stress was evaluated using

$$\sigma = 4\,P/\,\pi\,d^2$$

Where P is the applied load, d is the diameter of the indenter. To get the creep stress, impression stress should be divided by a factor of 3. The strain is calculated by

$$\varepsilon = \delta/d$$

Where δ is the displacement. Since we are using the cylindrical punch, constant load corresponds to the constant stress.

8.3 Results and discussion

.

Figs 1 to 6 shows the obtained creep curves and the corresponding strain rate versus strain plots at three different temperatures namely 293 K, 323 K and 343 K. At temperature 293 K, creep tests were carried out at stress values of 344 MPa, 436 MPa and 531 MPa.. At 323 K, creep tests were carried out at stress values of 399 MPa, 436 MPa and 610 MPa and at temperature 343 K, creep tests were carried out at 217 MPa, 344 MPa and 399 MPa. At all the temperatures studied, at a given stress value, attainment of steady state can be evidenced from the corresponding strain rate versus strain plots [Figs 2, 4 & 6]. The steady state creep rates were evaluated by taking the slopes of the creep curves in steady state region. At all temperatures, we can see the increment in steady state

strain rate with increases in stress [Table 1]. The stress exponents were calculated by plotting the steady state strain rate values vs stress (at a given temperature, after compensating for the variations in G with temperature [Table 2]) and taking the slope of the resultant plot. The measured stress exponents are 6.46 at 293 K, 5.1 at 323 K and 11.4 at 343 K [Fig 7]. Activation energy was calculated by plotting the steady strain rate vs 1/T at a constant stress (436 MPa) and measuring the slope of the resultant plot. The obtained slope multiplied by the universal gas constant (R) yields the activation energy. In the present study it was 70±2 kJ/mole [Fig 8]. The high values of the stress exponents obtained in the current study do not account for any creep mechanism controlled by grain boundaries. However the activations is energy is close to that of grain boundary diffusion for aluminum.

The steady state creep rate for coarse grained materials is given by the well known Dorn equation:

$$\dot{\varepsilon} = \frac{ADGb}{kT}\left(\frac{b}{d}\right)^{p}\left(\frac{\sigma}{G}\right)^{n}$$

Where $\dot{\varepsilon}$ = steady state creep rate

A= dimensionless constant

d = grain size

σ = applied stress

D= diffusion coefficient = D_0 exp (-Q/RT)

D_0 = pre-exponential term

Q= activation energy

R= Universal gas constant

T= Temperature in K

b = Burger's vector

G= Shear modulus

n= Stress exponent

p= inverse grain size exponent

Creep properties of coarse grained metals and alloys were investigated extensively and the governing creep mechanisms were identified [10]. The studies on evaluation of creep properties of nanostructured materials are very limited so far and they were reviewed by Mohamed and Li [11]. Since the nanocrystalline materials contains increased volume fraction of grain boundaries (or in other words finer grain size), it was believed that these materials will exhibit poor creep resistance. However, in nanocrystalline Cu, Pd and Al-Zr it was showed that the measured steady state creep rates were smaller than that predicted by the Coble creep equation [6]. They attributed the observed very low creep rates to two factors, a) the presence of twin boundaries and low angle boundaries that resist boundary sliding and that are poor paths for vacancy diffusion b) the limitation on dislocation activity due to the smaller grain sizes. Wang et al [7] studied the creep behavior of electrodeposited nanocrystalline Ni of different grain sizes varying from 6 nm to 40 nm. They observed stress exponents (n) ranging from 1 at 6 nm to 5 at 40 nm. However they did not report the values of activation energy. Yin et al [12] investigated the creep characteristics of nanocrystalline Ni at two different temperatures namely 290 K and 373 K. At 290 K, the n value was 1 but it increased to 6.5 at 373 K. However the

measured activation energy 0.72 eV is in good agreement with the activation energy for grain boundary diffusion in Ni (1.08 eV). They concluded that the creep mechanism at 290 K was controlled by Coble creep, however it might be changing to multiple mechanisms at 373 K. Recently Kottada and Chokshi [13] investigated the creep behavior of electrodeposited nanocrystalline Ni under compressive conditions. They observed very high values of stress exponents and are not predicted in the Coble mechanism. However the measured activation energy ~ 90-120 kJ/mole suggests that the grain boundary diffusion is the dominant mechanism. The creep behavior of cryomilled and extruded ultra fine grained Al-Mg alloy [14] predicts stress exponent values of 7.2-7.4. However, the activation energy is in good agreement with the activation energy for grain boundary diffusion in aluminum.

Although there are few investigations on creep behavior of different nanocrystalline metals and alloys [11], there was not even a single report on creep characteristics of nanostructured pure aluminum. In the current investigation, from the measured high stress exponent values, it appears that the creep mechanism does not follow grain boundary sliding (n~2). However, the calculated activation energy of nanostructured aluminum, 70±2 kJ/mole [Fig 8] is half of that of the lattice diffusion in aluminum (142 kJ/mole). Earlier studies on creep of nanostructured materials yielded high stress exponents [13 and 15]. However the activation energy was for that of grain boundary diffusion [13]. The current study on creep of nanostructured aluminum also falls on the similar lines (high stress exponent and activation energy for grain boundary diffusion) Hence it suggests that, the creep mechanism in nanostructured aluminum in the current study is controlled by grain boundary diffusion. Prior to this, the impression creep testing

was used to determine the creep properties of several conventional coarse grained metals and alloys [16-17]. This is the first report that suggests that the impression creep testing can be used to evaluate the creep properties of nanostructured materials

8.4 Summary and conclusions

The creep characteristics in nanocrystalline aluminum were investigated using impression creep testing at different temperatures and over a range of stresses. Our report shows that impression creep testing can be used to evaluate the time dependant deformation characteristics of nanostructured materials. The creep in nanocrystalline aluminum in the current study is controlled by grain boundary diffusion although the calculated n values are higher than those for Coble creep (or grain boundary mediated processes).

References:

1. M. A. Meyers, A. Mishra, D. J. Benson, Prog. Mat.Sci 51 (2006) 427.
2. K. S. Kumar, H. Van Swygenhoven, S. Suresh, Acta mater 51 (2003) 5743.
3. T. R. Malow and C. C. Koch, Acta Mater, 46 (1998) 6459.
4. T. R. Malow, C. C. Koch, P. Q. Miraglia, K. L.Murty, Mater Sci Eng, A 252 (1998) 36.
5. X. Zhang, H. Wang, C. C. Koch, Rev. Adv. Mat. Sci, 6 (2004) 53.
6. P. G. Sanders, M. Rittner, E. Kiedaisch, J. R. Weertman, H. Kung and Y. C. Lu, Nanostruct. Mater. 9 (1997) 433.
7. N. Wang, Z. Wang, K. T. Aust, U. Erb, Mater. Sci. Eng., A237 (1997) 150.

8. B. Cai, Q. P. Kong, P. Cui, L. Lu, K. Lu, Scripta mater. 45 (2001) 1407.

9. Q. P. Kong, B. Cai, M. L. Xiao, Mater. Sci. Eng., A234 (1997) 91.

10. Creep in metallic materials by J. Cadek, Elsevier (1988), ISBN 0444989161, p. 13.

11. F. A. Mohamed, Y. Li, Mater. Sci. Eng., A298 (2001) 1.

12. W. M. Yin, S. H. Whang, R. Mirshams, C. H. Xiao, Mater. Sci. Engg. A301 (2001) 18.

13. R. S. Kottada and A. H. Chokshi, Scripta mater. 53 (2005) 887.

14. R. W. Hayes, V. Tellkamp, E. J.Lavernia, Jour. Mater. Res., 15 (2000) 2215.

15. R. Hayes, V. Tellkamp, E. Lavernia, Scripta mater., 41 (1999) 743.

16. J.C.M Li, Mater. Sci Engg, A 322 (2002) 23.

17. P. S. Godavarti and K. L. Murty, J. Mat. Sci. Lett., 6 (1987) 456.

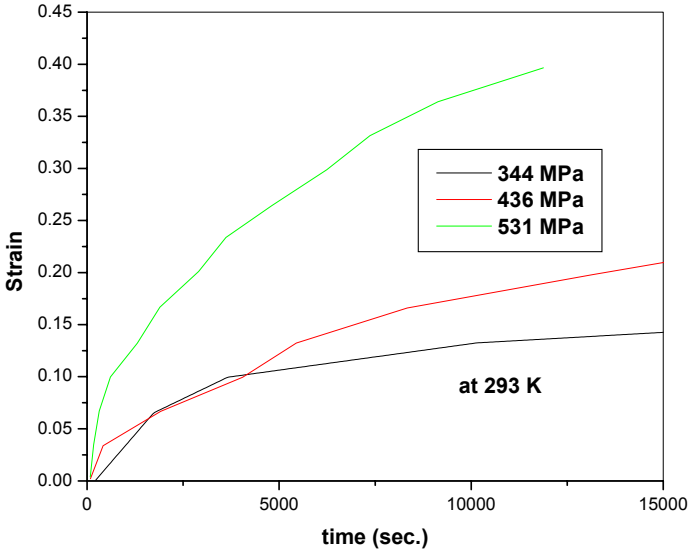

Fig 1 Creep curves of nanostructured Al at 293 K

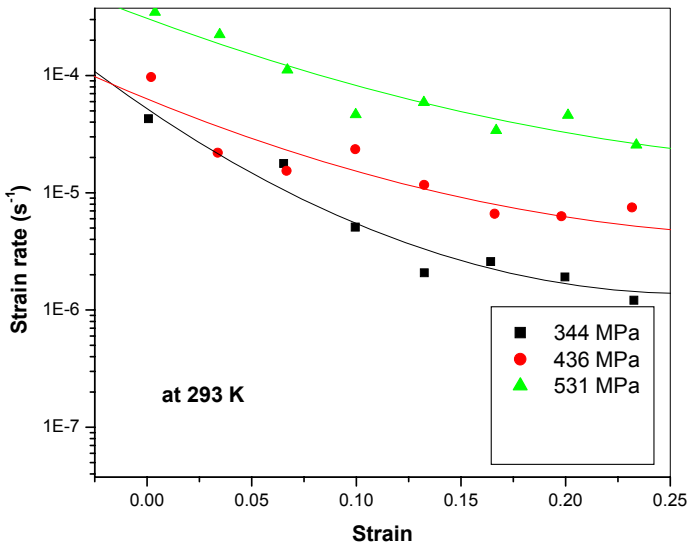

Fig 2 Strain rate vs strain curves at 293 K

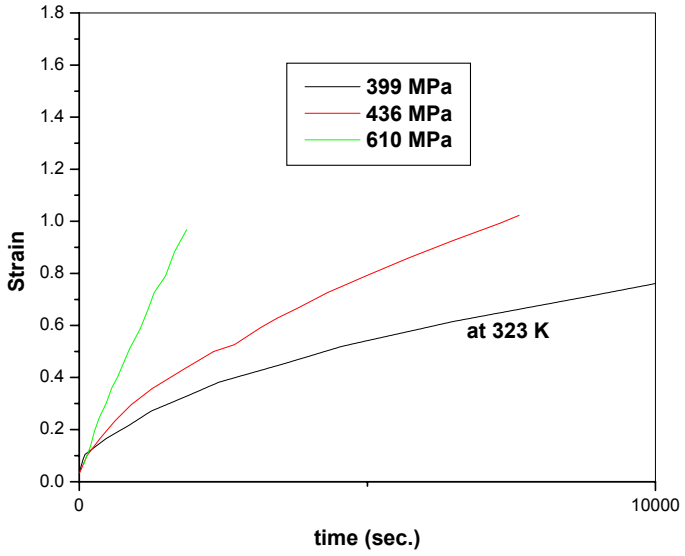

Fig 3 Creep curves of nanostructured Al at 323 K

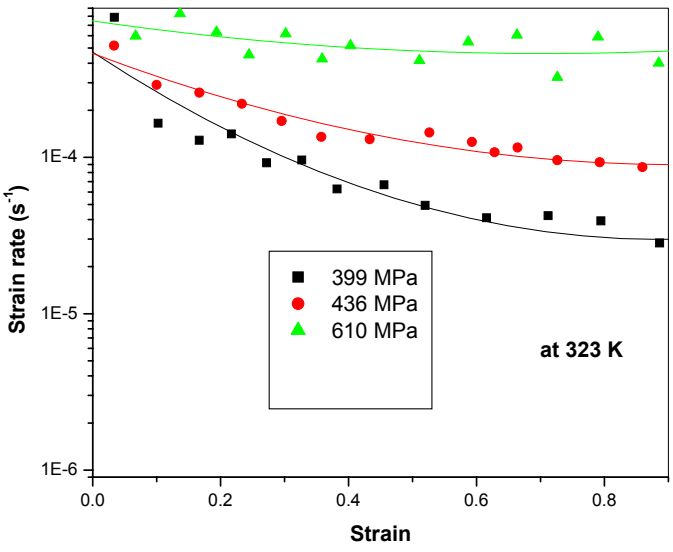

Fig 4 Strain rate vs strain curves at 323 K

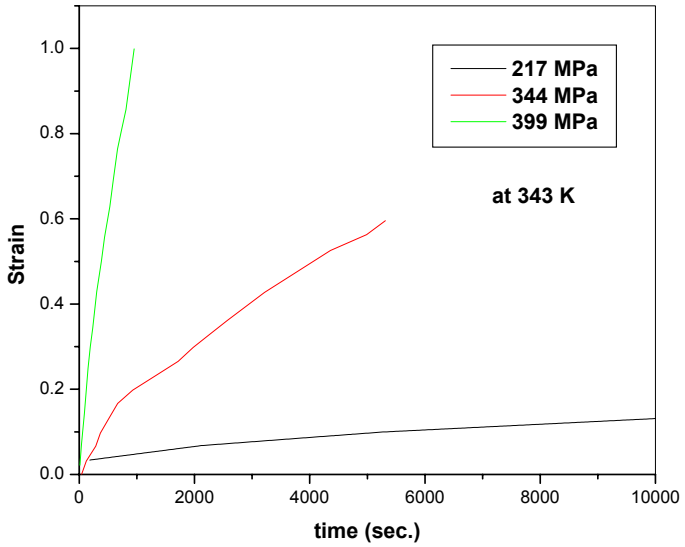

Fig 5 Creep curves of nanostructured Al at 343 K

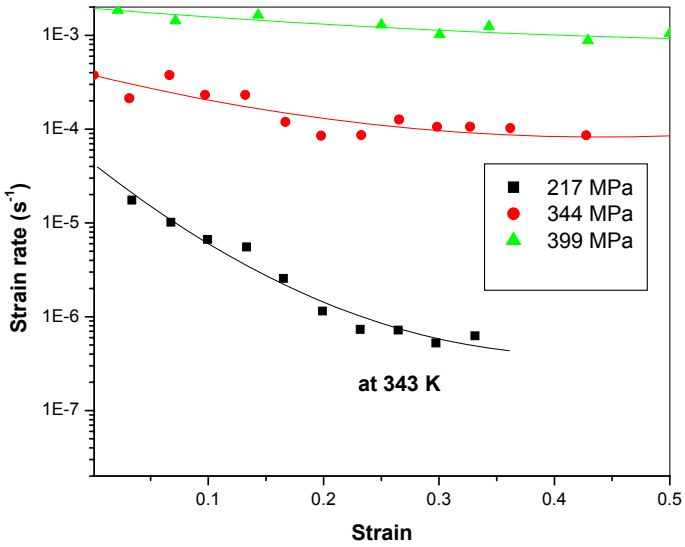

Fig 6 Strain rate vs strain curves at 343 K

Table 1 Experimental creep data on nanostructured Al (of d=32 nm) evaluated by impression creep testing

Temperature (K)	Stress (MPa)	Steady state strain rate (s^{-1})
293	344	1.6E-6
293	436	5.3E-6
293	531	2.7E-5
323	399	5.2E-5
323	436	7.6E-5
323	610	5.0E-4
343	217	6.3E-7
343	344	8.5E-5
343	399	8.1E-4

Table 2 Variation of G with temperature for Al

Temperature (K)	G (MPa)
293	25495.28
323	25086.92
343	24814.68

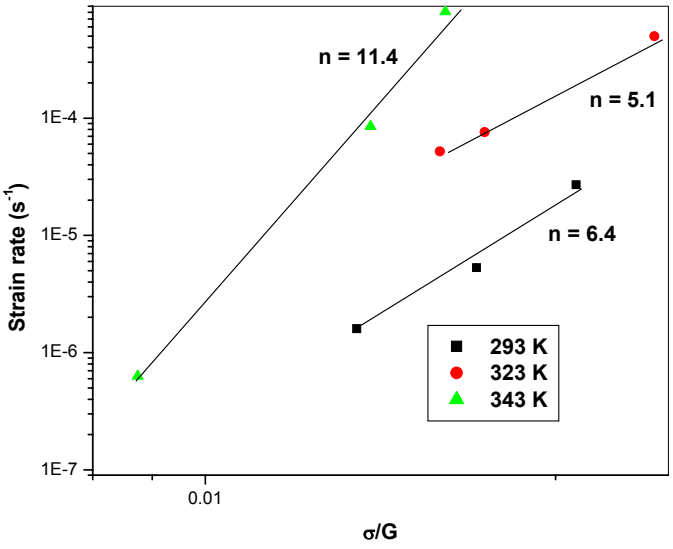

Fig 7 Steady state strain rate vs stress/G at different temperatures, 293 K, 323 K and 343 K.

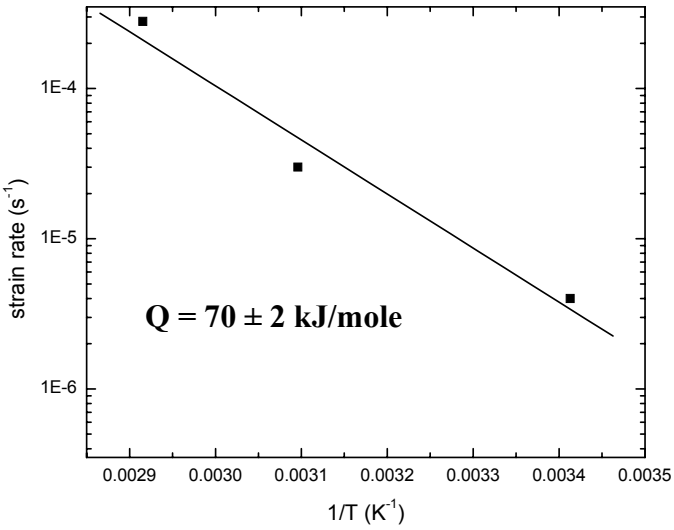

Fig 8 Plot of strain rate vs 1/T. The activation energy was calculated from the slope of this plot. The data points of strain rate given in this plot are for a stress value of 436 MPa. For Al, Q_l = 142 kJ/mole; Q_{gb}= 84 kJ/mole.

Chapter 9

Summary and conclusions

Nanocrystalline aluminum was synthesized using ball milling at room temperature. The obtained powders were compacted at 573K in an argon atmosphere. The powders were also consolidated using high pressure torsion (HPT). The nanocrystalline aluminum attained hardness as high as 1200 MPa after HPT. This high strength was derived from the grain refinement, increase in dislocation density, and probable presence of twins in nanocrystalline aluminum. It was successfully demonstrated that a combination of ball milling and high pressure torsion can be used to synthesize bulk nanostructured materials with high end mechanical properties. In the end, the nanocrystalline aluminum was 6 times harder than its coarse grained counterpart.

Nanocrystalline Al-W composites of varying compositions were synthesized using combination of ball milling and high pressure torsion. Although the equilibrium phase diagram of Al-W shows the presence of some intermetallics in the compositions studied, there was not any formation of a metastable/stable compound, solid solution or an intermetallic. It was purely a two phase composite structure at nano scale. This nano scaled microstructure was not disturbed during HPT. The grain size of the aluminum matrix in these alloys is about 30 nm and the W particle size is around 500 nm. An addition of 4.0 atomic % of W to nanocrystalline aluminum increases the strength of the aluminum from 934 MPa to 1600 MPa. The hardness of these composites monotonically increases with increase in W content. This strengthening behavior is successfully explained by composite model using rule-of-mixtures.

Nanocrystalline Al-Pb composites of different compositions were synthesized by two different routes. In one route, ball milling was done on Al and Pb with the addition of 1.5 wt % of stearic acid at room temperature and the obtained powders were warm compacted at 573 K. In the other route, spherical balls were synthesized using in situ consolidation technique, i.e., milling at cryogenic temperature followed by milling at room temperature. The grain size of aluminum was about 28 nm and the particle size of the Pb varies from 5 nm to 500 nm. In both the cases, addition of minute amounts of Pb to the nanocrystalline aluminum caused a drastic softening. The obtained hardness values are far below than the ones predicted by rule-of-mixtures. This interesting phenomenon was explained based on defect generation under applied external load becoming easier because of the presence of Pb in the nanocrystalline aluminum grain boundaries.

Nanocrystalline Al-0.7%Pb composite synthesized by in situ consolidation technique was further strained by HPT. The mean grain size of Al before HPT was around 30 nm and it did not change significantly after HPT. However the hardness of the material was decreased by 24 %. The mean grain size of Pb before HPT was 11 nm and it was refined to 5 nm after HPT. The lattice strain of aluminum increased after HPT. This could be because of the increase in dislocation density and the strain resulted from the rearrangement of the microstructure during HPT. However, the reasons for the softening observed in this material after HPT are unknown at this time.

Creep properties of bulk nanostructured aluminum (of grain size 32 nm) were evaluated by impression creep testing technique at various temperatures (293 K, 323 K and 343 K)

and over a range of stresses. The stress exponent values were larger than those for the Coble creep mechanism (~2). However, the measured activation energy is close to that of grain boundary diffusion in aluminum.

In the end, addition of a soft phase (Pb) softens the nanocrystalline aluminum matrix drastically whereas the hard phase (W) strengthens the nanocrystalline aluminum. However, the governing mechanisms for these two effects appear to be different.

Chapter 10

Suggestions for the future work

1. Detailed characterization of the microstructure using HRTEM is needed in case of HPTed nanocrystalline aluminum to see if there are any deformation twins developed at the nano scale during HPT. If there are any, need to quantify the contribution of these twins to the hardening.
2. Microstructural characterization using DF and HRTEM in HPTed aluminum in longitudinal as well as torsion directions is to be carried out to check for the microstructural homogeneity.
3. The reasons for the abnormal characteristics (i.e., not following the equilibrium phase diagram) in nanocrystalline Al-W at the nano scale are need to be identified. Microstructural investigations need to be carried out using TEM on Al-W nano composites to detect the presence of W in nanocrystalline Al grain boundaries if there is any. If it is present, its contribution to the strengthening should be evaluated.
4. The dependence of the lattice strain on dislocation density should be examined by evaluating the dislocation densities at various positions using X ray peak profile analysis.
5. In case of Al-Pb, HRTEM should be performed in all the samples in as milled condition as well as the HPTed condition to check for the nature of the interface between Al and Pb at the nano scale. And it should be correlated with the mechanical properties. The changes in the grain boundary properties (ex., energy

and misorientation) in nanocrystalline aluminum caused by Pb atom segregates should be monitored with the DSC and the HRTEM.

6. The variation of the mechanical properties in nanocrystalline Al-Pb composites with the temperature should be investigated both in the as milled condition and HPTed condition.
7. Detailed tensile testing should be performed on nanostructured Al, Al-W and Al-Pb to investigate the changes in ductility caused by W/Pb in nanocrystalline aluminum. The influence of W/Pb on the fracture morphology of nanocrystalline aluminum should be studied.
8. The atomistic mechanism responsible for the hardening/softening caused by W/Pb in nanocrystalline aluminum need to be explored using both the experimental data and theoretical predictions.